Bone Material Characteristics Influenced by Osteocytes

Dissertation

zur Erlangung des akademischen Grades

doctor rerum naturalium

(Dr. rer. nat.)

im Fach Physik

eingereicht an der

Mathematisch-Naturwissenschaftlichen Fakultät I

der Humboldt-Universität zu Berlin

von

Diplom Physiker Michael Kerschnitzki

Präsident der Humboldt-Universität zu Berlin:

Prof. Dr. Jan-Hendrik Olbertz

Dekan der Mathematisch-Naturwissenschaftlichen Fakultät I:

Prof. Dr. Andreas Herrmann

Gutachter/innen: 1. *Prof. Dr. Dr. h.c. Peter Fratzl*

2. *Prof. Dr. Franz Pfeiffer*

3. *Prof. Dr. Norbert Koch*

Tag der mündlichen Prüfung: *24.02.2012*

Kurzfassung

In dieser Doktorarbeit wird die Hypothese geprüft, ob Osteozyten einen direkten Einfluss auf die Knocheneigenschaften in ihrer unmittelbaren Umgebung haben. Der zentrale Experimentieransatz ist dabei die Korrelation der Organisation des Osteozytennetzwerks mit den Mineraleigenschaften des Knochens auf der Submikrometerebene. Es wird gezeigt, dass bereits die anfängliche Ausrichtung der Osteoblasten entscheidend für die Synthese von hoch ausgerichtetem Knochenmaterial ist. Die dabei entstehenden Osteozytennetzwerke sind so organisiert, dass die Osteozyten und ihre Zellfortsätze jeweils einen möglichst kleinen Abstand zum Knochenmineral haben. Deshalb wird vermutet, dass genau diese Netzwerkorganisation mitentscheidend ist, wie gut die Zellen das Mineral in ihrer Umgebung beeinflussen können. Messungen der Knochenmineraleigenschaften auf Submikrometerebene mit Röntgenkleinwinkelstreuung bestätigen diese Vermutung. Dabei wird deutlich, dass Knochenmaterial in der Nähe der Osteozyten durch andere Mineraleigenschaften geprägt ist. Um zu klären, wie Osteozyten Mineral in ihrer direkten Umgebung verändern können, werden Mechanismen der passiven Mineralherauslösung aus der mineralisierten Oberfläche des Osteozytennetzwerks untersucht. Es wird gezeigt, dass kalziumarme ionische Lösungen unter physiologischen Bedingungen große Mengen von Kalzium-Ionen aus dem Knochen lösen und diese dann durch die Osteozytennetzwerkstrukturen diffundieren können. Zum Abschluss wurde medullärer Knochen von Hühnern als ein Modellsystem für rasanten Knochenumbau untersucht. Dieser spezielle Knochentyp dient den Hennen als labiles Kalziumreservoir und ermöglicht dadurch die tägliche Eierschalenproduktion. Experimente am medullären Knochenmaterial zeigen insbesondere die Bedeutung von weniger stabilen Mineralstrukturen die benötigt werden um den Knochen an den schnellen, sich wiederholenden Knochenauf- sowie Abbau optimal anzupassen.

Knochenaufbau, Osteozytennetzwerke, Osteozytische Osteolyse, Kleinwinkelstreuung, Konfokale Mikroskopie

Abstract

This thesis aims to test the hypothesis whether osteocytes have a direct influence on bone material properties in their vicinity. In this regard, the concomitant analysis of osteocyte network organization and bone ultrastructural properties on the submicron level is the central approach to answer this question. In this work, it is shown that already initial cell-cell alignment during the process of bone formation is crucial for the synthesis of highly organized bone. Furthermore it is proposed that the occurrence of highly ordered osteocyte networks visualized with confocal laser scanning microscopy (CLSM) has a strong impact on the ability of osteocytes to directly influence bone material properties. These highly organized networks are another consequence of initial cell-cell alignment and are found to be arranged such as to feature short mineral cell distances. Examination of submicron mineral properties with scanning small angle x-ray scattering (sSAXS) shows that bone material in the direct vicinity of osteocytes and their cell processes shows different mineral properties compared to bone further away in the depth of the tissue. Moreover, mechanisms of passive mineral extraction from the mineralized surface of the osteocyte network, due to the treatment with calcium poor ionic solutions, are investigated. It is shown that this chemical process occurring under physiological conditions leads not only to the dissolution of considerable amounts of calcium, but also to efficient diffusion of these ions through the osteocyte network structures. Finally, medullary bone which is intended as a labile calcium source for daily egg shell formation in hens is used as a model system for rapid bone turnover rates. This bone type in particular indicates the importance of uniquely adapted, less stable mineral structures to fit the requirements for rapid bone resorption as well as re-formation.

Bone formation, osteocyte networks, osteocytic osteolysis, small angle x-ray scattering (SAXS), confocal laser scanning microscopy (CLSM)

Contents

1   Introduction

Bone is one of the most intensively studied biological materials, composed from inorganic hydroxyapatite mineral crystals which are embedded in an organic extracellular collagen matrix. Bone features several levels of hierarchy, which together involve unique implications on macroscopic bone material properties (Weiner and Wagner 1998; Currey 2002; Fratzl and Weinkamer 2007). Furthermore bone is the main mineral reservoir for maintaining body calcium and phosphate homeostasis (Aarden, Burger et al. 1994; Bonewald 2007). A detailed understanding of the dynamic processes of bone formation and remodeling during physiological growth, healing and aging as well as in the case of pathological cases of bone diseases has high clinical relevance. Bone development and adaptation involves not only various cellular interactions (Cowin 2004; Chen, Liu et al. 2010) but also depends on dynamic chemical processes of bone mineral crystallization (Weiner and Traub 1992; Landis 1995; Olszta, Cheng et al. 2007). Thus, bone research is a highly interdisciplinary field at the interface of medicine, chemistry, biology and material science.

Bone remodeling is traditionally attributed to osteoblasts and osteoclasts – cells which deposit and resorb bone, respectively (Buckwalter, Glimcher et al. 1995). These cells are also the primary target of treatments against bone diseases leading to an imbalance of bone formation and resorption and thus to substantially decreased bone quality (Rodan and Martin 2000; Roschger, Paschalis et al. 2008). Osteocytes are the cells residing within the bone matrix, deriving from osteoblasts which get embedded during the process of bone deposition (Franz-Odendaal, Hall et al. 2006) and create a network of extracellular spaces by which the bone tissue is perfused (Lanyon, Rubin et al. 1993). Osteocytes are known to orchestrate the delicate activity of osteoclasts and osteoblasts (Burger and Klein-Nulend 1999; Bonewald and Johnson 2008; Nakashima, Hayashi et al. 2011). However, to date more evidence arises, that osteocytes are also directly involved in bone mineral homeostasis. The surface area of the osteocyte network can be estimated 100 fold greater than the surface available to osteoblasts and osteoclasts (Aarden, Burger et al. 1994; Teti and Zallone 2009). Therefore, it seems possible that osteocytes may act directly on the bone material they are in contact

with, having some ability to deposit and resorb mineral (Bonewald 2007; Bonucci 2009; Teti and Zallone 2009) and thus directly control bone quality as well as fragility.

1.1   Scope and Aims of the Work

In this PhD thesis, the hypothesis will be tested whether osteocytes directly influence bone material in their vicinity. This implies that bone material adjacent to osteocytes and their cell processes could be more dynamic and thus, may have a different structure as compared to bone further away in the bulk of the tissue. The chosen approach to solve this complex problem is a combination of techniques to reveal osteocyte network organization together with the measurement of bone ultrastructural properties on the submicron level. This concomitant analysis offers the possibility to better understand the influence of cell-cell organization during the dynamic processes of bone formation and remodeling as well as the possibility of cell-matrix interactions – with particular regard to osteocytes. This will improve the understanding of the impact of osteocyte network organization in conjunction with osteocyte activity on bone tissue characteristics such as matrix orientation and mineralization. As these factors mainly influence bone quality as well as bone fragility, these new insights can help to better understand the role of osteocytes during calcium and phosphate homeostasis. Furthermore, these insights may clarify whether these cells should be considered more urgently as a target for drug development in the context of bone diseases featuring deficient bone mineral homeostasis, such as osteoporosis.

The work is based on five different experimental steps: **(i)** Confocal laser scanning microscopy (CLSM) combined with rhodamine staining which allows the three-dimensional visualization of osteocyte networks in undemineralized bone sections. Furthermore, experimental procedures are developed to accommodate the assessment of bone material properties at the same location with various techniques such as back-scattered electron microscopy (BSE) and scanning small angle x-ray scattering (sSAXS). **(ii)** Subsequently, osteocyte network organization is visualized and correlated with bone tissue characteristics in different bone types from different species in order to better understand common geometries of the osteocyte network arrangement in conjunction with the surrounding bone

matrix. Moreover, implications on the dynamic processes of bone formation, bone healing and remodeling are made as osteocyte networks show the direct location of former osteoblasts during the process of bone deposition. **(iii)** To test whether bone material in the direct vicinity of the osteocytes and their cell processes shows different characteristics, high resolution sSAXS techniques are used to measure submicron bone mineral properties which are further correlated to the organization of the osteocyte networks. **(iv)** To further understand how osteocytes could modify bone mineral properties in their vicinity, passive mineral extraction from the mineralized surfaces exposed within the osteocyte network is performed. These experiments show the proposed potential of calcium ion dissolution and successive transportation through the osteocyte network structures. **(v)** Finally, medullary bone of egg laying chicken is investigated to better understand the requirements on bone material uniquely adapted for bone resorption as well as re-formation.

1.2   Outline of the Thesis

The thesis starts with a brief introduction, distinguishing between bone as a material and a living tissue. Firstly bone hierarchy and individual structural characteristics of different bone types will be explained, but also the main bone cells which control bone formation and remodeling will be introduced. This section is followed by the 3rd chapter briefly introducing the theoretical background of physical methods used, focusing on confocal laser scanning microscopy, electron microscopy and small angle x-ray scattering. In the 4th chapter initial preparation of bone samples as well as experimental setups are explained. A detailed description of all methods and sample preparation protocols especially developed during this PhD-project can be found in the 5th chapter. In the 6th chapter, experimental findings are discussed in detail, followed by general conclusions and a perspective for future research in the 7th chapter.

2   Bone and Bone Mineral

Bone is the main component forming the skeletal system in all vertebrates. The human skeleton consists of approximately 206 different bones, individually in shape, size and mechanical properties, depending on their anatomical position and function. As an example, the skull must be flexible during stages of growth but still protective to prevent external impacts on the brain, whereas auditory ossicles residing inside the ear are, due to acoustical reasons, stiff and brittle (Currey 2003). Additionally to their multifunctionality, bones continuously adjust to external stimuli by remodeling, performed by coordinated interactions of bone cells (Duncan and Turner 1995). Thus bone is not only a static material but continuously undergoes adaptation throughout its whole lifecycle (Frost 1987; Currey 2003; Fratzl and Weinkamer 2007). In the following these two approaches to firstly understand bone as a 'static material' but also secondly as a living organism, will be described.

2.1   Bone as a Material

Bone material features a complex hierarchical structure ranging over several levels of hierarchy from the molecular- up to the macroscopic level (Rho, Kuhn-Spearing et al. 1998; Weiner and Wagner 1998; Currey 2002; Fratzl and Weinkamer 2007). At lowest levels of hierarchy bone is a nano composite formed from collagen type 1 molecules and carbonated hydroxyapatite mineral particles (Fratzl, Gupta et al. 2004). Triple helical collagen molecules self-assemble to approximately 100 nm thick fibrils in such way, that adjacent collagen molecules are staggered in axial direction by 67 nm leading to banded structures showing the characteristic gap and overlap zones (Petruska and Hodge 1964; Landis, Hodgens et al. 1996). Collagen fibrils are mineralized with carbonated hydroxyapatite mineral crystals. It was reported that nucleation of those starts in the gap regions (Landis, Hodgens et al. 1996; Landis, Hodgens et al. 1996) however a recent report states a initiation of mineral nucleation in the overlap zone (Nudelman, Pieterse et al. 2010) with further growth to flat plate-like crystals (Weiner and Traub 1992; Landis, Hodgens et al. 1996). Water is the third major component at lowest levels of hierarchy located within and between the fibrils

and collagen molecules. During processes of mineralization, water is partly substituted with bone mineral (Fratzl, Fratzl-Zelman et al. 1993).

Mineralized collagen fibrils further assemble to fibrillar arrays building up diverse organizational patterns which can be generalized to 4 different bone types (Weiner and Wagner 1998): **(i)** Parallel-fibered bone features arrays of collagen fibrils arranged in a parallel manner over ranges of micrometers and even millimeters. This type of bone is very rapidly formed and usually can be found in tendons, skeleton of fish, amphibians and the bovid family. Opposing to parallel fibered bone **(ii)** woven fibered bone is characterized by no long range order. Fibrils are arranged to poorly oriented and loosely packed bundles with diameters up to 30 μm. Woven bone forms and mineralizes very rapidly but only offers poor mechanical properties. It is found to be the first deposited bone type after fractures and during early stages of embryonic development and subsequently gets replaced by other bone types. **(iii)** Plywood-like structures feature sets of parallel fibrils arranged in layers, with alternating fibril orientation between individual layers. Lamellar bone as one example of twisted plywood-like structures is very often found in mammals centrically arranged around the Haversian canal containing the blood vessel. It features excellent mechanical properties and is formed at lower rates as compared to parallel-fibered or woven bone. **(iv)** Another structural motif of fibrillar arrays is the radial fibril orientation, characteristic for the inner layer of teeth. Fibrils are aligned in plane, radial to the surface of the tubule present in the bulk of dentin (Figure 1).
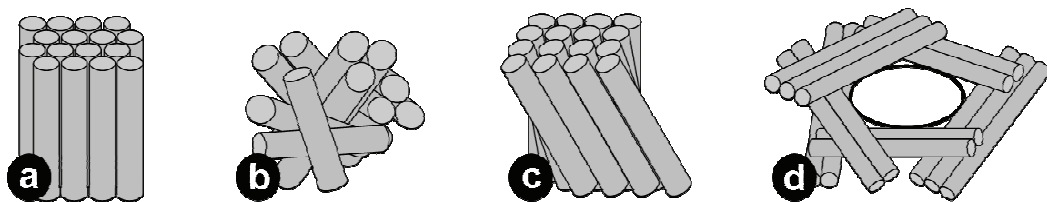
Figure 1: Scheme of the 4 different bone types: (a) parallel fibred bone, (b) woven bone, (c) plywood-like lamellar bone and (d) radial fibril orientation. Adapted from (Weiner and Wagner 1998).

In larger mammals, in particular in cattle, fibrolamellar bone can be found (Currey 2002; Mori, Kodaka et al. 2003; Mori, Hirayama et al. 2007). This bone

type features a mixture of poorly aligned, rapidly growing woven bone and highly aligned parallel-fibered or lamellar bone. This structural composition is beneficial as these animals have to grow fast but still, bones need to withstand high mechanical loading.

At the next hierarchical level, the structure of bone is distinguished in compact cortical and spongy trabecular bone. Cortical bone forms the outer bone shell and is characterized by low porosity (< 10 %), which is mainly due to the occurrence of blood vessels and cellular spaces which also can act as initiation points for cracks (Nicolella, Bonewald et al. 2005; Nicolella, Moravits et al. 2006; Ebacher and Wang 2009). Whereas human cortical bone is composed of numerous osteons ensuring good blood supply, cortical bone in cattle and horses is mainly composed of fibrolamellar bone featuring less supply with blood, which leads to longer healing times in case of fracture. In areas of heavy compressive loading such as the head of the femur or the vertebrae, the cortical bone shell is filled with spongeous trabecular bone featuring high porosity (> 80 %). The individual lamellar bone struts with a diameter ranging between 100 and 300 μm are not supplied with blood as nutrition of bone cells is assured by the surrounding bone marrow.

On the macroscopic level, shapes of bones range from long bones like the femur which provide stability against bending and buckling, over flat bones as the scapula to block-shaped or plate-shaped bones as the vertebrae or skull providing stability against bending as well as protecting vital organs.

The complex hierarchical structure of bone has several implications for bone mechanics as every level of hierarchy contributes to macroscopic mechanical properties of the bone material. Just to mention some examples, in literature it is suggested that at the nano-scale, strong mechanical heterogeneity accounts for crucial mechanisms of energy dissipation during mechanical loading (Tai, Dao et al. 2007). In this regard, inorganic mineral particles provide stiffness but also being shielded from strong deformation by the ductile organic collagen matrix which takes up the deformation energy by shearing (Jager and Fratzl 2000; Gupta, Wagermaier et al. 2005; Gupta, Seto et al. 2006). However, also at higher levels of hierarchy, mechanisms of crack deflection at microscopic interfaces can

dissipate deformation energy (Peterlik, Roschger et al. 2006; Koester, Ager et al. 2008).

2.2 Bone as a Living Tissue

Bone is a dynamic living tissue as it features the unique ability not to be only statistically predefined by its genetic blueprint. Furthermore it is able to continuously adapt to changing external biophysical stimuli of its environment to improve functionality (Thompson 1992; Fratzl and Weinkamer 2007; Meyers, Chen et al. 2008). Even without a change in stimulus, dynamic self-healing mechanisms continuously remediate damage and thus strengthen the bone material.

In bone the ability of adaption derives from permanent processes of remodeling of the entire bone material. Remodeling is beneficial as it **(i)** increases the blood supply, **(ii)** removes dead bone, **(iii)** takes out microcracks, **(iv)** changes the grain which leads to improved mechanical properties and **(v)** contributes to body mineral homeostasis (Currey 2002). Processes of remodeling are a consequence of interplay of the bone cells. Osteoclasts resorb bone leaving small cavities. Osteoblasts subsequently fill those with new, completely unmineralized bone material. Subsequent mineralization of the newly deposited material is very rapid during the first days – reaching about 50 % of the final degree of mineralization – followed by a phase of continuous slow mineralization leading to a permanent increase in mineral content (Fratzl, Gupta et al. 2004; Ruffoni, Fratzl et al. 2008). In trabecular bone, due to its high surface to volume ratio, osteoclasts have access to the whole bone volume just by resorbing cavities of approximately 60 µm (Jee 2001). Whereas in compact cortical bone (low surface to volume ratio), osteoclasts resorb a tunnel with a speed of approximately 20 – 40 µm/day (Jee 2001). These remaining tunnels get later filled with new lamellar bone material deposited by osteoblasts – forming a new haversian system also called secondary osteon which improves blood supply (Figure 2). Secondary osteons are separated from their surrounding older bone material by an impermeable cement line acting as an outer border. Thus, cells residing in the old bone are not supplied from the blood vessel anymore leading to cell death. Hence, in these areas the rate of formation of new secondary osteons is increased (Currey 2002).
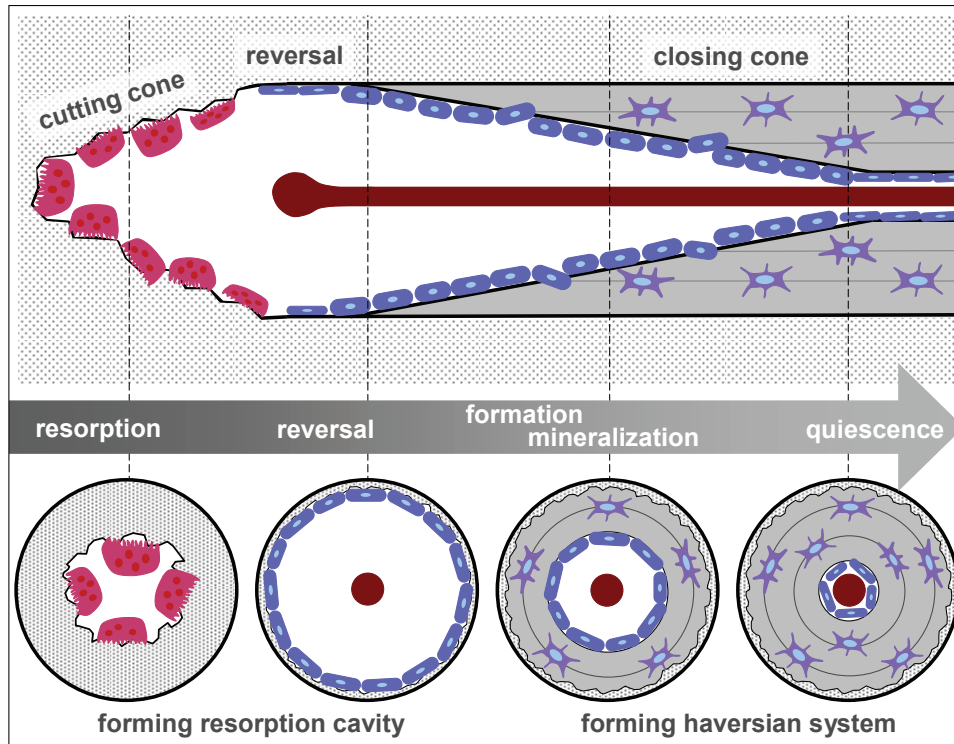
Figure 2: Scheme of the formation of a secondary osteon in cortical bone. During resorption phase, osteoclasts in the cutting cone build a tunnel, which is followed by the reversal phase at which osteoblasts align at the surface of the resorbed cavity to subsequently deposit new lamellar bone material. After closure of the cone, remaining osteoblasts at the surface go to quiescence. Adapted from (Stroncek and Reichert 2008)

During the deposition of new bone, some osteoblasts get buried within the bone matrix and differentiate to osteocytes (Franz-Odendaal, Hall et al. 2006; Nicolella, Moravits et al. 2006). Osteocytes reside inside their cell lacuna within the bulk of the bone material and are interconnected mutually as well as with the bone cells acting at the bone surface (Aarden, Burger et al. 1994; Marotti 2000; Palumbo, Ferretti et al. 2004; Bonewald and Johnson 2008). In recent reviews osteocytes are often called to be 'multifunctional', 'smart' or even 'amazing' cells (Bonewald 2007; Bonewald 2011). Source of this nomenclature is the still remaining lack of knowledge of the particular role of this cell-type during bone homeostasis. Osteocytes are known to orchestrate bone remodeling in response to mechanical and microenvironmental changes as they have the capability to sense strain rates in their surrounding bone matrix (Klein-Nulend, Vanderplas et al. 1995; Burger and Klein-Nulend 1999; Bonewald and Johnson 2008). This

mechanosensation either occurs over direct straining of the cell (Nicolella, Moravits et al. 2006), or via the detection of flow of interstitial fluid as a result of mechanical loading (Weinbaum, Cowin et al. 1994; Zeng, Cowin et al. 1994; Owan, Burr et al. 1997).

Moreover, osteocytes have long been suspected to play a direct role in bone mineral homeostasis. The surface of the osteocyte network is estimated to be 100 fold greater than that of trabecular bone and even 400 fold greater than all the surfaces of the haversian systems in compact bone – thus surfaces typically available to osteoclasts and osteoblasts (Qing and Bonewald 2009; Teti and Zallone 2009). This leads to the conclusion that osteocytes, facing this enormous surface could potentially contribute to bone mineral homeostasis as they have some ability to deposit and resorb mineral in their vicinity (Baud 1962; Belanger 1969; Baylink, Wergedal et al. 1971; Parfitt 2003; Teti and Zallone 2009). Receptors for calcium regulating hormones (Boivin, Mesguich et al. 1987; Vanderplas and Nijweide 1988) as well as ion channels for the control of calcium and phosphate levels (Ravesloot, Vanhouten et al. 1990; Ravesloot, Vanhouten et al. 1991; Teti and Zallone 2009; Bonewald 2011) could be found in osteocytes. Furthermore the existence of molecules regulating mineralization such as Dmp1 (Toyosawa, Shintani et al. 2001) and sclerostin (van Bezooijen, Roelen et al. 2004; Gardner, van Bezooijen et al. 2005; Poole, van Bezooijen et al. 2005) were detected, implying that osteocytes are not only capable of controlling ionic concentrations in their vicinity but also directly influence mineralization of the bone material they are facing (Baylink, Wergedal et al. 1971; Lane, Yao et al. 2006). This further implies that mineral and the matrix in the neighborhood of osteocytes and their cell processes must be more dynamic and thus may have a different structure compared to bone further away in the depth of the tissue (Belanger 1969). In this sense it was proposed that a thin layer of amorphous or highly crystalline mineral is present at the surface of each osteocyte lacuna, which acts as a small mineral reservoir, being formed – and as needed – resorbed by the osteocyte (Bonucci 1990; Bonucci 2009). However, to reveal these modest morphological and ultrastructural changes of the bone material residing in the vicinity of osteocytes, a combination of sophisticated experimental techniques are needed which are capable of mapping bone material properties as a function of the distance to these cells.

3   Theoretical Background of Physical Methods Used

In this PhD-thesis, experimental techniques were applied to study osteocyte net-work morphologies and correlate these with bone ultrastructure at the micron- and the submicron scale. For this purpose confocal laser scanning microscopy – to measure osteocyte network organization – scanning electron microscopy – to further qualitatively measure bone mineralization – and small angle x-ray scatter-ing – to determine submicron mineral characteristics – were used. In this chapter, the theoretical background of these physical methods is briefly introduced. Fur-ther information on the mutual accommodation of these complementary methods can be found in the following chapter 4 – *Materials and Methods* and 5 – *Devel-opment of Experimental Procedures*.

3.1   Confocal Laser Scanning Microscopy

In conventional light microscopy, image quality strongly depends on the thick-ness of the illuminated sample, as light coming from scattering objects above and below the focal plane reduces image contrast. Confocal microscopy is designed to remove obscuring out-of-focus light which further leads to an increase of lat-eral resolution (Price and Jerome 2011). In the confocal microscope light is fo-cused to a defined point within the specimen. Light emerging from this defined point is further collected and focused by the objective lens to a spot at the image plane. Light arising from out-of-focus areas within the sample is focused differ-ently from the objective lens. This stray light is rejected by a small pinhole aper-ture which only allows light coming from the focal point to further pass towards the detector (Minsky 1988). A single point alone does not provide much informa-tion of the specimen. Thus, image information within the focal plane is collected sequentially by scanning the spot across. Confocal laser scanning microscopes (CLSM) utilize lasers as the luminous source. Here exhibition can be performed in transmission as well as in reflection mode in which fluorescent samples can be observed. Fluorescence imaging in reflection mode has the big advantage to pro-vide a high contrast signal to maximally exploit the ability to remove out-of-focus light from the image (Price and Jerome 2011). For this purpose the excita-tion light which only gets reflected at the specimen and emission light arising

from the fluorescent characteristics of the sample is separated by appropriate filters only allowing certain defined wavelengths to pass.
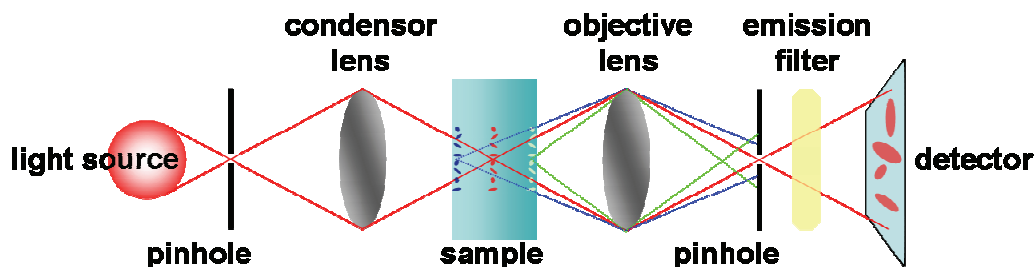
Figure 3: Principle design of a confocal microscope. Light from the photon source is focused at the first entrance pinhole, collected by the condenser lens and focused to the sample. Light emerging from this focal plane is further collected by the objective lens and focused at a second exit pinhole. Entrance, focal sample plane and exit pinhole are in conjugate focus (red lines). Light further reaches an emission filter only allowing a certain range of wavelengths to pass to the detector. Light emerging from out-of-focus planes (blue and green lines) is not transmitted to the detector as it reaches the exit pinhole out of focus. Adapted from (Price and Jerome 2011).

In confocal laser scanning microscopy, either auto fluorescent materials or non-fluorescent materials which get specifically stained with fluorescent molecules (fluorochromes) can be measured in reflection mode. Here the fluorochromes absorb photons with a specific energy respectively wavelength (fluorochrome excitation). During this excitation the fluorochrome molecules undergo an electronic transition to a higher electronic state for which a certain amount of energy is required. In this regard only energies close to the excitation energy are absorbed by the fluorochromes thus offering specificity to the process of fluorescence. This specificity of certain staining media can be used due to utilization of different exciting lasers during the fluorescence measurement. After excitation, the molecule relaxes to lower vibration states within the electronic state before it eventually goes back to the ground state by generation of a photon. During the internal conversion of vibration relaxation, the energy is transferred in non-photon-generating reactions, mainly in the form of heat. This loss of energy leads to the generation of lower energy photons, respectively an increase in wavelength of the emissive light, which is called Stokes shift. Confocal microscopy benefits from this shift to longer wavelengths as it allows filtering the excitation from the

emissive light. Hence, final images only contain fluorescence information providing high contrasts.
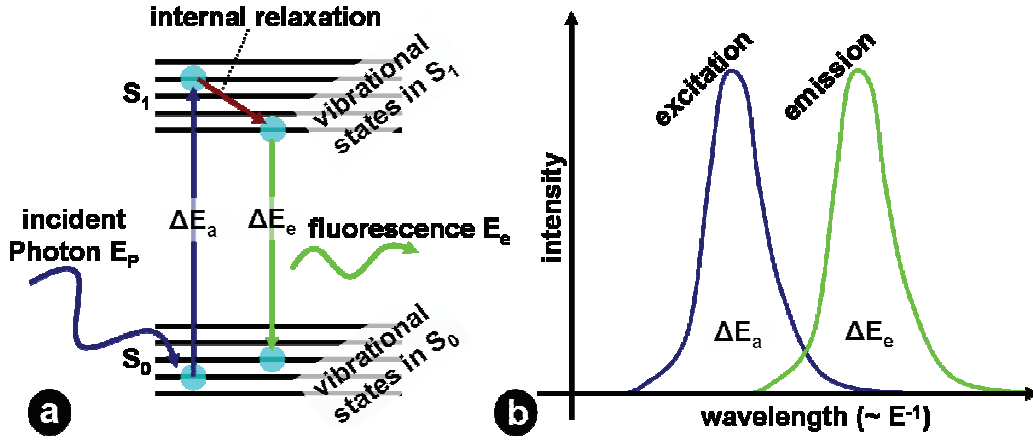
Figure 4: (a) Jablonski diagram showing the excitation of a molecule due to absorption of an incident photon with the energy E_P from the S_0 to the S_1 state with $\Delta E_a = E_P$. Subsequent relaxation from S_1 to S_0 with emission of a photon with the energy E_e predominantly occurs after nonradiative processes of internal relaxation which leads to a loss of energy ($\Delta E_a = \Delta E_e$). (b) Schematic plot showing the excitation and emission spectra. These are not discrete since excitation and emission can occurs from and to different vibration states within distinct electronic states. Due to separation of individual excitation and emission spectra, emitted light can be easily distinguished from incident light.

Excited molecules not only loose energy by emitting light. There are also other competing processes leading to relaxation to the ground state such as heat generation and energy transfer to neighboring molecules. These alternative nonradiative processes can decrease the amount of fluorescence and lead to worse imaging quality. The attribute of each fluorochrome to convert absorbed photons in fluorescence emission is specified by the quantum yield.

$$QY = \frac{\# \, photons, emitted}{\# \, photons, absorbed} = \frac{k_f}{k_f + k_{nr}}$$

(Price and Jerome 2011) with *QY* as the quantum yield, k_f as the rate of fluorescence and k_{nr} as the rate of all other nonradiative processes. A perfect emitter would feature *QY = 1*, emitting one photon of lower energy for each photon absorbed and thus assure strong fluorescence signals even at focal planes deep

inside the specimen. In bone, specific staining of bone cells or cavities within the bone material can be used to visualize long range organization of the material. Due to the requirement of low transparency of the material and high penetration depths of the measurement (Schneider, Meier et al. 2010), staining with fluoro-chromes having a high quantum yield is necessary.

3.2 Back-scattered Electron Imaging

In opposition to conventional light microscopy techniques, scanning electron microscopy allows to examine samples in scanning mode by utilizing a focused electron beam. During measurement, interactions of the electrons with the specimen lead to processes of elastic and inelastic scattering accounting for back-scattered- as well as the generation of secondary electrons, respectively (Boyde and Jones 1996). During elastic scattering the energy of the electrons remain un-changed, only the trajectories of flight are affected. As a consequence a portion of the incoming electrons is scattered backwards. The amount of back-scattered electrons (BE) carries information on the atomic composition of the target area (Roschger, Plenk et al. 1995). During processes of inelastic scattering the energy of the electrons is altered due to several interactions with the sample leading – amongst other processes – to the generation of secondary electrons (SE). Secon-dary electrons show lower energies as compared to the primary beam energy. Due to high attenuation of low energy electrons in matter, SEs reaching the de-tector originate only from a thin layer at the surface of the sample. As a conse-quence, detection of secondary electrons provides topographical information of the target area, as surfaces have strong impact on the SE-signal (Koshikaw.T and Shimizu 1974).
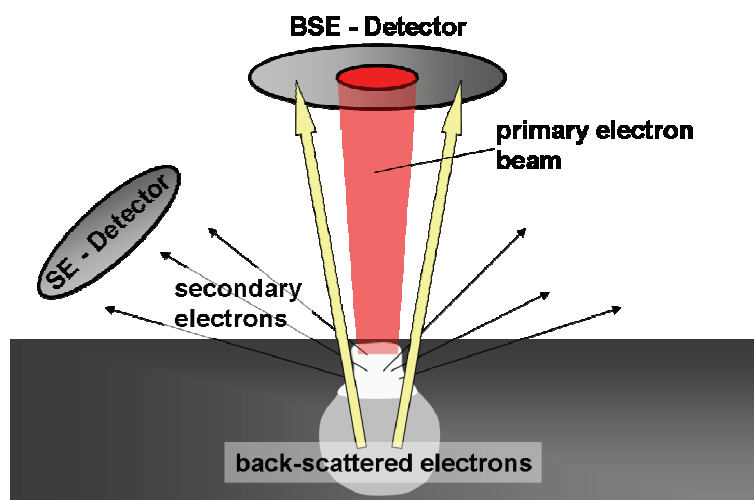
Figure 5: Scheme depicting the origin of the two different signals measured with scanning electron microscopy. Secondary electrons (SE) are generated due to inelastic scattering events between the primary electron beam and the material. Due to strong reabsorption of SE, only those generated within a thin layer at the surface can escape the material. Back-scattered electrons (BSE) are a result of elastic scattering events. The amount of back-scattered electrons carries information on the atomic composition of the material. Adapted from (Johnson 1990).

In bone tissue calcium atoms have the highest atomic number ($Z = 20$) and consequently dominate the BE-signal. Thus back-scattered electrons can be used to measure the local calcium concentration, respectively the degree of mineralization – also an indication for bone age (see chapter 2.2) – which can additionally give useful implications on bone growth and remodeling dynamics (Roschger, Paschalis et al. 2008).

3.3   Small Angle X-ray Scattering

X-rays as electromagnetic waves interact with matter by means of absorption as well as elastic and inelastic scattering. Processes of absorption, involving subsequent processes of fluorescence, can be used for elemental analysis as well as for the structural studies such as radiography. Processes of elastic scattering provide information on the submicron structure of the examined material. Commonly it is distinguished between x-ray scattering which is a result of elastic interactions between waves (or photons) and a material without long range order (no regular arrangement of atoms) and x-ray diffraction as a result of elastic interaction with

materials featuring long range order (regular arrangement of atoms) and thus leading to characteristic patterns of interference behind the illuminated object.

In this thesis, small angle x-ray scattering (SAXS) was one of the main experimental techniques. SAXS is a diffuse elastic scattering up to angles of 5° describing randomly oriented systems containing two phases with different electron densities with sharp interfaces (Kratky, Porod et al. 1951; Porod 1951; Porod 1952) in the range from 1nm up to 1 μm. In bone, two phases are represented by the collagen phase with low electron density and the mineral phase with high electron density. Information on the size, orientation and shape of submicron mineral particles can be derived from the scattering intensity distribution $I(\vec{q})$

$$I(\vec{q}) = \frac{K}{V} \left| \int_V \rho(\vec{r}) \cdot \exp(i\vec{q}\vec{r}) d^3 r \right|^2$$

with $\vec{q}$ as the scattering vector (Figure 6), V as the sample volume and K as an instrumental constant. The scattering vector $\vec{q}$ is defined to be the difference of the wave vector of the scattered beam $\vec{k}'$ and the wave vector of the incident beam $\vec{k}$ with $\left|\vec{k}\right| = \left|\vec{k}'\right| = 2\pi/\lambda$ for elastic scattering. Accordingly, the modulus of $\vec{q}$ can be derived from

$$\left|\vec{q}\right| = 2k \cdot \sin\theta = \frac{4\pi}{\lambda}\sin\theta$$

Furthermore, Porod's law states that in systems containing two phases of different mean electron densities, separated with sharp interfaces, the following equation is valid for large q values:

$$I(q) \xrightarrow{q \to \infty} \frac{P}{q^4}$$

with *P* as the Porod constant calculated from the Porod-plot (see chapter 4.3.2) and *B* as the background. This equation points out that in all biphasic systems with distinct interfaces the scattering intensity decreases with q^{-4}.
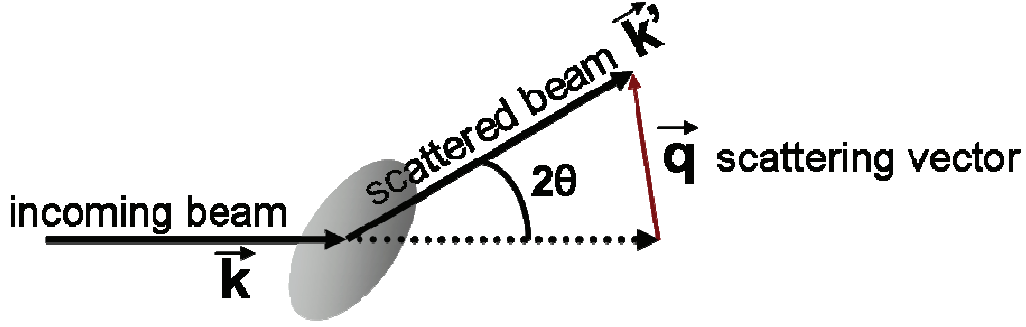
Figure 6: Scheme of SAXS scattering: the scattering vector q is calculated from the incoming wave vector k and the scattered wave vector k'. 2θ is the scattering angle between k and k'.

Whereas the degree of mineral particle orientation is obtained from the two-dimensional shape of the SAXS-scattering signal (see chapter 4.3.2 for azimuthal integration), information on the mean mineral particle thickness (T-parameter) can be derived from the decay of the scattering signal with larger scattering vectors $\vec{q}$ which is described in detail elsewhere (Fratzl, Fratzl-Zelman et al. 1991; Fratzl, Groschner et al. 1992; Rinnerthaler, Roschger et al. 1999). Accordingly the T-parameter reflecting the mean mineral particle thickness is calculated as

$$T = \frac{4}{\pi P}\int_0^\infty q^2 I(\vec{q})dq = \frac{4\phi(1-\phi)}{\sigma}$$

with P as the Porod constant, ϕ as the volume fraction of the mineral phase and σ as the surface area of mineral particles per unit volume. Furthermore, supposing that *N* mineral particles reside in a volume V_0 and each mineral particle is a uniform parallelepiped with the edge lengths *a, b, and c*, the T-parameter can be rewritten as

$$T = 2(1-\phi)\frac{abc}{ab+bc+ac}$$

with $\phi = N \cdot abc/V_0$ and $\sigma = 2N(ab+bc+ac)/V_0$. Moreover, the assumption that the mineral particles are platelets with a as the mineral platelet thickness being the shortest dimension and thus $a << b,c$ simplifies the equation to

$$T \approx 2(1-\phi)a$$

showing the connection between the T-parameter, the mineral particle thickness a and the degree of mineralization ϕ (Zizak, Roschger et al. 2003). Consequently, the T-parameter is only a direct measure of the mineral particle thickness if volume fractions of the mineral phase equals $\phi = 0.5$.

4 Materials and Methods

The characterization of bone material in correlation with the organization of the osteocyte network involves a combination of various experimental techniques. These techniques to some extend require different sample preparations which have to be mutually accommodated. This chapter states the different types of bones which have been used for experiments. Furthermore different experimental methods in combination with its required sample preparation techniques are described and explained.

4.1 Types of Bone Samples

4.1.1 Murine Bone

Murine femurs used in a different study as reference samples, were obtained from the University of Potsdam. Sections were collected from the midshaft region of the femur of mature, 12 month old mice.

4.1.2 Ovine and Bovine Bone

Native ovine bone samples obtained in a different study from the Julius Wolff Institute, Charite Berlin were collected from the midshaft region of the femur of a mature 5 year old sheep. To exhibit patterns of bone formation, structurally comparable samples from the midshaft region of the femur of a growing 2-3 year old cow were used. For fracture healing samples, sections of the callus had been collected in a previous study of an osteotomy model of a 2.5 year old sheep. A monolateral external fixator (6 Schanz screws and 2 steel tubes) was attached to the medial aspect of the tibia after the surgery. Intraoperatively, the osteotomy of the tibial diaphysis was performed and distracted to 3 mm (Schell, Epari et al. 2005). The examined bone samples (cortex and callus) were harvested 2 and 9 weeks after osteotomy.

4.1.3 Equine bone

Osteonal equine bone sections obtained from the Hebrew University of Jerusalem, Israel from the 3rd metacarpal bone (wrist bone) from a 7 year old horse was

harvested. The 3rd metacarpus is structurally comparable to the midshaft region of the equine femur. Advantages of the smaller sizes of metacarpal bone make it more feasible for specimen collection.

4.1.4 Medullary Bone from Egg Laying Hens

Egg laying hens were sacrificed at the Hebrew University of Jerusalem, Israel. The ethics permit was issued by the appropriate committee of ethics in animal experiments at the University. Samples were collected after intravenous anesthetization according to their egg laying cycle at 13 different time points, starting from t_0: directly after laying the egg, every 2 hours up to t_{12}: 24 hours after lay (n=2 per time point). Both femora were harvested. Additionally blood samples were taken to determine calcium and phosphate ion concentration during the egg laying cycle.

4.2 Initial Sample Preparation

After harvesting, bone samples were stored without any further treatment (dry) in the freezer at -20°C. For initial preparation samples were cut with a low speed diamond saw (IsoMet, Buehler GmbH, Düsseldorf, Germany) to an initial thickness of 200 microns and subsequently polished in an automatic polisher (Logitech PM5, Logitech Ltd., Glasglow, UK). Due to the diversity of experimental techniques and its required sample dimension, further steps of sample preparations are explained and discussed in a greater detail in context with each experimental method in chapter 4.3. All experimental procedures which had been separately developed to address the characterization of certain sample features are discussed in chapter 5.

Ovine bone samples undergoing chemical treatment were initially infiltrated with non-ionic detergent (Nonidet P-40) to dissolve diffusion barriers and enhance ion exchange. Subsequently the samples were treated with 10 ml of sodium chloride solution at neutral pH and put to the shaker for 72 hours. Reference samples were treated in phosphate buffered saline (PBS) at neutral pH.

4.3   Specimen Characterization

4.3.1   Microscopy

For microscopical analysis samples were polished to a final thickness of around 80 microns. Samples were kept wet throughout the whole preparation process. Until further usage, samples were wrapped in cotton gauze soaked in phosphate buffered saline (PBS) solution (Sigma Aldrich GmbH, Germany) and stored at 4 °C.

4.3.1.1   Light– and Polarized Light Microscopy

Hydrated samples were examined by transmission light microscopy using a Leica (DM RXA2) microscope, equipped with a DFC 480 camera. The associated linear polarizer was used for polarized microscopy. Polarizer and analyzer were set into a cross-polarization position 90 degrees to each other. Due to the birefringence of collagen, highly arranged bone matrix lights up if it is not parallel arranged to both the polarized and analyzer.

4.3.1.2   Confocal Laser Scanning Microscopy (CLSM)

Fresh samples were stained for 3 days with rhodamine-6G (Sigma Aldrich GmbH, Germany) which was dissolved (0.02 % wt) in phosphate buffered saline (PBS) solution. After washing with PBS at neutral pH for three times, CLSM micrographs of hydrated samples were taken with a Leica DM IRBE (Leica Mikroskopie und Systeme GmbH, 35530 Wetzlar) equipped with a 100x oil immersion microscope objective with a numerical aperture of 1.4. The excitation wavelength was set to 514 nm, while the emission was measured at a range from 550 up to 650 nm. Image stacks were measured until a penetration depth of 10 μm with a spatial z-resolution of 0.2 μm. The spatial pixel resolution of each image in the stack was 0.2 x 0.2 μm. For additional measurement of fluorochrome labels the excitation wavelength was set to 488 nm. Emission of calcein labeling was measured from 505 up to 530 nm, emission of alizarin complexon from 660 up to 760 nm. Individual filters to measure emissive radiation were set in a way to prevent an overlap of the intensities of rhodamine, calcein and alizarin complexon.

For rhodamine staining in combination with PMMA embedding, 0.002 % wt of rhodamine was dissolved in methyl metacrylate (MMA) and used as staining solution (3 times 1 day) during the dehydration series of the bone samples. Subsequently bone samples were embedded in covered plastic containers with PMMA solution containing 400 ml MMA, 100 ml nonylphenyl- polyethylene-glycol acetate (NPA) and 10 g dibenzoyl peroxide (BPO). During embedding samples were put to an oven at 42 °C for 12 hours, 48 °C for another 12 hours and for final hardening to 58 °C for 24 hours.

4.3.1.3 Scanning Electron Microscopy and Back-scattered Electron Microscopy

Dry bone samples were glued on an object holder with double sided tape and mounted on an aluminum stub. For examination a FEI-Quanta 600FEG electron microscope (FEICompany, Oregon, USA) was used in low vacuum mode (0.75 Torr) at a working distance of 10 mm. Images were taken with a solid state detector (SSD) at 15kV measuring the back-scattered-electron signal from the surface of the sample.

4.3.1.4 Cryo Scanning Electron Microscopy

Cryo SEM was performed in cooperation with Julia Mahamid at the Weizmann Institute of Science (WIS), Rehovot, Israel. To maintain transient mineral phases, samples had to be examined under the electron microscope using cryo conditions. This preparation protocol for bone samples is described elsewhere (Mahamid, Sharir et al. 2008). Fresh medullary bone pieces of approximately 500 x 500 x 200 microns were taken from the medullary cavity of the femur of a chicken directly after harvesting the bones. The samples were immediately immersed in 10% Dextran (Fluka – Sigma Aldrich GmbH, Germany), mounted between two metal discs (3 mm diameter, with 0.1 or 0.2 mm cavities) and cryo-immobilized in a high pressure freezing device HPM10 (Bal-Tec, Germany). Subsequently samples were transferred to a Freeze Fracture device BAF 60 (Bal-Tec, Germany) and fractured at -140 °C, etched for 20 min and coated. Samples were observed in an Ultra 55 SEM (Zeiss, Germany) using a secondary electron in-lens detector and a backscattered electron in-lens detector (operating at 5 kV) in the frozen-hydrated state by use of a cryo-stage at a temperature of -120 °C.

4.3.1.5 Quantitative Back-scattered Electron Imaging

These measurements were performed in cooperation with Paul Roschger from the Ludwig Boltzmann Institute of Osteology in Vienna. More information about the experimental setup and calibration can be found elsewhere (Roschger, Fratzl et al. 1998). Bone samples containing a transversal fibrolamellar bone structure from the periosteal region down to the endosteal region were embedded in blocks of polymethylmethacrylate, polished and carbon coated by vacuum evaporation (SCD 004 Balzers, Liechtenstein). Examination was performed with a digital scanning electron microscope (DSM 962, Zeiss, Oberkochen, Germany) equipped with a four quadrant semiconductor back-scattered electron detector. The microscope was set to an accelerating voltage of 20 kV and a working distance of 15 mm.

4.3.2 Small Angle X-ray Scattering Measurements

Small angle x-ray scattering is used to measure inhomogeneities of the nanostructure of a sample by elastic scattering of the x-ray beam. The signal contains amongst others information about the size and shape of macromolecules or pores. In bone SAXS is used to study the dimension and the alignment of mineral particles which allows a better understanding of bone formation and remodeling. Within this project bone samples were studied at two different synchrotron beamlines – the µSpot at BESSY II (Helmholtz-Zentrum Berlin für Materialien und Energie GmbH, Berlin, Germany) as well as the Nanofocus beamline ID13 at the European Synchrotron Radiation Facility (ESRF), Grenoble, France. The most relevant difference between these beamlines was the size of the x-ray beam and thus the maximum scanning resolution accessible. At BESSY a nominal beam size of ~ 15 µm could be obtained whereas at ID13 a beam size of ~ 500 nm could be used for scans. Here the experimental setup and measurement parameters at both beamlines are briefly described. Data correction and analysis of experiments with FIT2D and Autofit is similar and described subsequently.

4.3.2.1 Experimental Setup at BESSY

Ovine and murine bone samples with a thickness of approximately 30 µm were measured at the µSpot beamline with multi layer setup and a monochromatic x-

ray beam of 15keV. Sample to detector distance was set to ~ 300 mm for measurement with a 2D position-sensitive CCD-detector (MarMosaic 225, Mar USA Evanston, USA) with 3072 x 3072 pixels and a corresponding pixel size of 73.242 x 73.242 μm^2. To improve measurement time the detector binning was set to 2 x 2 (1536 x 1536 pixels, corresponding pixel size of 146.484 x 146.484 μm^2) and the sample detector distance increased to ~ 400 mm to assure sufficient q-resolution. Bone samples were fixed with a lead tape and mounted on a sample holder screwed on an xyz translation stage which could be moved perpendicularly to the beam, allowing to measure the sample in scanning mode with a step size of 10 μm. Additionally an x-ray fluorescence (XRF) detector (ASAS-SDD, KETEK Germany) was used to measure calcium fluorescence signal simultaneously. For data correction, transmission intensity of each scanning point was measured with a diode before each area scan. The exposure time for the transmission measurements was set to 0.3 seconds. For measurement of the scattering pattern, exposure times were set accordingly to the binning factor, sample properties and the x-ray beam intensity between 4 and 30 seconds. A detailed description of the beamline can be found elsewhere (Paris, Li et al. 2007).

4.3.2.2   Experimental Setup at ESRF

At the Nanofocus beamline at ESRF ovine bone samples with a thickness of approximately 30μm were measured. A monochromatic x-ray beam with an energy of 14 keV was used. Scattering patterns were measured with an ESRF FReLoN detector with 2048 x 2048 pixels and a corresponding pixel size of 51.5 x 50.7 μm^2 (after flat field correction). To reduce measurement time detector binning was set to 4x4 (512 x 512 pixels, corresponding resolution of 205.9 x 202.8 μm^2). The sample to detector distance was set to approximately 720 mm. Ovine bone samples were framed with a lead tape and screwed on a sample holder which was magnetically mounted to the sample stage. During the scan the stage was translated in yz direction, perpendicularly to the beam, with a step size of 1 μm. Simultaneously to the measurements of the scattering patterns, the calcium fluorescence signal was obtained with an XRF detector which was moved approximately 20 mm apart from the sample. Before each scan, transmission intensity of each scanning point was measured with a diode for later data correction. The exposure time for the transmission measurements was set to 0.1 seconds. For

measurement of the scattering patterns, exposure times were set between 0.1 and 1 second.

4.3.2.3 Data Correction

Using Fit2d (Hammersley, Svensson et al. 1996) the sample to detector distance and the exact beam center position was determined from the diffraction patterns of hydroxyapatite (HAP) standard powder measured before and after each scan. In order to correctly correlate background measurements with the measured scattering patterns a correction factor was determined:

$$t = t_1 * t_2 = \left(\frac{I_{sample,diode}}{I_{EB,diode}} \right) \cdot \left(\frac{Monitor_{sample,mar}}{Monitor_{EB,mar}} \right)$$

with t_1 as the correction of the transmission intensity which is the ratio of the Intensity at the Sample (I_{sample}) and the empty beam intensity (I_{EB}); and t_2 as the correction of the decreasing beam intensity during scanning – measured with a beam monitor – due to the decrease of the ring current. For t_1 the decrease of the ring current during the transmission scan was neglected since transmission scans were very short. Additionally the calcium fluorescence signal was corrected with t_2 since a reduction in beam intensity leads to a lower fluorescence signal. The intensity correction of the scattering patterns was calculated by Autofit as followed:

$$I_{corrected} = \frac{I_{sample,mar}}{t} - I_{EB,mar}$$

4.3.2.4 Data Analysis

The data were analyzed using Autofit (custom made analysis software, C. Li, MPI of Colloids and Interfaces, Potsdam, Germany). For calculation of the T-parameter the following equations were used:

$$T = \frac{4}{\pi} \cdot \frac{\bar{I}}{P}$$

with $\bar{I}$ as the integration of the Kratky plot (Figure 7) and P the Porod constant as the intercept of the Porod fit with the ordinate (Figure 7). $\bar{I}$ was further calculated with

$$\bar{I} = \int_0^\infty q^2 I(\vec{q})dq = \int_0^{q,Kratky,\min} q^2 I(\vec{q})dq + \int_{q,Kratky.\min}^{q,Porod,\min} q^2 I(\vec{q})dq + \int_{q,Porod,\min}^\infty q^2 I(\vec{q})dq$$

which further simplifies to

$$\bar{I} = \frac{1}{2} I_{Kratky,\min} \cdot q_{Kratky.\min} + \int_{q,Kratky,\min}^{q,Porod,\min} q^2 I(\vec{q})dq + \frac{P}{q_{Porod,\min}}$$

as for biphasic systems the following equation is valid

$$I(q) \xrightarrow{q \to \infty} \frac{P}{q^4}$$

Fitting parameters for the Porod plot were set accordingly to different bone samples, since different bone types feature different mineral particle sizes. For ovine bone the Porod fit was set from Porod$_{min}$ = 1.5 to Porod$_{max}$ = 2.8 nm^{-1}. The Porod fit parameters for murine bone were set from 1.8 to 3.1 nm^{-1}. The fit parameter Kratky$_{min}$, from which the run of the Kratky plot is interpolated for small q-values (due to insufficient q-resolution), was set constantly to 0.3 nm^{-1}.

For the calculation of the Rho-parameter the scattering intensity integrated over q as a function of the azimuthal angle χ is analyzed. The distribution of the integrated intensity over χ shows two peaks (Figure 8) which are fitted with two Gaussian functions. The peak position of each Gaussian indicates the alignment of the mineral particles. To calculate the Rho-parameter, which describes the ratio of aligned particles to the total amount of particles in the illuminated area, the following equation is used:

$$Rho = \frac{Mineral_{aligned}}{Mineral_{aligned+unaligned}} = \frac{A_1 + A_2}{A_1 + A_2 + A_0}$$

with A_1 and A_2 as the area under both Gaussians respectively, interpreted as the amount of aligned particles and A_0 as the area under the baseline of both Gaussians which can be interpreted as the fraction of unaligned particles.
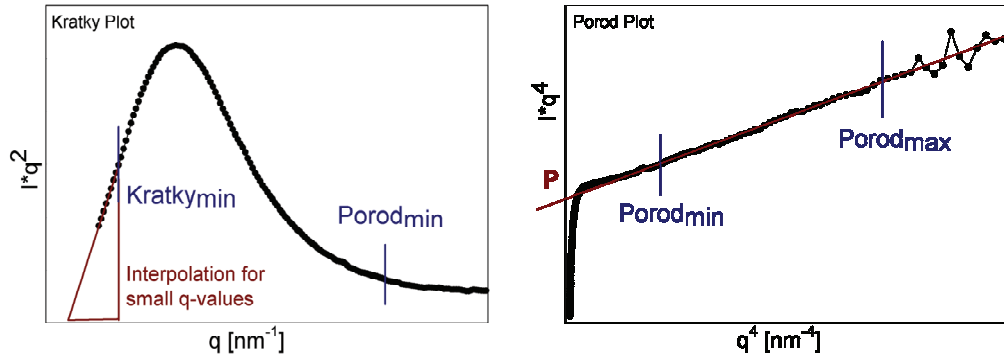

Figure 7: Kratky and Porod plot from radially integrated SAXS patterns. The T-parameter calculation needs the user input of following parameters: Kratky$_{min}$ Porod$_{min}$, Porod$_{max}$
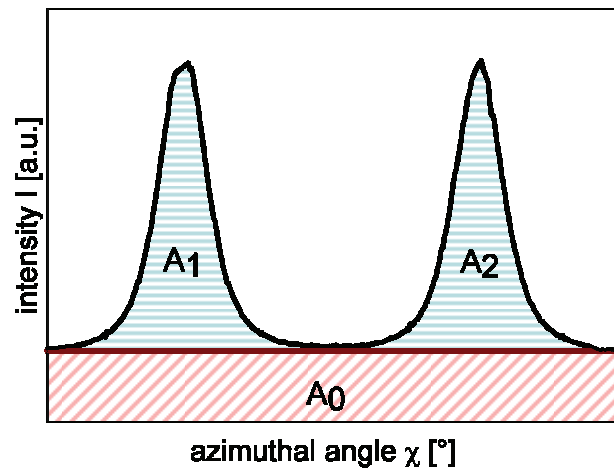

Figure 8: Azimuthal plot of the scattering intensity showing two peaks which are 180° separated. A_1+A_2 describes the fraction of aligned particles, A_0 the fraction of randomly aligned particles.

4.3.3   Quantitative Synchrotron Micro Computer Tomography

Medullary bone samples from chicken at 4 different time points (0, 6, 12, 18 hours after lay, 2 samples each) were examined using a 23 keV x-ray beam at the BAMline at BESSY II Helmholtz-Zentrum Berlin für Materialien und Energie GmbH, Berlin, Germany) to determine bone properties such as the degree of mineralization and trabecular architectures. For measurements, 1 cm long intact sections from the midshaft of the femur were embedded in blocks of poly-methylmethacrylate as fixation. Samples were prepared completed anhydrously (see chapter 5), stacked onto each other and mounted to a rotation stage. For quantitative measurement of the bone mineral density, the sample to detector distance was set to 15 mm to prevent the influence of straylight and the measurement of coherence effects. For phase enhanced imaging, which improves the visualization of macroscopic edges of the bone architecture, the sample to detector distance was set to 40 mm. For each scan a total number of 1200 projections was measured with different resolutions ranging from 0.876 up to 4.34 µm. A more detailed description of the beamline setup can be found elsewhere (Rack, Zabler et al. 2008). The projection images were normalized and reconstructed using PyHST (Mirone, Wilcke et al. 2009)

4.3.4   Ptychography at the Swiss Light Source (SLS)

The experiments were performed in cooperation with Martin Dierolf from the Technical University Munich at the cSAXS beamline at the Swiss Light Source (SLS) which is part of the Paul Scherrer Institute (PSI), Villigen, Switzerland. In this experiment ovine bone samples, which where chemically treated with Sodium chloride solution and subsequently cut to small 2 mm long beams with a cross section of approximately 50 x 50 microns were scanned. As a standard measurement single spheres of HA powder with a diameter of approximately 30 µm were scanned. The cSAXS beamline is optimized for coherent SAXS applications. A monochromatic x-ray beam with an energy of 6.2 keV, running through a small aperture, with a diameter of 2 to 3 µm was used. The detector (Pilatus 2M) was located at a distance of 7.19 m behind the sample in order to fulfill the required conditions for coherent diffractive imaging. The small beams of treated ovine bone were glued at the tip of a syringe and mounted close behind

the beam-defining pinhole to a three-axis piezo scanning stack located on top of an air bearing rotation stage. For each tomographic scan, 361 projections with a step size of 0.5° were taken. For each projection a ptychographic raster scan contains approximately 450 single scan points which overlap at adjacent positions. Due to the overlap an improved convergence behavior of the image reconstruction is obtained. With an exposure time of 0.1 seconds with an additional scanning overhead of another 0.1 seconds, scanning a field of view of approximately 65 x 20 μm^2 took about 12 hours. A more detailed description of ptychography measurements and data analysis as well as reconstructions can be found elsewhere (Dierolf, Menzel et al. 2010).

4.3.5 Infrared Spectroscopy

Infrared (IR) spectroscopy was performed together with Yotam Asscher from the Weizmann Institute of Science (WIS), Rehovot, Israel. More information on the influence of different sample preparation procedures can be found elsewhere (Asscher, Weiner et al. 2011). Freshly dissected pieces of medullary bone were washed with acetone to remove fatty tissue components. Samples were subsequently crushed in an agate mortar with sodium hypochlorite solution (6%) added for 5 minutes at room temperature. The suspension was then transferred into Eppendorf tubes and centrifuged at 14,000 rpm for 3 min in an Eppendorf 5417C micro centrifuge to remove the supernatant. The pellet was washed three times with double distilled water saturated with calcium and phosphate and twice with 100% ethanol. The pellet was resuspended in ethanol and sonicated (Ultrasonicprocessor W-380; Heat Systems Ultrasonics). This procedure is known to not alter transient mineral phases (Mahamid, Sharir et al. 2008). The freshly suspended medullary bone mineral particles were subsequently exposed to a heat lamp in order to remove the remaining ethanol. The residual bone mineral was lightly crushed in an agate mortar, mixed with potassium bromide (KBr) and a 7-mm pellet was prepared. The IR-spectra were measured with a Nicolet 380 FTIR spectrometer. The splitting factor of the phosphate υ_4 peak describing the crystallinity of the bone material was calculated following Weiner and Bar-Yosef (Weiner and Bar-Yosef 1990).

## 4.4 Data Treatment and Visualization

All images obtained from microscopy-techniques as well as reconstructions from micro CT were edited and processed in ImageJ (National Institutes of Health, USA). Three-dimensional volumes were visualized using Drishti – Volume Exploration and Visualization Tool (VizLab, The Australian National University). Plotting of Data was done in SigmaPlot (Systat Software, Inc., USA) and Origin (OriginLab Corporation, USA).

5 Development of Experimental Procedures

The position resolved correlation of bone material properties with the osteocyte network geometries requires a variety of complementary experimental methods which all have to be performed at the same sample area. Thus bone preparation- and experimental procedures become a crucial issue and all have to be mutually accommodated. This chapter describes experimental- and sample preparation procedures which were developed during this project. These procedures such as the three-dimensional visualization of osteocyte networks, anhydrous sample preparation to not alter mineral properties as well as special labeling of scanning areas for confocal microscopy and scanning SAXS are essential for addressing the question whether osteocytes can influence their surrounding bone material.

5.1 Visualization of Osteocyte Networks

Visualizing osteocyte networks in undecalcified bone tissue is yet a great challenge (Schneider, Meier et al. 2010) since resolving of canaliculi structures featuring diameters smaller then 100 nm involves scanning techniques with high spatial resolution. In principle two main approaches for visualization of the network structures are possible: Firstly micro- or even nano-computed tomography allows the assessment of volumes of various shapes (optimal signals with cylindrical shapes). These can be performed either at lab sources or at the synchrotron. The final resolution of the scan is hereby defined by the technical setup and – even more important – by the dimension of the exposed sample volume. This leads to the fact that an increase in scanning resolution involves more sophisticated sample preparation since scanned volumes need to be smaller. As an example, for μCT scans at the BAMline at BESSY with a resolution of 3.5 μm cylindrical objects of a maximal height of 14 mm and maximal diameter of 9.3 mm was measured. For a maximal resolution of 0.22 μm sample dimensions are already limited to a maximal height of 0.9 mm and a diameter of 0.6 mm. However, to visualize canaliculi connecting the cells, a final pixel resolution smaller then 100 nm is required (Figure 9).
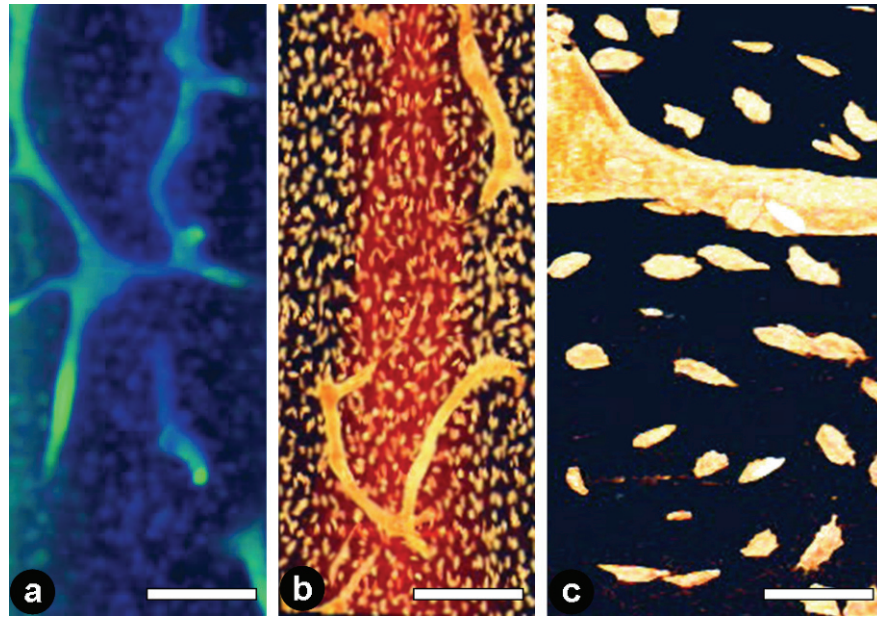
Figure 9: Visualization of osteocyte networks with different micro CT setups: (a) Skyscan 1072 with a pixel resolution of 10µm, (b) BAMline at BESSY II with a pixel resolution of 440 nm and (c) Skyscan NanoCT 2011 with a pixel resolution of 150 nm. Scale bars: (a), (b) 200µm, (c) 50 µm. None of these setups is capable of resolving canalicular structures in bone.

Secondly Confocal Laser Scanning Microscopy (CLSM) combined with fluorescent staining was applied on thin bone sections with a maximum thickness of 200 µm. The fluorescent dye gets excited by a laser with a suitable energy. The position of the emitted light was measured in a three-dimensional mode since the laser is accurately focused over the different z-levels of the sample (minimal step size of 0.2 µm) leading to a three-dimensional data output comparable to reconstructed data of a CT-scan. A substantial advantage of CLSM is the required sample dimension. These are fairly similar to those needed for different microscopical techniques as well as x-ray scattering measurements. Thus, a correlation of data from complementary experimental techniques from identical sample areas becomes feasible. Here rhodamine was used as staining solution diffusing through the blood vessels and osteocyte network binding to the cell membranes and mineral edges. Due to the high quantum efficiency of nearly one, high penetration depths of the measurement up to 50 µm are achievable (Figure 10). Even though a maximum pixel resolution of only approximately 0.2 µm is possible,

canalicular structures can be still resolved since staining leads to an amplification of these tiny sample features (smaller then a single pixel).
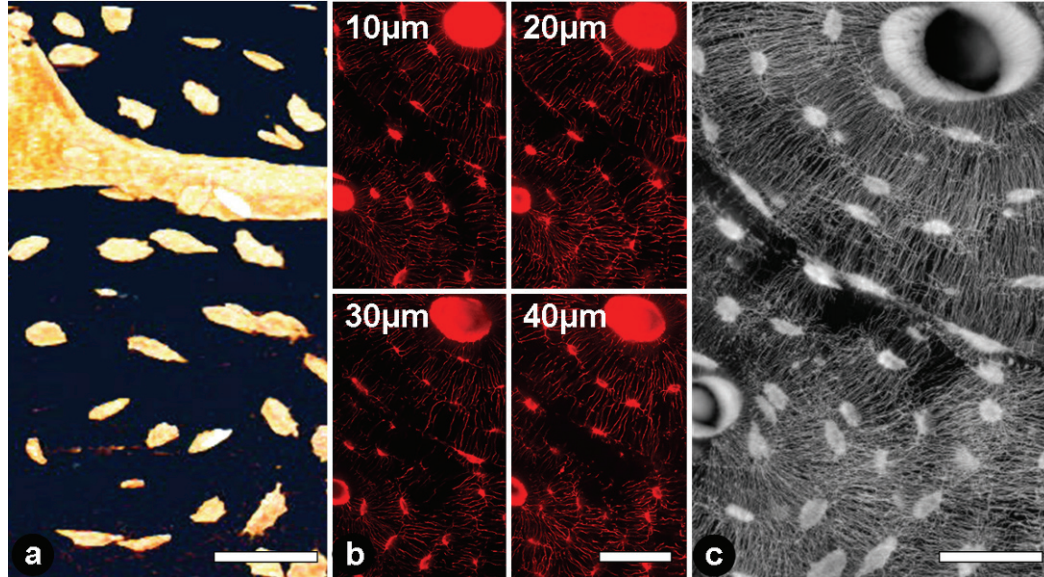

Figure 10: Comparison of a high resolution CT scan with CLSM: (a) 3d reconstruction of a Skyscan NanoCT 2011 scan with a pixel resolution of 150 nm, (b) CLSM scan of different z-levels (10, 20, 30, 40 μm from sample surface) from osteonal bone stained with rhodamine, (c) 2d projection of the CLSM scan of 50 μm scanning depth (251 images with a step size of 0.2 μm). CLSM combined with rhodamine allows visualization of the osteocyte lacunae as well as the canalicular network. Scale bars are 50 μm.

Due to the advantages in sample preparation and the possibility of correlation with different experimental techniques, CLSM is a perfect tool to visualize osteocyte networks in bone. Another considerable aspect is the accessibility of the instrument and time of such a measurement. High resolution CT-scans, depending on the setup, not even considering the time of data reconstruction, take many hours or even require beamtime applications at a synchrotron. However, the scan of a 100 x 100x 50 μm area with the confocal microscope takes less then 10 minutes. Thus the measurement of adjacent scan areas which can be stitched together is feasible and greatly helps greatly to understand the long range arrangement of the osteocyte network in conjunction with the alignment of macroscopic bone features such as blood vessels or even the macroscopic shape of the bone.

Recently two other methods visualizing osteocyte networks in bone were developed by different groups. Focused ion beam (FIB) combined with scanning electron microscopy (Schneider, Meier et al. 2011) allows quantitative three-dimensional measurement of osteocyte networks as well as the distribution of mineral by serial sectioning of the sample. Hereby the resolution is determined by the optics of the SEM device. Ptychographic x-ray computed tomography (Dierolf, Menzel et al. 2010) offers the same information with a maximum pixel resolution of 65 nm. However, both techniques are very time-intensive and involve highly sophisticated sample preparation and experimental techniques. Additionally, due to the high scanning resolution, measurements are restricted to tiny sample volumes of about 50 x 50 x 50 μm. In other words, this limits the exposed scanning area to a maximum of two osteocytes. Nevertheless, the complementary determination of the mineral content in correlation with the osteocyte network structures facilitates essential supplementary information on bone material properties as a function of the distance to the osteocytes. This information is not measureable with CLSM.

## 5.2   Rhodamine staining in bone sections with high porosity

Confocal laser scanning microscopy requires thin sample sections. Preparing such sections from compact bone specimens (porosity < 10 %) is a straight forward procedure just by polishing down the bone samples. In trabecular bone which features porosities larger then 80 %, polishing would lead to a disruption of the bone sample due to a decrease of connectivity of the individual bone segments (or trabeculae). To overcome this limitation an external fixation such as PMMA embedding to stabilize the individual bone segments is needed. However subsequent staining of embedded bones is not possible anymore since all cavities and voids from the blood vessels and the osteocyte network are blocked by the hardened PMMA. Thus, staining already during the procedure of embedding becomes possible. This can be done by dissolving rhodamine powder in methyl metacrylate (MMA) solution which is used during the embedding process for dehydration and as the basis of the PMMA embedding medium (more information on the embedding protocol in chapter 4.3.1.2).
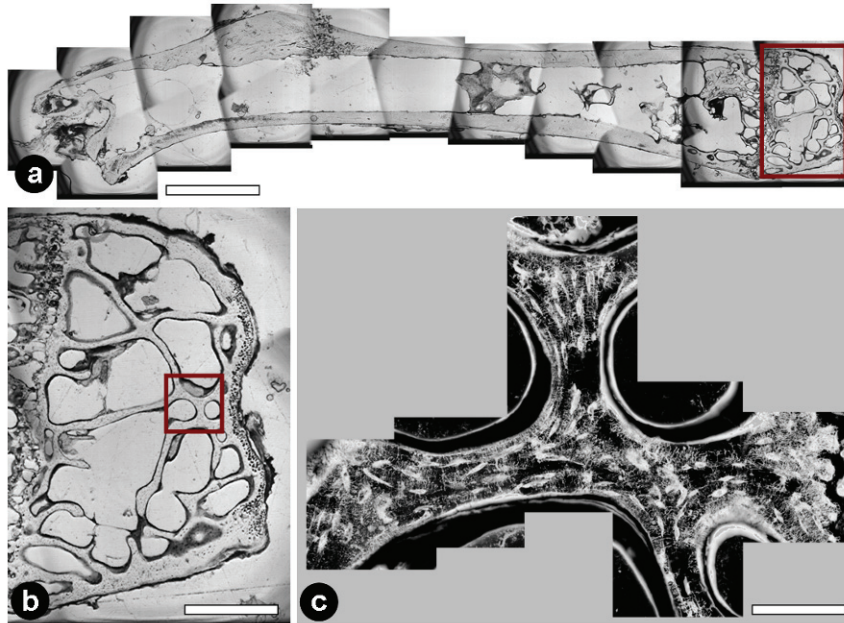
Figure 11: CLSM of a 50 µm thick PMMA embedded murine femur: (a) stitched brightfield scan as an overview of the whole bone, (b) magnification of the femoral epiphysis labeled in (a), (c) visualized osteocyte network in trabecular epiphyseal bone. PMMA embedding is a good mechanical stabilization for less connected noncompact bone after polishing. Scale bars: (a) 2 mm, (b) 600 µm and (c) 80 µm.

In order to stain bone samples during the process of PMMA embedding another issue needs to be taken into account to assure good staining quality. Hereby the limiting factor is the size of the embedded bone section since firstly, rhodamine is not penetrating deeply enough due to diffusion rate and secondly, membranes acting as diffusion barriers at macroscopic surfaces from intact bones may inhibit the penetration of external fluids to the bulk of the bone. Consequently, large samples show considerable less quality of staining in areas further away from the macroscopic bone surfaces. Thus, introducing artificial surfaces by e.g. longitudinal cutting of bone samples helps to enhance penetration depth of the staining medium. As an example, long bones can be cut longitudinally into half before staining and embedding in PMMA. For this purpose samples are mounted on a sample holder with dental glue which provides more stability during the cutting procedure. During PMMA embedding, rhodamine solution can more easily access the bulk of the bone sample since the artificially created surface is not covered with any diffusion-blocking membranes. After embedding, the plastic block

including the sample is polished from the outer sample surface towards the artificial cutting plane to its final thickness (Figure 12) since quality of staining is best close to the cut surface. As a result, pre-cut samples show more homogeneous staining compared to non-cut samples (Figure 13).
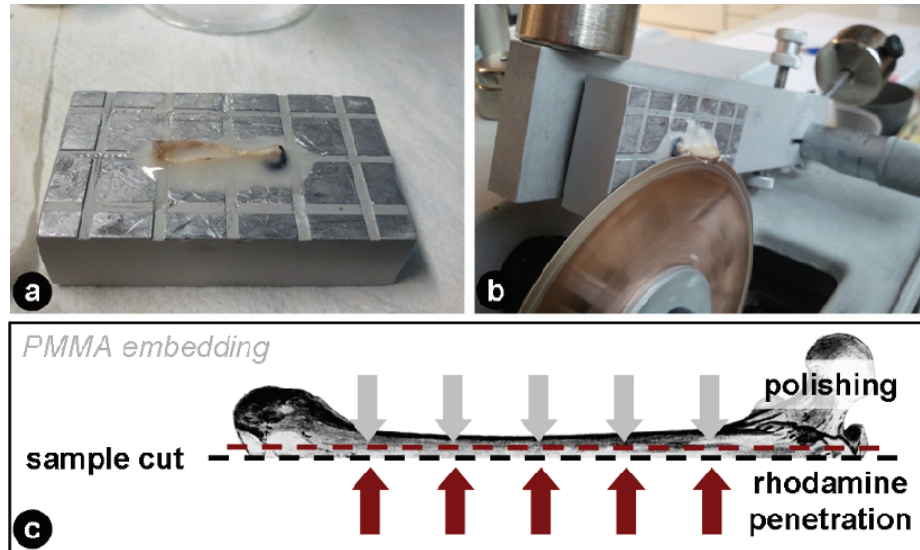
Figure 12: Pre-cutting of longitudinal bone samples: (a) murine tibia is aligned and fixed with dental glue on a sample holder and (b) longitudinally cut with a diamond saw into half. (c) During embedding in PMMA, rhodamine can penetrate from the cutting surface into the bone. After embedding, the thin sample section is prepared by polishing down the plastic block parallel to the artificial cut surface.
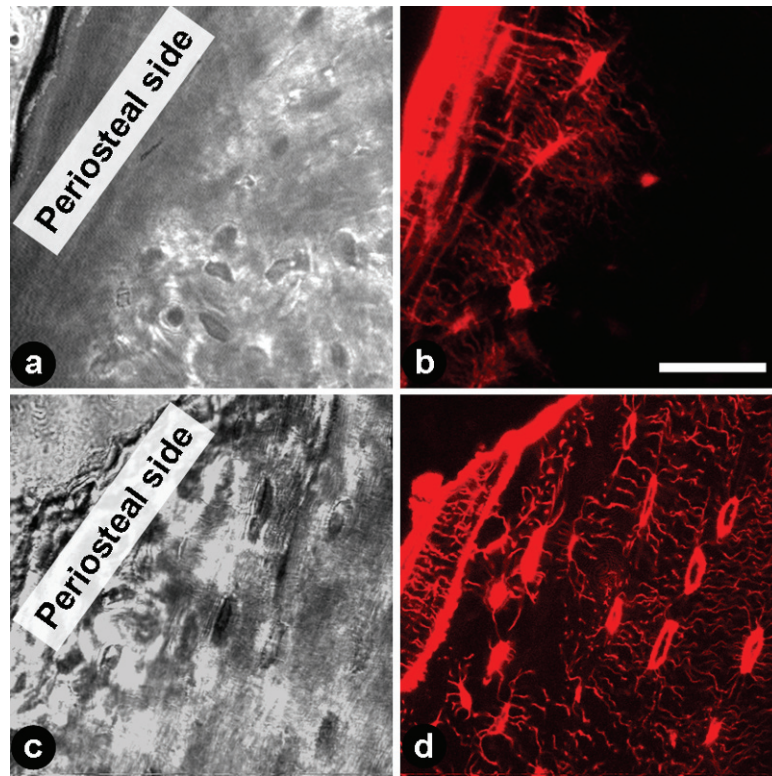
Figure 13: Comparison of staining between a non-cut bone sample ((a) brightfield image, (b) rhodamine staining) and a pre-cut sample ((c) brightfield, (d) rhodamine staining). Images show a considerably better penetration of staining medium. The periosteal (outer side) of the bone is indicated. In case of the non-cut sample, rhodamine can only penetrate from the periosteal side of the bone. In the opposite case of the precut sample, rhodamine penetrates from the artificially induced cut which is parallel to the visualized section. Scale bar: 25 µm.

5.3   Anhydrous Sample Preparation to Prevent Alteration of Mineral Properties

To test the hypothesis whether bone material properties in the vicinity of osteocytes differ from tissue further away from the cells, it has to be assured that sample preparation is not altering mineral properties and thus, introducing artifacts to the processed bone samples. Water is known to play a key role during the mineralization process of bone tissue (Fratzl, Fratzl-Zelman et al. 1993; Olszta, Cheng et al. 2007) and also controls the maintenance of transient, less stable mineral phases appearing for example in early stages of bone mineralization (Landis and Glimcher 1978; Landis, Paine et al. 1980; Mahamid, Sharir et al. 2008). More-

over, water can interact with the stable hydroxyapatite mineral phase leading to a dissolution of mineral ions and thus to a demineralization at mineral surfaces (Figure 14). Although interactions only alter tiny portions of mineral at exposed surfaces, the impact on the bulk of the material can be tremendous since the surface area of the osteocyte network and thus the amount of exposed mineral are vast. Therefore, establishing appropriate anhydrous sample preparation techniques which ensure that mineral in the vicinity of osteocyte lacunae and canaliculi is not dissolved or modified during preparation becomes a crucial issue.
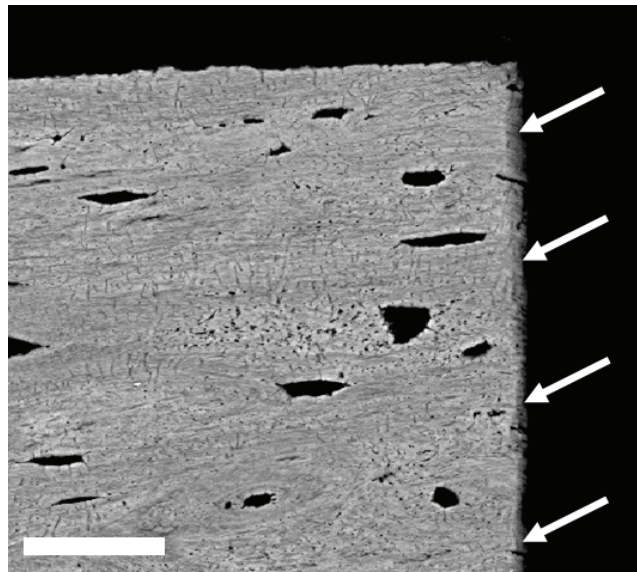
Figure 14: Back-scattered electron imaging of an ovine bone sample after 1 day exposure to water shows demineralization at the macroscopic bone edges. Dissolution of bone mineral at microscopic bone surfaces of osteocyte lacunae and canaliculi are not visible since alterations are very settle. Scale bar: 30 μm.

Water is a basic element during various steps of conservative sample preparation. It is used in dehydration series' before PMMA embedding of biological samples, as a polishing medium, during various microscopy techniques as an infiltration medium to keep samples in a liquid environment or during microtome cutting. Moreover, it is a basis of ionic solutions such as phosphate buffered saline (PBS) which are used as a storage medium for bone samples. In order to establish water free sample treatment, all these steps involving the contact of samples with water have to be reconsidered and modified: **(i)** Dehydration series' before PMMA embedding must start with pure alcohol since already few amounts of water mixed

with ethanol could interact with the bone mineral. **(ii)** For polishing and micro-scopical techniques water must be substituted with certain water-free polishing media such as ethylene glycol. **(iii)** Bone samples must be stored either in the freezer under dry conditions or within 100% ethanol. However, storage in pure ethanol leads to a dehydration of the whole bone tissue which results in shrink-age of the organic phase and higher fragility, thus, introducing cracks to the bone material. This in particular becomes apparent when cutting and polishing dehy-drated or PMMA embedded bone samples in cross section. Here individual bone lamellae connected via soft interfaces mainly run along the cross sectional plane. Due to the shrinkage of the individual lamellae, cracks can easily propagate along the soft interfaces leading to a macroscopic rupture of the bone section (Figure 15). Interestingly this is less pronounced when cutting bone in long sec-tion, which makes this cutting direction more feasible for dehydrated samples.

This consequently leads to some practical considerations regarding sample preparation based on the subsequently performed experiments. For x-ray diffrac-tion studies in which thin, anhydrously prepared samples are needed, bone tissue needs to be cut in longitudinal direction in order to prevent the formation of mac-roscopic cracks. For sole structural studies of the organization of the osteocyte network – for example at different anatomical positions – anhydrous sample preparation is not needed and thus preparing samples in cross sectional direction becomes more feasible. Furthermore, different structural features of the bone material become even more apparent when cutting along the cross sectional plane.

In some cases, due to practical reasons, water can not be substituted by another solution such as ethanol or ethylene glycol. For example, sophisticated tech-niques like microtome cutting need water to wet the blade and to straighten the thin sample sections after cutting. Here ethylene glycol, which is too viscous and thus leads to unsatisfactory cutting quality as well as pure ethanol which evapo-rates too fast, are inappropriate substitutes. For this purpose double distilled wa-ter can be saturated with calcium phosphate powder and subsequently filtered to assure the absence of calcium phosphate particles which were not dissolved (Mahamid, Sharir et al. 2008) Due to its saturation, this aqueous solution will not dissolve bone mineral from exposed surfaces.
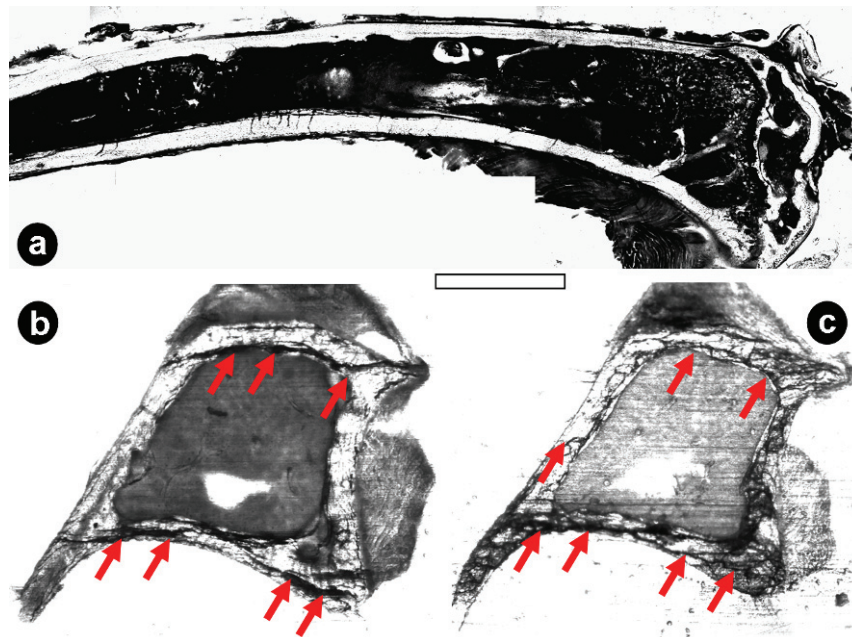
Figure 15: Different cutting directions of anhydrously prepared, 50 µm thick murine tibiae: (a) stitched brightfield image of a long section showing the tibial epi- and diaphysis, (b) and (c) stitched brightfield images of different cross sections. Red arrows indicate macroscopic cracks which run along the bone lamellae induced by anhydrous sample preparation. Interestingly, long sections do not show macroscopic cracking due to anhydrous sample preparation. Scale bar: (a) 2mm, (b) and (c) 1.5mm.

5.4 Passive Dissolution of Bone Mineral due to Chemical Treatment

The potential of water to interact with exposed mineral at the surfaces of the osteocyte lacunae and canaliculi implies the possibility of passive mineral dissolution and transportation through the osteocyte network. Furthermore it is conceivable that such passive processes of mineral extraction play an important role during calcium homeostasis in the body. To test this hypothesis bone samples were treated with physiological (pH neutral) sodium chloride (NaCl) solution that spontaneously dissolves mineral from the bone tissue. Physiological NaCl was used intentionally, since it is a main constituent of the body fluid und thus also surrounding and infiltrating the bone tissue. Initially, bone samples are pretreated with a non-ionic detergent which dissolves proteins from membranes covering blood vessels, osteocyte lacunae or canaliculi. Washing out these diffusion barriers leads to a strong enhancement of ion exchange between the subsequently used NaCl solution and the bone tissue. Preliminary mechanical experi-

ments show that this treatment even leads to measurable mechanical changes of the bone tissue (Kerschnitzki 2008).

5.5 Marking of Samples for SAXS scanning

An important issue during sample preparation is the labeling of regions of interest (ROIs) which are measured consecutively with the different experimental techniques. In case of microscopy, regions of interest are fairly easy to identify if intrinsic structural features of the sample such as the macroscopic shape of the bone or some unique arrangements of blood vessels are present. In order to find regions of interest during SAXS scanning experiments at the µSpot beamline at BESSY II, transmission scans are performed which are not capable of resolving most of the intrinsic sample features. Additionally, some bone tissues show very uniform sample features which make an identification of the ROI more difficult. Thus additional labeling becomes mandatory since it also allows more accurate superimposition of data obtained from similar sample areas by complimentary experiments.

During this project two different approaches of ROI labeling were applied. Firstly, sample areas were marked with TEM grids which were glued under microscope on the bone sample (Figure 16). A substantial disadvantage of this method is the 'one shot only' mode for which still hands are needed. At worst, the area which was supposed to be measured subsequently could be glazed with glue or parts of it covered by the grid. Considering the amount of available samples as well as the required time for individual sample preparation including pre-characterization of potential ROIs, makes this uncontrollable approach not suitable as a standard ROI-labeling method. The second more automated and thus more controlled approach is the labeling of ROIs with a laser cutter which resects parts of the bone by short time laser pulses. Moreover the laser cutter works like a usual microscope which allows to directly mark ROIs after identification. By introducing macroscopic notches to the sample, ROIs in the vicinity of the notch are substantially easier to find by all different experimental techniques. Even at the µSpot beamline, macroscopic notches can be resolved by fast low resolution diode scans of the transmission or the calcium fluorescence signal (Figure 16).
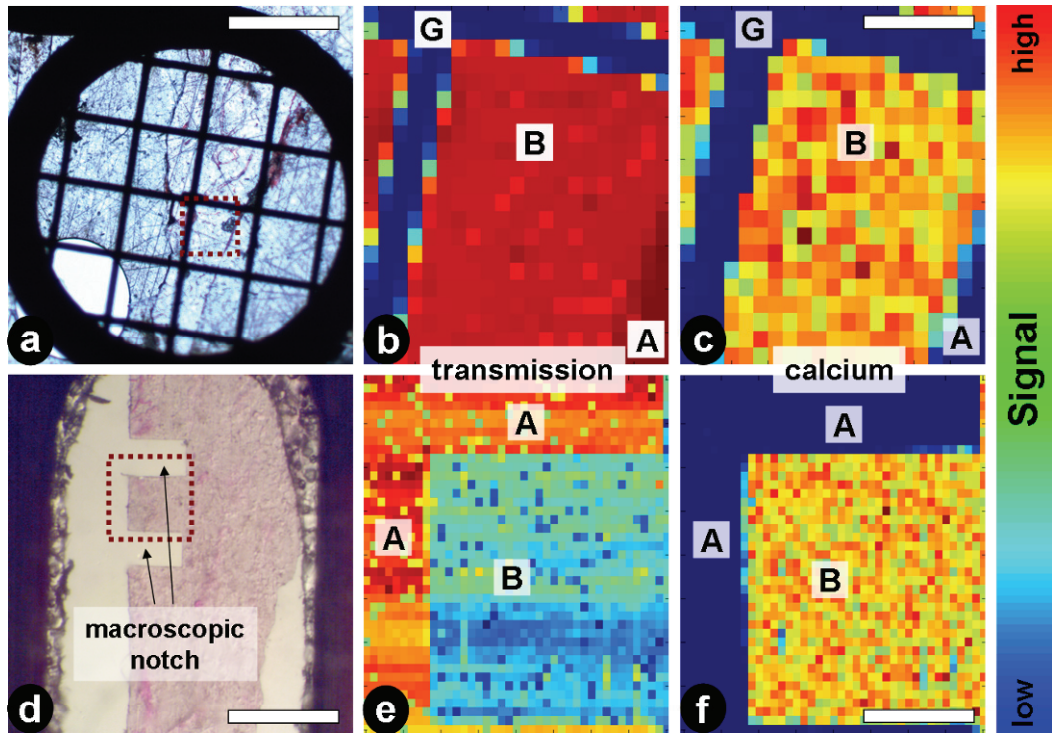
Figure 16: Different possibilities of sample area labeling for SAXS scanning: (a) – (c) murine femur labeled with a TEM grid, (d) – (f) ovine femur marked with laser cutting. (a) & (d) light microscopy overview image which shows the scanned ROIs (red pointed box). Identification of labeled areas at the µSpot beamline at BESSY II with the transmission signal (b) & (e) and the calcium signal (c) & (f) from a fast diode scan. Scale bars: (a) 1 mm, (b) & (c) 150 µm, (d) 800 µm, (e) & (f) 300 µm. G – TEM grid, A – air, B – bone

5.6   Computational Analysis of Osteocyte Networks

Visualization of the organization of osteocyte networks yields qualitative structural information on the cellular level of bone tissue. Furthermore it offers the possibility to quantify these network structures in regard to their orientation, density and bone porosity in different bone types. Moreover, the obtained geometrical information can be correlated to material properties of the bone tissue such as the degree of mineralization, the organization of the organic collagen matrix and mineral particle properties. The correlation of these complementary data allows deep insights into the interaction between the osteoblastic as well as osteocytic cells and the bone material they are either synthesizing or facing, respectively, for instance during formation and remodeling. For quantifying osteocyte network data obtained from confocal laser scanning microscopy of rhodamine stained bone samples various image processing techniques are applied which will be briefly described. This project has been realized in close collaboration with Philip Kollmannsberger (MPI of Colloids and Interfaces, Potsdam, Germany).

The original data are 8-bit intensity images that contain the fluorescent signal from the network together with noise. Signal and background is separated by image binarization. For this purpose an intensity threshold is defined by interpreting the histogram of pixel intensities of the image as a bimodal distribution consisting of two overlapping distributions for signal and noise. Here, three different thresholding methods are applied and compared after original data were smoothed using 3D Gaussian blurring. After thresholding, morphological closing is applied to the binarized images (dilation followed by erosion) in order to fill holes. **(i)** Using Otsu's method of histogram variance is the classical method for automatic thresholding. It assumes two classes of pixels (signal and background) and finds the threshold that minimizes the combined intra-class variance. It is robust and works for different images, as it does not consider any specific constrains of the data. For the noisy osteocyte network images, a threshold 20 % below the Otsu threshold yielded reasonable results, whereas for clean images, the Otsu method resulted in too high thresholds, leading to loss of parts of the network. **(ii)** Another possibility is to fit two functions that describe noise and signal, respectively, which sum corresponds to the intensity distribution of the image. A threshold can then be found by defining a minimum ratio of signal to

noise and then discarding all pixels below that intensity value. This method does not work well on noisy images, or if the number of voxels is too small. **(iii)** Using the number of components (or particles) in the binarized image as a criterion is the third possibility of thresholding. For a range of thresholds between 0 and 1, the number of individual components in the binarized image is calculated. Low thresholding leads to many isolated noise pixels which remain in the image. For large thresholds, the network breaks up into many small pieces, leading again to a large number of components. The optimum threshold is somewhere in between, e.g. at the value that yields the lowest number of components. However, it cannot be excluded, that this threshold leads to artificial connections that lower the number of components. Thus, the threshold should be set somewhere above this value.

After thresholding, thinning of the canalicular structures (skeletonization) of the osteocyte network is the next step of image processing. This step is mandatory since due to the strong fluorescence signal from rhodamine staining, submicron structures appear magnified. For this purpose firstly cells and blood vessels need to be segmented, as these structures are not to be skeletonized. The criterion that defines a cell or blood vessel is its size, i.e. the distance of the innermost voxels from the surface. A distance transform is applied to the negative of the image, yielding an image where the intensity of each voxel corresponds to its Euclidean distance from the background. All voxels above a certain distance are defined as candidates for being inside a cell or vessel, and all other voxels are set to zero. Of all connected components in the remaining image, only those are kept that contain at least one voxel above a second threshold that defines the minimum cell size. All remaining positive voxels that are not part of a cell/vessel are identified as the canalicular network. In the original and binarized images, an individual canaliculus has diameters of several pixels due to the point spread function of the microscope, while the real diameter is somewhere between 70-100 nm, which is below the diffraction limit of the optical microscope. From the binarized images, the actual network is reconstructed by computing the medial axis skeleton of the measured canaliculi. Although the canalicular diameter cannot be measured by this method, it yields a close approximation of the true network. Several methods exist to compute the medial axis skeleton of three-dimensional volumes. Here distance-ordered homotopic thinning is applied, which is described elsewhere in

greater detail (Lee and Wang 1994; Pudney 1998). After image processing data can be analyzed according to different structural parameters such as the bone porosity due to network structures, as well as network orientations and average distance between the network and its surrounding mineralized matrix.
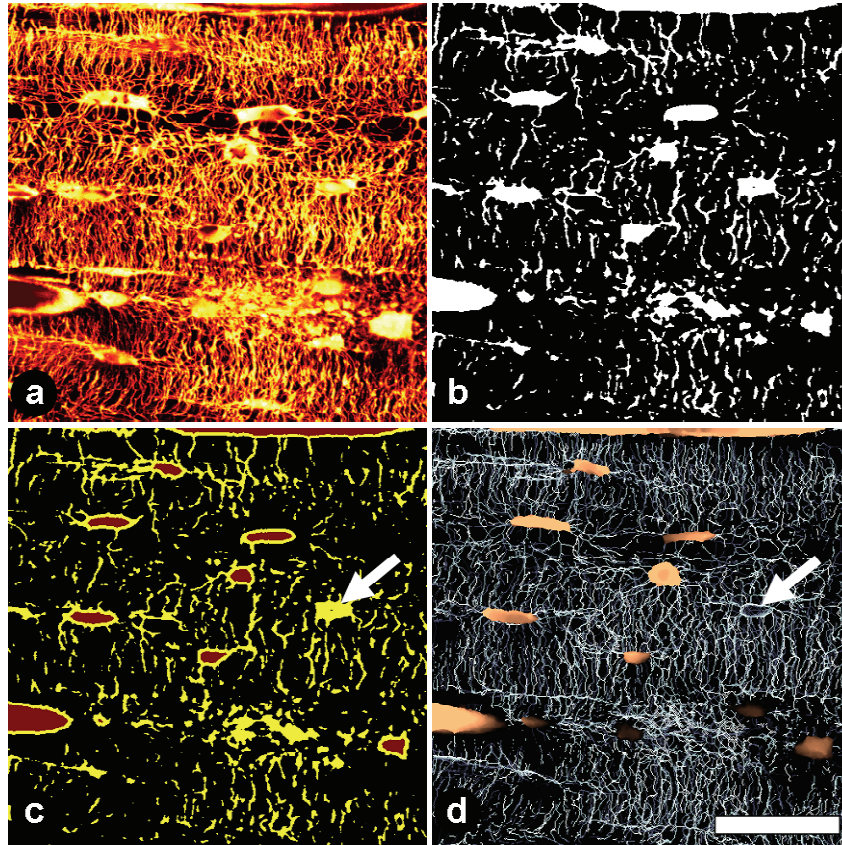
Figure 17: Different steps of image processing: (a) original image data, shown as standard deviation projection in z direction, (b) single image from the binarized stack, (c) same binarized image after segmentation of cells and blood vessels and (d) 3D projection of the network with segmented cells and the thinned canalicular network. Arrows indicate an example of a cell which not gets segmented und thus skeletonized. Scale bare: 30 μm.

6 Results and Discussion

This chapter describes and discusses different subprojects which have been accomplished during the PhD project in order to understand how initial coordination of osteoblasts already determines the organization of bone during physiological growth and remodeling as well as osteocyte-material interactions during mineral homeostasis. In this regard the hypothesis whether osteocytes can modify bone material in their vicinity will be addressed and discussed.

Firstly in section 6.1 osteocyte networks from different bone types are visualized with confocal laser scanning microscopy combined with rhodamine staining and subsequently characterized and quantified. Secondly, in section 6.2 implications on bone tissue formation and remodeling processes such as bone healing are derived from the correlation of structural parameters of the osteocyte network and the material properties of bone tissue in which the cells are embedded. Subsequently, in section 6.3, bone material properties on the submicron level obtained from SAXS scanning are correlated to osteocyte network geometries. These correlations yield additional information on the interaction of cells and their surrounding material. Finally two model systems are studied: In section 6.4 passive mineral extraction through blood vessels and osteocyte network structures is examined showing the potential of osteocytes to act as membranes and thus directly control dissolution of calcium and phosphate ions under physiological conditions. In section 6.5 medullary bone from egg laying hens is studied. This special bone type serves as a mineral reservoir for daily eggshell production. Due to the tremendous daily mineral turnover for eggshell production, medullary bone facilitates a unique model system to study potential interactions between bone material and osteocytes as well as implications on bone material properties to better fit the requirements of fast turnover. The conjunction of the individual subprojects will help to better understand the potential role of osteocytes during bone mineral homeostasis, in other words, whether osteocyte action may have a direct influence on bone material quality.

## 6.1   Characterization and Quantification of the Osteocyte Network

Undemineralized cortical bone sections from femurs from horse (equine), sheep (ovine) and mouse (murine) were stained with rhodamine. Staining leads to a labeling of all internal bone surfaces, revealing blood vessels, the osteocyte lacunae and canaliculi. Thus, the whole osteocytic network is dyed with a fluorescent medium that can be visualized and analyzed in a 3-D mode. Subsequent combination of confocal laser scanning microscopy data with polarized light microscopy and back scattered electron microscopy offers the possibility to correlate bone material properties with osteocyte network organizations.

6.1.1   Osteocyte Networks in Equine Osteonal Bone

Equine metacarpal bone (Figure 18) consists of the initially built fibrolamellar bone matrix, as well as secondary osteons which get formed during processes of cortex remodeling. In both systems, osteocyte networks are highly oriented. Lacunae are aligned with their long dimension along the bone lamellae, concentric around the blood vessel (Haversian canal) which is situated in the centre of the osteons. In the initial, unremodeled bone matrix, lacunae and bone lamellae are aligned linearly. Canaliculi run mainly perpendicular to the bone lamellae as well as to the long axis of the osteocyte lacunae, connecting the cells with each other and ultimately with the haversian canals. The newly remodeled (younger) bone matrix, abundant in secondary osteons, is less mineralized than the older initially built bone as visualized by the lower grey values of the backscattered electron microscope image (Figure 18d).

From literature it is known that during the remodeling process the pre-existing matrix gets resorbed by osteoclasts, including the osteocytic network, followed by a so-called reversal phase, where the eroded surface is smoothened and covered with a non-collagenous protein-rich substance (cement line) (Burr, Schaffler et al. 1988; Skedros, Holmes et al. 2005). On such prepared surfaces the new bone matrix is then deposited by the osteoblasts. At these zones it becomes apparent, that the rhodamine stained osteocyte network is disrupted and the new osteonal osteocytes line up along the cement line (Figure 19).
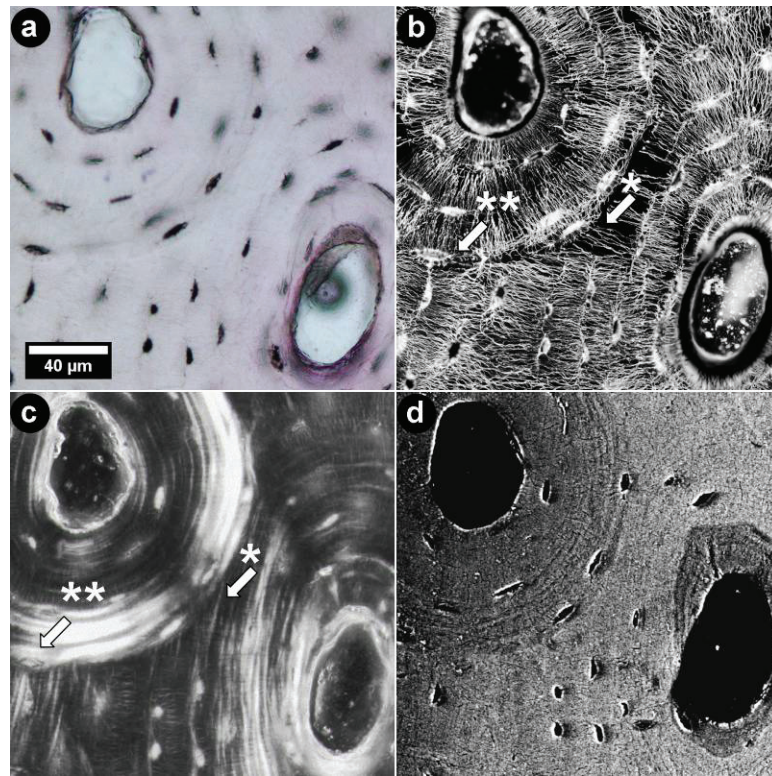
Figure 18: Osteons in equine metacarpal bone; (a) rhodamine stained sample under light microscope, (b) same area visualized with confocal microscopy, (c) polarized microscopy from the same area, note that the oriented bone lamellae run perpendicular to the canaliculi visualized in (b), (d) backscattered electron microscopy image: the grey value of the mineral shows the degree of mineralization. Newly remodeled bone is less mineralized (darker); these parts are separated from the older, more highly mineralized bone (brighter parts) by a cement line that also disrupts the osteocytic network (see magnification of indicated areas with asterisks in Figure 19). With permission from Elsevier (Kerschnitzki, Wagermaier et al. 2011)

Their processes run towards those boundary layers, but since passing through is impossible they turn their direction and follow the outer border of the osteon along the cement line. Canaliculi in the older, unremodeled bone that run towards the new built osteon are cut off as a result of the remodeling process. Due to the concentric alignment of the osteocytic network around the Haversian canal in the osteon, matrix orientation and cell network alignment differs from the unremodeled bone, which is mainly linearly aligned. Confocal and polarized microscopy shows this missing adaption between the newly built osteon and the surrounding older bone (Figure 19).
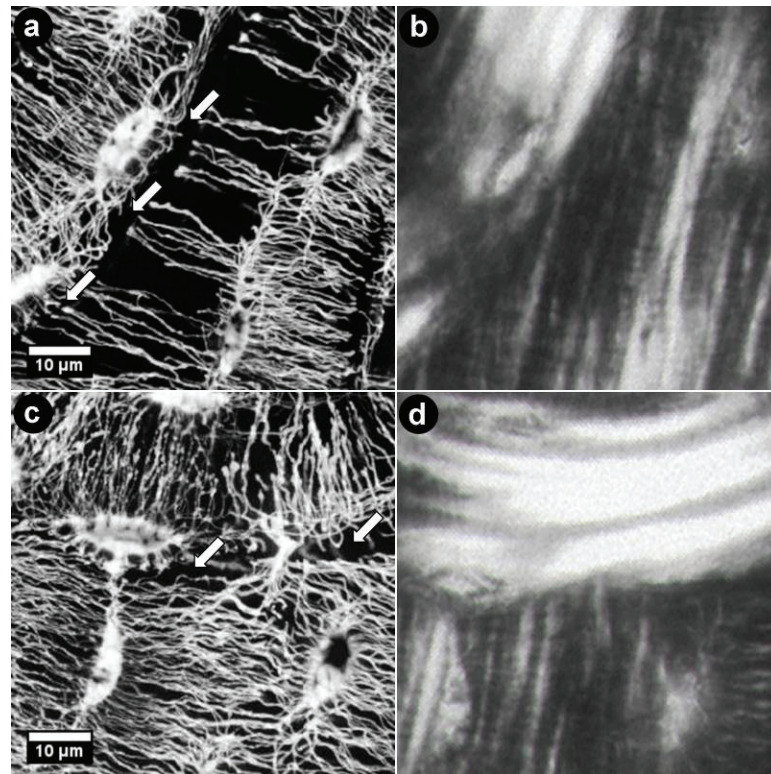
Figure 19: Magnification of area * and ** from Figure 18: the cement line disrupts the osteocyte network (arrows), (a) orientation of canaliculi as well as bone lamellae shown in (b) between the old and the remodeled bone is parallel; (c) canaliculi of the old and the remodeled bone run perpendicular to each other; (d) also the lamellae show a corresponding alignment. With permission from Elsevier (Kerschnitzki, Wagermaier et al. 2011)

6.1.2 Osteocyte Networks in Ovine Fibrolamellar (Plexiform) Bone

The cortex of the fibrolamellar ovine femur (Figure 20) consists of many non-remodeled bone packets which are bordered by the blood vessels. Osteocyte networks around the bordering blood vessel are highly aligned in parallel layers. These layers correspond to the individual bone lamellae, following the orientation of the blood vessels. Canaliculi run mainly perpendicular through the lamellae mutually interconnecting the cells and the blood vessels. In the mid zone of each bone packet a thin layer that is less penetrated with canaliculi is present. Polarized microscope images of the fibrolamellar cross section show dark and bright areas in the ordered parts of the bone packet. This indicates a collagen fiber orientation being mainly in plane close to the blood vessels and out of plane close to the middle layer which is less penetrated with canaliculi. This arrange-

ment of fibers is confirmed by polarized light microscopy of long sections of fibrolamellar bone showing complementary patterns of interference. Backscattered electron microscopy in low vacuum mode of the same area shows brighter, more mineralized parts of the bone matrix, which correspond to those thin bone layers with a low degree of organization.
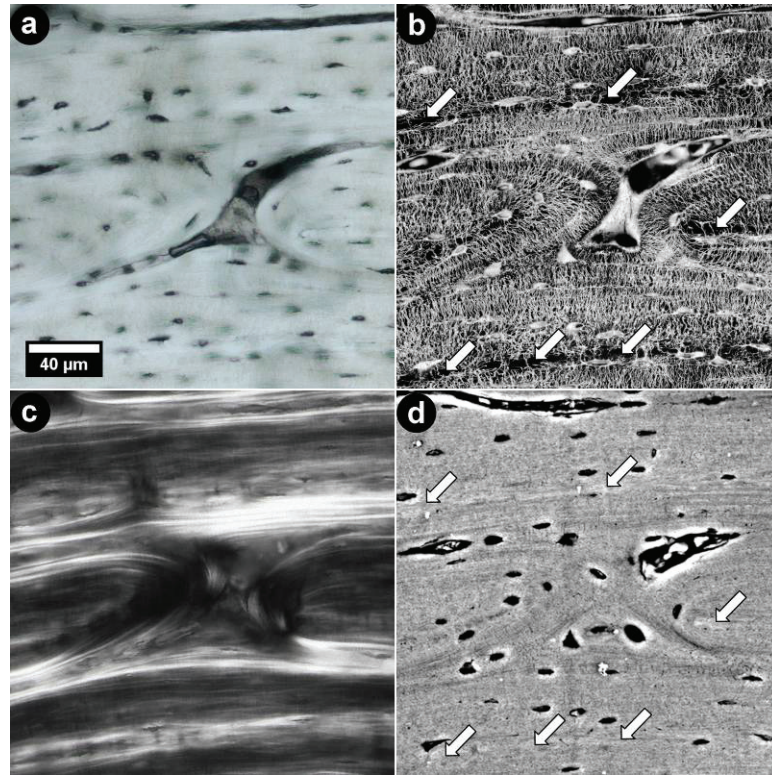
Figure 20: Fibrolamellar ovine femur: (a) rhodamine stained sample under light microscope, (b) same area visualized with confocal microscopy: note the linear areas of the matrix (arrows) between the blood vessels that are less penetrated with canaliculi, (c) polarized microscopy from the same area: note that the oriented bone lamellae run perpendicular to the canaliculi visualized in (b), (d) backscattered electron microscopy: brighter parts (arrows) that are more mineralized, correspond to the areas in (b) which are less penetrated with canaliculi. With permission from Elsevier (Kerschnitzki, Wagermaier et al. 2011)

6.1.3   Osteocyte Networks in Murine Bone

Cross sections from the murine cortex in the femur (Figure 21a) reveal several areas with different degrees of osteocyte network alignment. In the periosteal region (top) areas with an abundance of osteocytes and their connecting canaliculi not showing a high degree of mutual alignment as well as areas barely showing any cells or canaliculi are present. The endosteal side of the cortex (bottom) exhibits well oriented osteocyte lacunae and canaliculi, which mainly run perpendicular to the long axis of the osteocytes. This layer-like structure can also be observed with cross polarized light microscopy with the sample in 45° position (Figure 21b). Areas which showed a higher degree of osteocyte network alignment appear brightly and thus feature a high degree of the collagen matrix alignment. Areas in which cells are absent appear darker, therefore corresponding to lower degrees of collagen orientation. Back-scattered electron imaging shows several areas having different degrees of mineralization (Figure 21c). Lower mineralized, darker parts of the cortex correspond to the areas featuring a high degree of collagen orientation respectively high mutual alignment of osteocytes and canaliculi. Highly mineralized areas match with areas showing a lower degree of collagen orientation. Additionally, the back-scattered images show cracks within the bone material, which have been introduced due to further sample preparation for electron microscopy. These cracks run parallel to the bone lamellae und thus can be used as indicators of the lamellar collagen orientation. It is obvious that in the periosteal region of the cortex, these cracks run parallel to the surface of the highly mineralized areas. In the endosteal region cracks run mainly circumferentially along the cortex.
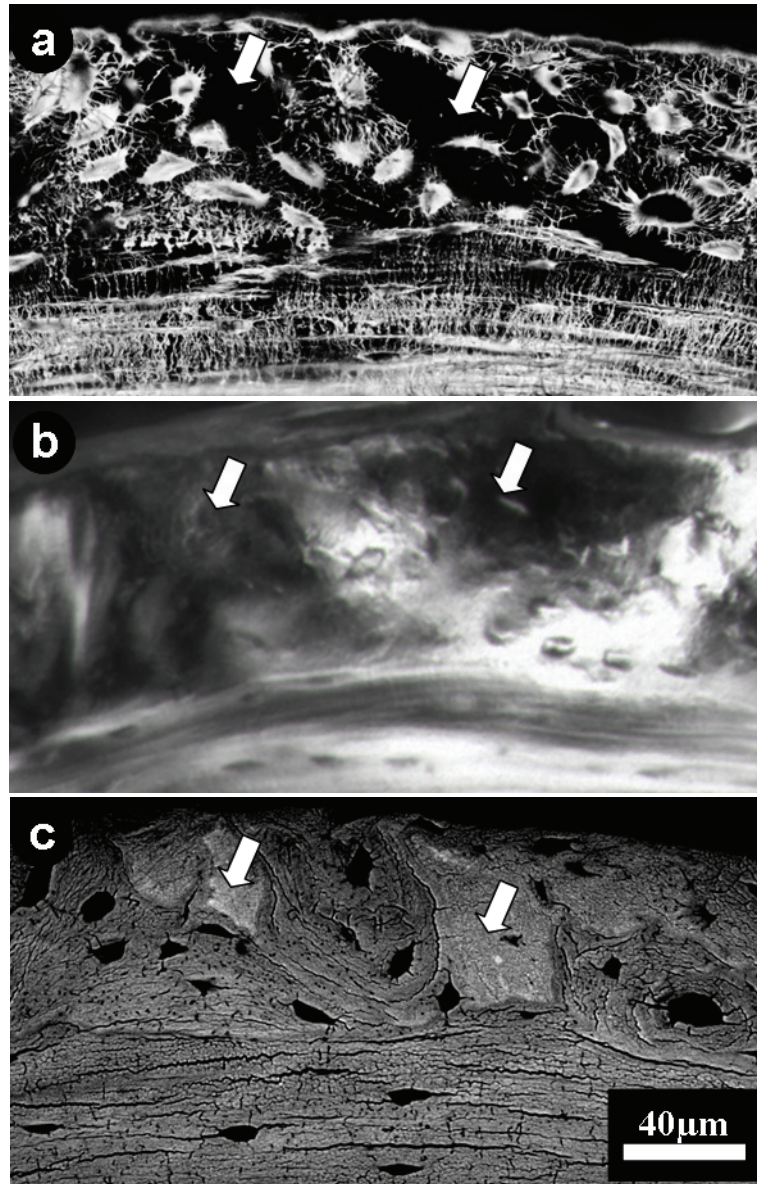
Figure 21: Visualization of an area of the cross section of a murine femur: (a) confocal microscopy showing the osteocyte network, which is less aligned at the periosteal side (top) and highly aligned at the endosteal side (bottom), black areas without staining correspond to (b) dark areas under the polarized microscope which indicate a low degree of collagen matrix alignment (arrows), (c) back-scattered electron imaging: less aligned areas (arrows) show higher degrees of mineralization (higher grey level), cracks within the lower mineralized regions (lower grey level) indicate the alignment of the collagen matrix.

6.1.4 Quantification of Osteocyte Networks in Murine and Ovine Bone

The different structural organization of the collagen matrix in poorly arranged murine bone compared to highly arranged equine and ovine bone leads to distinct mechanical implications on these tissues. Furthermore, due to the osteocyte network organization, which varies correspondingly strong in different bone types, additional considerations on potential osteocyte - mineral interactions can be made. For this purpose, qualitative fluorescence data of rhodamine stained bone samples are used to quantify osteocyte networks in different bone types regarding their average distances of bone mineral to the lacunar-canalicular network. This information is a theoretical measure for the amount of accessible bone mineral within a certain penetration depth in context of osteocyte-controlled mineral exchange between bone matrix and blood. The intensity of each voxel in the distance-transformed image corresponds to its Euclidean distance in microns to the nearest positive voxel in the thinned image. Plotting the relative amount of mineral as a function of the distance from the cells or their cell processes reveals different mineral distributions in different bone types (Figure 22).
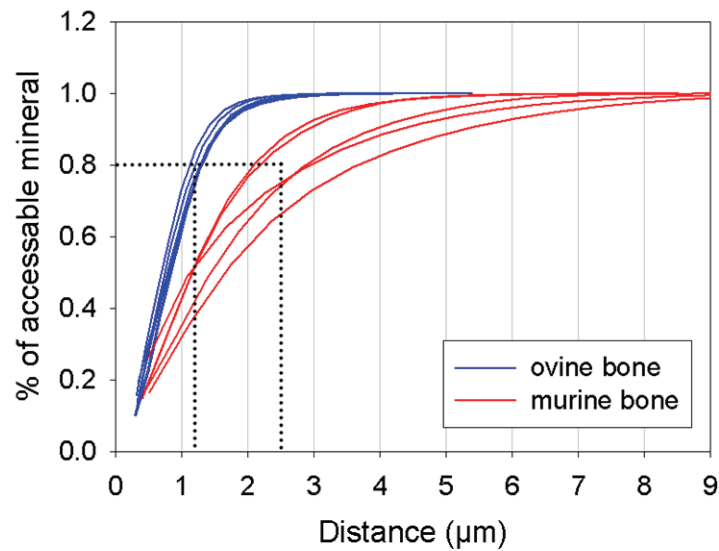
Figure 22: Plot of the relative amount of reachable mineral within a certain distance from an osteocyte. Various measured ovine bone areas show similar curve progression of reachable mineral. 80 % of ovine mineral resides within a distance of only 1.1 µm. In murine bone curve progression of reachable mineral varies strongly between different bone areas with 80 % of mineral residing from 2 µm to 4 µm distance from the osteocytes.

In highly arranged ovine bone already 80 % of the mineral resides within only 1.1 μm and thus is rapidly accessible by diffusion, whereas in murine bone, less then 50 % of mineral is located within 1.1 μm. In particular maximum distances between cells and mineral differ greatly in these two tissue types (Figure 22). In fibrolamellar bone, 100 % of mineral can be reached already within approximately 3 μm. In murine bone maximum penetration depth of more then 9 microns would be required to reach 100 % mineral. Moreover curve progression of the relative amount of reachable mineral is considerably more uniform in fibrolamellar ovine bone compared to murine bone. The reason for this is the high degree of structural alignment of the osteocyte network in fibrolamellar (or lamellar) bone. Here canaliculi are homogeneously distributed over the whole bone matrix such as to feature uniform distances between the cells and their processes and the surrounding material. In contrast murine bone consists of different structural units of woven or lamellar bone, either showing poorly or highly arranged osteocyte networks with either low or high amounts of accessible mineral, respectively (Figure 23). Consequently this inhomogeneous structural organization gets apparent in the strongly varying curve progression of the relative amount of reachable mineral residing within a certain distance. Thus, curves with higher slopes indicate murine bone areas with relatively large fractions of lamellar bone, whereas bone areas with high fractions of modestly aligned woven bone show lower slopes.
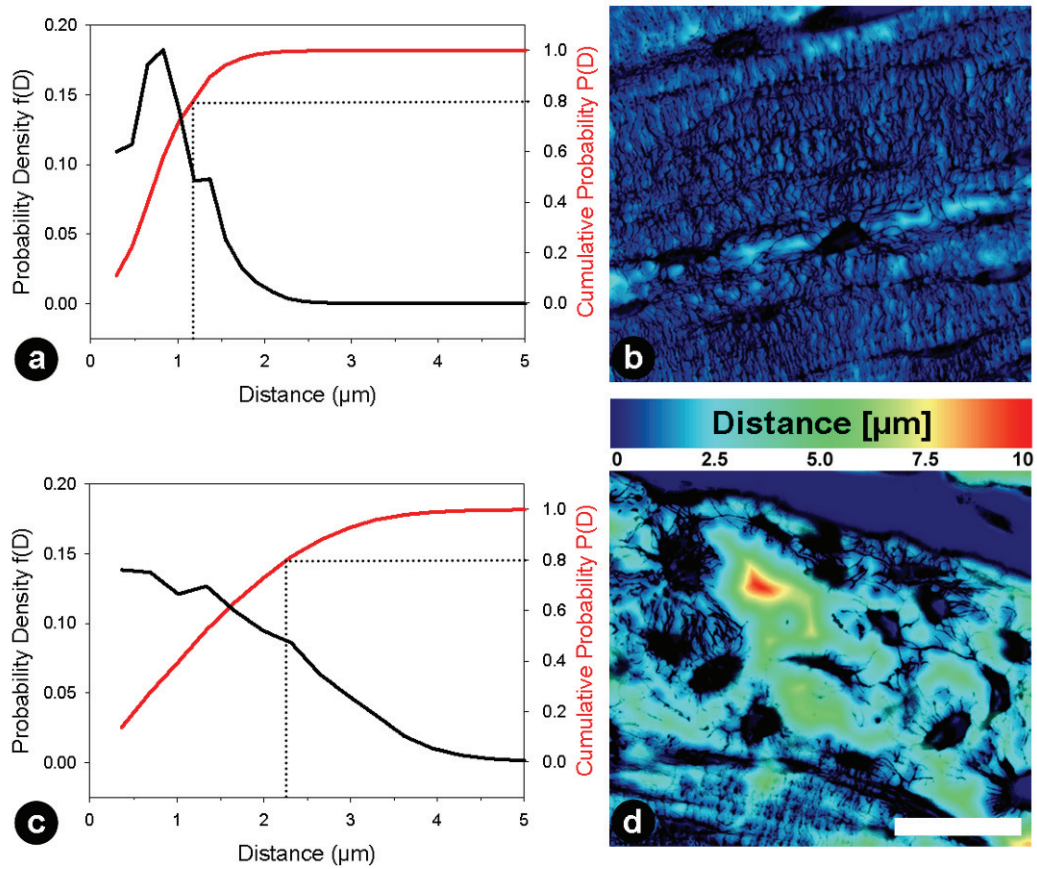
Figure 23: Examples of a fibrolamellar ovine (a) & (b) and murine (c) & (d) bone area. (b) & (d) showing the distance map of mineral in each bone type. In fibrolamellar bone due to the homogeneous alignment of the osteocyte network a high fraction of mineral resides in the proximity of the cells. (a) Mineral distance distribution (probability density – black curve) peaks below a value of 1 μm. In murine bone mineral is broadly distributed over the distances (c) with high amounts of accessible mineral in highly arranged areas of parallel fibred or lamellar bone. In areas where cells are absent, mineral is barely accessible (d). Scale bar 30 μm.

6.1.5 Implications on Osteocyte Network Organization in Different Bone Types

Comparing the structural arrangement of osteocytes and the extracellular collagen matrix in different bone types from different animals leads to the conclusion that the organization of the osteocytic network mirrors the extracellular matrix orientation. Equine metacarpal bone and ovine fibrolamellar bone as well oriented tissues (Weiner and Wagner 1998; Currey 2002) exhibit highly oriented

networks of osteocytes aligned to the bone lamellae in a parallel manner and canaliculi running perpendicularly to them. In equine bone secondary osteons built by tissue remodeling are not adapted to the older bone matrix (Currey 2002), showing a different structural arrangement of osteocyte networks and corresponding collagen matrix organization. Murine bone as an example of a barely oriented tissue consists of modestly arranged parts of woven bone as well as layers of parallel fibred and lamellar bone (Enlow 1962; Hörner, Loeffler et al. 1997; Price, Herman et al. 2005). This is demonstrated by the black white patterning showing up in different areas with polarized microscopy. The osteocytic network shows a corresponding arrangement to the collagen matrix, no mutual alignment of osteocytes and their canaliculi in the not-oriented woven bone layer, but high alignment of the osteocytes parallel to the fibers with canaliculi running perpendicular to them in parallel fibred and lamellar bone at the edges of the cortex.

The theoretical amount of accessible mineral is considerably smaller for murine woven bone than for fibrolamellar bone, indicating that the latter is more suited for dynamic mineral exchange and thus the control of mineralization. As a consequence, tissue mineralization during growth and maintenance of dissimilar bone tissues could be different. From literature it is known that woven bone material in a mature state features higher degrees of mineralization as compared to highly arranged parallel fibred or lamellar bone (Weiner and Wagner 1998; Currey 2002). Yet this is explained by the different alignment of collagen bundles. In woven bone, these do not show long range orientation being rather interwoven and thus facilitating more and larger interfibrillar spaces for the growth of bone mineral particles then compared to the tightly aligned collagen fibrils in parallel fibred or lamellar bone. Both, bigger sizes or higher numbers of these mineral particles lead to an overall higher degree of mineral content in bone (higher calcium content).

Due to the different degrees of osteocyte network alignment featured by woven compared to parallel fibred or lamellar bone, another explanation for the dissimilar degrees of mineralization becomes feasible. In bone tissue featuring high osteocyte network organization, most of the material resides in the proximity of the cells leading to high relative amounts of accessible mineral. Furthermore, osteo-

cytes are known to being capable of inhibiting bone mineralization in order to not becoming mineralized (Baylink, Wergedal et al. 1971; Lane, Yao et al. 2006). Thus, it might well be possible that osteocytes control mineralization in their proximity. As an example, the degree of mineralization of bone areas in which osteocytes did undergo apoptosis is continuously increasing and osteocyte lacunae get filled with mineral (Busse, Djonic et al. 2010; Vuong and Hellmich 2011). Poorly arranged woven bone is in a comparable situation to apoptotic bone. Here osteocytes are still present but high fractions of mineral reside further away from the cells and their processes (distances larger then approximately 5 µm) and thus can be less controlled. As a consequence, mineral content in these areas is higher due to a continuous increase of mineralization as in case of apoptotic bone. However in the proximity of the cells residing within woven bone type, below a distance of a few micrometers, mineral content is visualized to be lower und thus, mineralization still well controlled by the cells (Figure 24).
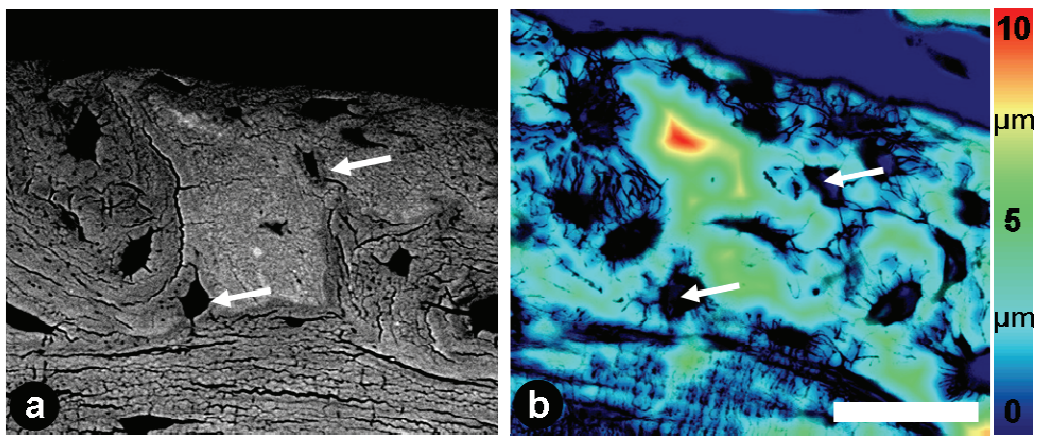
Figure 24: Comparison of the degree of mineralization and the corresponding distance to the nearest cell: (a) back-scattered electron microscopy image and (b) map of the mineral cell distances merged with a confocal image of the osteocyte network in that area. Highly mineralized bone is mainly located in areas with distances to the next cells or its processes larger then approximately 5 µm. Arrows indicate cells within the highly mineralized woven bone type. Mineral in the proximity of those cells is still controlled and thus shows lower degrees of mineralization. Scale bar 30 µm.

6.2 Osteocyte Network Organization during Bone Formation and Remodeling

Examination of bone samples with a combination of confocal laser scanning microscopy, polarized light microscopy and back scattered electron microscopy shows that the organization of the osteocyte networks mirrors the extracellular collagen matrix orientation. Furthermore, information about the mineral content indicating the age of the bone combined with the spatial alignment of the osteocyte network together with the arrangement of the collagen matrix can give implications on the dynamics of bone formation during the processes of **(i)** bone tissue growth as well as **(ii)** bone remodeling and healing which will be described and discussed in the following.

6.2.1 Bone Deposition during Tissue Growth

At the periosteal side of the growing fibrolamellar ovine cortex, formation of new bone packets starts with the deposition of highly mineralized linear areas of primary bone revealed by back-scattered electron imaging. These primers in the centre of each bone packed are abundant in the whole cortex (Figure 25). Visualizing the osteocyte network in the fibrolamellar cortex with confocal laser scanning microscopy also reveals these linear regions showing less canaliculi penetration. Whereas osteocytes are poorly ordered within these primarily deposited regions, they are well lined up along their surfaces. Between the highly mineralized regions, the osteocyte network is formed of parallel cell layers with highly ordered canaliculi (Figure 25). These layers correspond to the alignment of individual bone lamellae and canaliculi run perpendicularly to collagen direction in these lamellae.
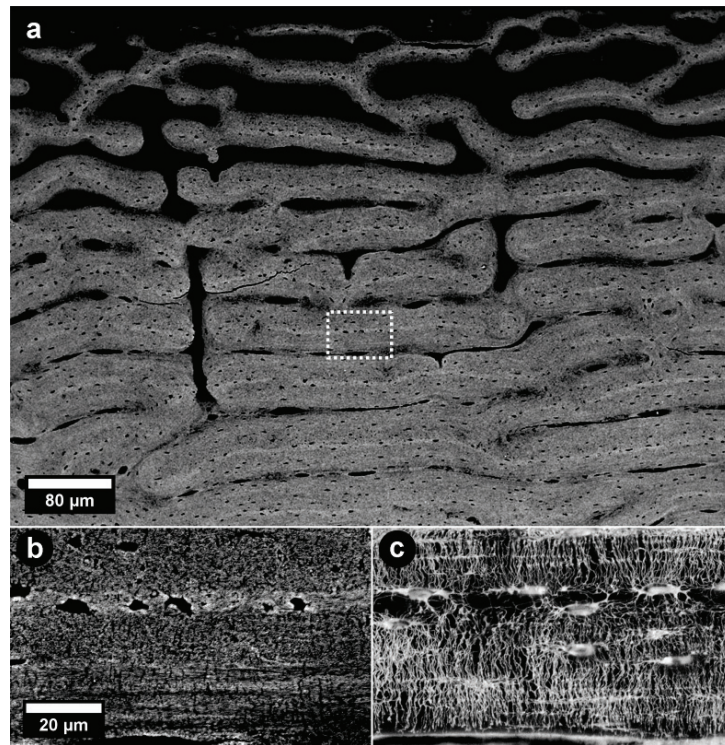
Figure 25: Fibrolamellar bovine femur: (a) high vacuum backscattered electron imaging shows highly mineralized linear areas abundant in the whole cortex, note that formation of fibrolamellar bone packets in the periosteal region (top) starts with the deposition of this highly mineralized primer, (b) magnification of a single bone packet with (c) corresponding cell network alignment measured by confocal microscopy. With permission from Elsevier (Kerschnitzki, Wagermaier et al. 2011)

6.2.2 Bone Deposition during Remodeling and Healing

Ovine fracture healing callus, 9 weeks after the osteotomy (Figure 26) consist of a mixture of less organized as well as highly oriented mineralized tissue. The callus at the periosteal side of the cortex further away from the osteotomy gap is almost completely filled with densely packed bony tissue. In this region, almost no poorly organized bone is still present and high fractions of lamellar bone are observed. This fraction of lamellar bone decreases with shorter distance to the osteotomy gap. Also the density of the callus decreases, having more unmineralized holes which are not yet filled with highly oriented lamellar bone. Higher magnification of a comparable region at 2 weeks and 9 weeks after the induced osteotomy exhibits the dynamics of callus formation regarding the organization of the deposited bone material. At a time point of 2 weeks (Figure 26b) only

poorly oriented bone, also showing a low degree of mutual osteocyte arrangement, is deposited. After 9 weeks (Figure 26c) also well oriented lamellar bone can be observed. Interestingly, the lamellae alignment runs parallel to the surface of the primarily deposited, poorly organized bone. Visible osteocyte lacunae in the lamellar bone are well arranged with their long axis parallel to the lamellar direction.
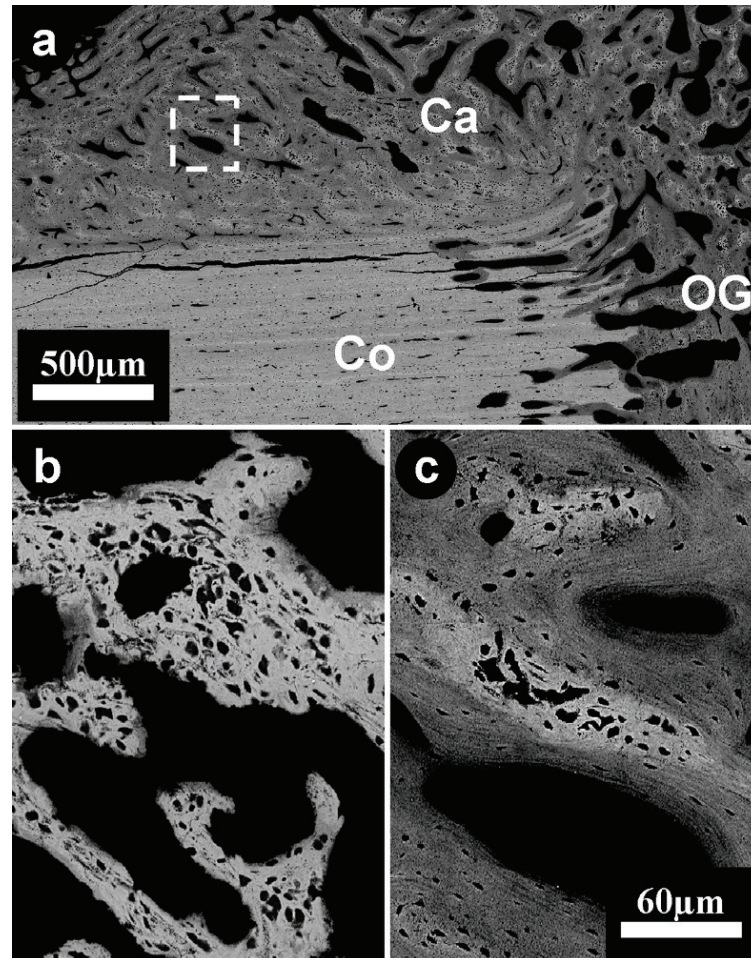
Figure 26: Long section of a healing ovine femur showing the ovine cortex (Co) the callus (Ca) and the osteotomy gap (OG), (a) backscattered electron imaging, 9 weeks after induced osteotomy, (b) magnification of the same region in a comparable sample 2 weeks after osteotomy only showing poorly organized bone material, (c) magnification of the same region, time point 9 weeks after osteotomy showing a further developed part of the callus. The orientation of the bone lamellae of the secondarily formed bone (less mineralized, darker areas) is parallel to the surface of the primarily deposited bone (highly mineralized, brighter areas). With permission from S. Karger AG, Basel (Kerschnitzki, Wagermaier et al. 2011)

Polarized light microscopy of the callus 9 weeks after osteotomy (Figure 27) confirms, that primarily formed bone merely shows poorly oriented collagen matrix which is only oriented around single cells indicated by the black-white pattern. The secondarily formed bone appears birefringent in polarized light showing high organization of the collagen matrix. Bone lamellae run parallel to the surface of the primarily deposited parts. Also osteocytes are poorly arranged, without any mutual alignment in the primarily deposited parts, opposing to osteocyte networks in the secondarily built parts which are aligned in layers following the lamellar alignment.
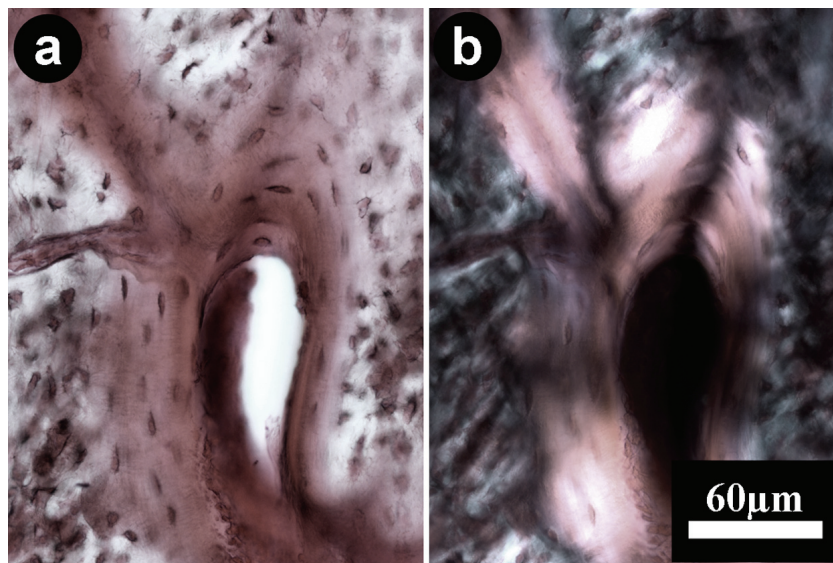
Figure 27: Magnified callus region in a long section of a healing fibrolamellar ovine femur 9 weeks after healing: (a) light microscopy image of a rhodamine stained sample showing a low degree of mutually aligned osteocytes in the primarily formed (whitish) regions. Osteocyte lacunae in the secondarily formed (reddish) regions are aligned in layers following the surface of the primarily formed bone. (b) Polarized light microscopy of the same area shows the corresponding collagen matrix organization, which is organized in domains around single osteocytes in the primary areas (black-white pattern) and lamellar in the secondarily formed bone. Note that the lamellar alignment corresponds to the alignment of the different osteocyte layers running parallel to the surface of the primarily formed bone. With permission from S. Karger AG, Basel (Kerschnitzki, Wagermaier et al. 2011)

6.2.3 Implications on the Dynamics of Bone Deposition during Tissue Growth and Healing

The detailed visualization of the arrangement of the osteocyte network in conjunction with the organization of the collagen matrix in growing ovine fibrolamellar bone implies a collective action of osteoblasts starting their synthesis-process from the surface of these substrate layers. This can be concluded from the fact that the secondarily formed bone lamellae, indicated by individual osteocyte layers, are always running parallel to the surface of the primarily formed parts. These structural features are also in agreement with findings by other groups (Stover, Pool et al. 1992; Currey 2002; Mori, Kodaka et al. 2003; Mori, Hirayama et al. 2007). These observations show, that initial spatial arrangement of osteoblasts is crucial in order to form bone featuring organized collagen matrix over large distances. Without the support by a solid surface, this coordinated action of bone forming cells is not possible, leading to formation of woven bone type. The dynamics of successive modestly arranged, primary and highly organized, secondary bone deposition suggests that a substrate layer, on which osteoblasts can assemble and align, helps in forming an ordered tissue whereby the collagen fibrils are arranged in parallel over distances beyond the range of a single cell.

Primary bone deposition serving as a substrate for subsequent formation of highly organized bone also plays a crucial role during growth of the murine cortex. Here primarily formed bone is highly mineralized and features a low degree of tissue organization. In these woven bone areas, almost no mutual alignment between osteocytes and no long range order of the collagen matrix orientation is present. In secondarily formed, lower mineralized bone, lamellae and corresponding osteocyte layers run parallel to the surface of the primarily formed areas. Here mutual alignment of osteocytes and canaliculi again implies, that formation of these areas starts at the surface of the primarily formed parts, at which the matrix synthesizing osteoblasts align. These results are in accordance to findings in histological studies (Hirose, Li et al. 2007) and to observations from growing murine femurs from rats (Idelevich, Kerschnitzki et al. 2011).

To conclude on the investigation of different bone types, the following scheme is suggested as a general model, representing osteocyte network and corresponding collagen matrix orientations (Figure 28). In less organized bone types no predominant mutual alignment between osteocytes is present. Canaliculi run mainly in radial direction from the lacuna towards the neighboring cells. The connectivity of the osteocytes is reduced in comparison to lamellar bone. This woven bone type, shows a short range order of collagen fibrils which are concentrically arranged around the osteocytes (drawn as red dashed lines) and are thus perpendicular to the radial canaliculi alignment. This organization of the collagen matrix can be defined as a microlamellar arrangement. In contrast, in lamellar bone, osteocytes are mainly aligned in layers along the bone lamellae which are connected by the canaliculi that run mainly perpendicular through those lamellae. This difference in organization suggests that a single osteoblast will organize the tissue only within a certain radius of action that is in the same order of magnitude as the spacing between osteocytes in microlamellar bone (approximately 20 to 30 microns – (Sugawara, Kamioka et al. 2005)). Only when osteoblasts are supported by a solid surface, such as a layer of modestly organized bone, they are able to coordinate their activity such as to synthesize a layer of parallel ordered collagen over distances much larger than a cell. Similar observations lead to the proposal that osteoblasts may exist in two differentiation stages, where they would either synthesize woven bone if they are loose, or parallel fibred lamellar bone if they are bonded to a surface (Shapiro 1988; Shapiro 2008).
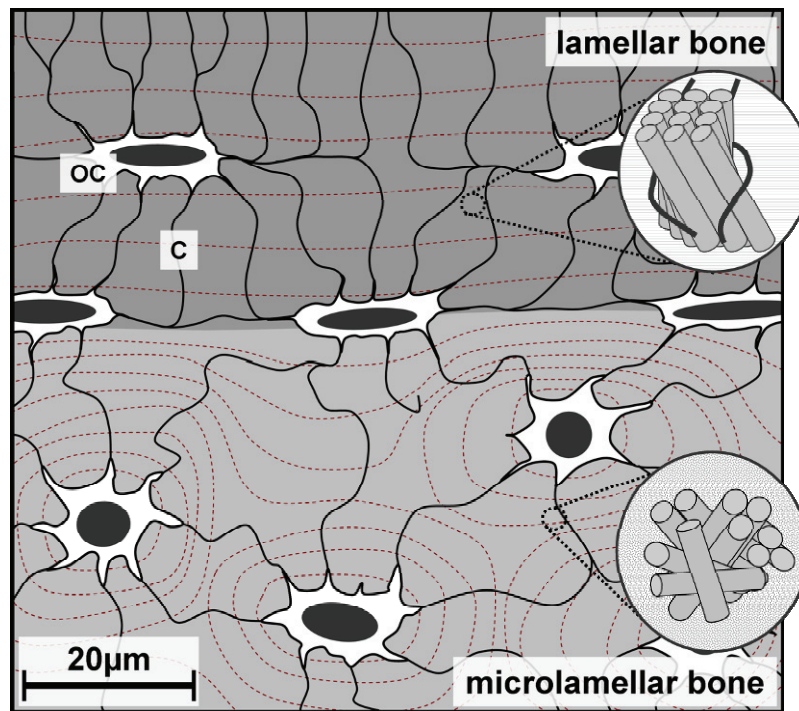
Figure 28: Scheme of the osteocyte network and corresponding matrix orientation (red dashed lines). Osteocyte networks are highly arranged in lamellar bone. In microlamellar bone, collagen is only oriented in domains, in the proximity around cells. No mutual alignment of osteocytes (OC) is present. Canaliculi (C) mainly run in radial direction from the cells. With permission from Elsevier (Kerschnitzki, Wagermaier et al. 2011)

The presence of substrate layers to direct subsequent osteoblastic action during collagen matrix synthesis is not only crucial during the process of bone growth. It also plays an essential role during processes of cortex remodeling. In osteonal equine metacarpal bone, which consists of numerous secondary osteons (Stover, Pool et al. 1992), the cement line separating the older bone matrix from the resorption cavity serves as a substrate layer for the coordinated deposition of lamellar bone. However, in osteonal bone, contrary to the primary substrate deposition by osteoblasts during bone growth, the surface of the solid substrate is formed by prior osteoclastic resorption (Figure 29). This implies that during the process of remodeling, osteoclasts are not only simply acting as bone resorbing cells – but rather as bone organizers – preparing surfaces which direct the organization of subsequently deposited bone. Thus, additionally the surface topography of resorbed bone becomes a crucial factor for the alignment and organization of subsequent bone formation. Consequently, dysfunctions in bone remodeling

could lead to deficient bone formation (Everts, Beertsen et al. 1988; Helfrich, Aronson et al. 1991). In some regions canaliculi situated in the older bone can be visualized to be "cut off" by the remodeling process and the deposition of a cement line at the interface to the newly formed osteon. This confirms the idea that the surrounding old bone serves merely as a substrate for new bone deposition, which therefore does not need to be guided by signals (Figure 29).
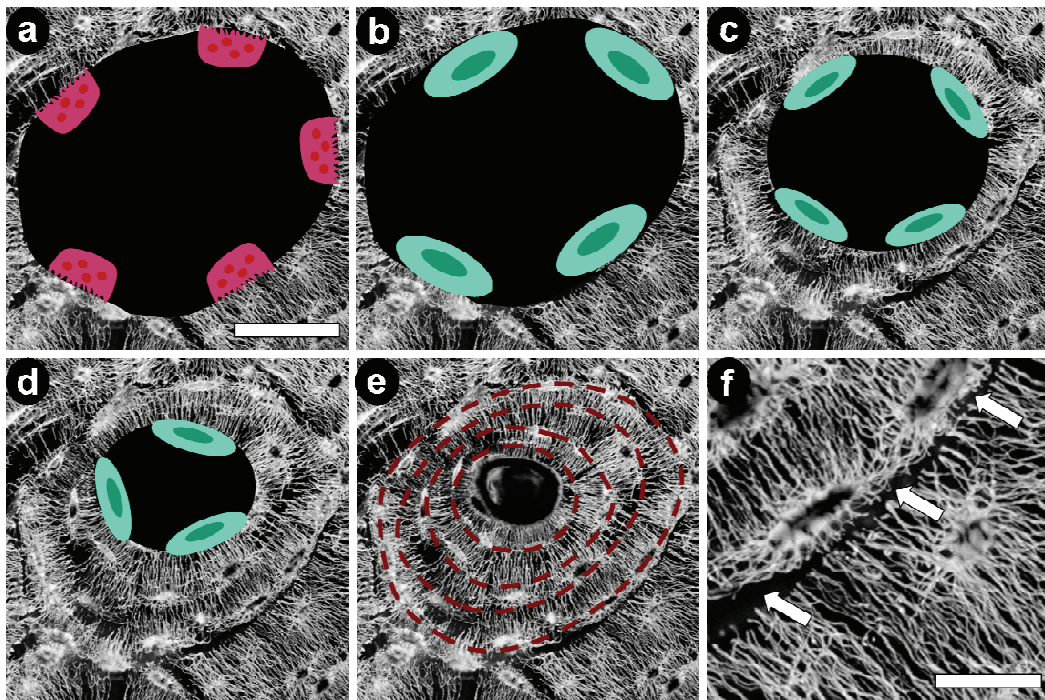
Figure 29: Sketch of secondary osteon formation: (a) osteoclastic resorption of old bone material, (b) – (d) layer like bone deposition by osteoblasts parallel to the surface of the old bone matrix, (e) completely formed secondary osteons showing different layers of osteocytes (former osteoblasts – red dashed lines) which got embedded during the formation of the osteons, (f) magnification of the cement line (arrows) which separates the old bone from the newly formed osteons. Scale Bars: (a) 50 μm, (f) 25 μm

The course of primary unorganized woven bone deposition with subsequent formation of highly oriented lamellar bone which is directed by the surface of the primary deposited material could again be demonstrated in ovine fracture healing callus (Kerschnitzki, Wagermaier et al. 2011). During callus formation, primarily deposited, poorly organized woven bone is deposited firstly such as to restore stability of the cortex. The missing mutual alignment of the osteocytes in these

regions indicates a process of bone formation by cells whose action has not been coordinated thus leading to unorganized collagen matrix over larger length scales. In contrast, secondarily formed, lower mineralized bone in the callus features a high degree of tissue organization. Interestingly, lamellae run parallel to the surface of the primarily formed parts. The mutual alignment of osteocytes as well as the lamellar arrangement implies, that formation of these areas starts at the surface of the primarily formed parts, at which the matrix synthesizing osteoblasts are aligned and in consequence being able to collectively synthesize collagen matrix. These results confirm findings with sSAXS that callus formation occurs in two waves of bone deposition, whereby a highly disordered mineralized tissue was built first, followed by a bony tissue with higher degree of mineral particle- (and thus collagen matrix-) alignment (Liu, Manjubala et al. 2010).

Taking together the dynamics of bone formation during physiological growth, remodeling and healing it becomes obvious that this process can be generally split into two different phases: (i) substrate formation by osteoblasts which are not attached to a surface and (ii) the following phase whereby deposition of oriented collagen matrix is performed by 'surface-osteoblasts'. Without the presence of a substrate, osteoblasts build microlamellar woven bone which can be subsequently used as a substrate layer.

In distinct animals bones consist of different relative amounts of woven (microlamellar) to lamellar bone (Currey 2002; Kerschnitzki, Wagermaier et al. 2011). In murine bone the fraction of woven bone is relatively high. However, light-weighted mice do not have high mechanical demands on their bones. Furthermore bones of mice need to grow relatively fast due to their prematurity at birth. In addition to that, synthesis of highly arranged bones is energy intensive and takes longer time since osteoblasts need to be coordinated along surfaces (Shapiro 2008; Kerschnitzki, Wagermaier et al. 2011). For the synthesis of modestly arranged woven bone larger numbers of cells can participate in the formation since they can be distributed over larger areas and do not need to be coordinated along surfaces. During the formation of this woven bone type, large holes reside within the material, which are filled with bone featuring higher material quality at later time points (Everts, Beertsen et al. 1988; Price, Herman et al. 2005; Idelevich, Kerschnitzki et al. 2011). This concept is advantageous since

animals can consequently grow fast and full formation and mineralization of bones to reach their final mechanical properties can take more time. Callus tissue during healing follows the same concept. Here fast formation of woven bone which gives some initial stabilization of the fracture is followed by formation of lamellar bone with superior mechanical properties (Liu, Manjubala et al. 2010; Kerschnitzki, Wagermaier et al. 2011). Secondary lamellar bone formation mainly occurs within the holes which reside in the primarily deposited woven bone type. Also bones from cattle (cow, sheep) and horses need to grow fast. However, in contrast to mice, these animals have high demands on their bones directly after birth. Thus, the fraction of bone featuring superior mechanical competence needs to be high. For this reason, during lateral growth, only thin layers of linear woven bone layers are deposited at which surface highly oriented bone (superior bone quality) can be formed as bone packets building up the fibrolamellar cortex. Since lateral growth of each of those bone packets proceeds to all directions, bone growth is considerably accelerated than compared to lateral growth due to sole apposition on the cortical edges.

6.3 Submicron Mineral Properties in the Vicinity of Osteocytes

So far, only the correlation between osteocyte networks and bone material properties on the cellular level has been addressed in the present work. To add another perspective, murine and fibrolamellar ovine bone samples were examined using scanning small angle x-ray scattering (sSAXS) in order to determine bone material properties on the submicron level. In the following findings from sSAXS experiments at the μSpot beamline at BESSY II, Berlin, Germany as well as at the Nanofocus beamline ID13 at the European Synchrotron Radiation Facility (ESRF), Grenoble, France will be presented and discussed. In both experiments hydroxyapatite particle thickness (T-parameter), particle orientation (Rho-parameter), calcium fluorescence signal (qualitative measure of calcium content) and transmission signal (another measure for the amount of absorbing material which is mainly calcium) is correlated with the osteocyte network geometry. At BESSY II areas were scanned with a resolution of 10 μm, at ESRF scanning could be performed with high resolution step size of 1μm.

6.3.1 Scanning SAXS Measurements at BESSY II with 10 μm Resolution

In murine bone absolute values of mineral particle orientation of the crystallographic c-axis (Rho-parameter) are low in primarily deposited bone material also showing the characteristic rudimentary, unarranged osteocyte networks (Figure 30). Moreover in these areas mineral particles seem to be arranged only in small domains which correspond to the sizes of single osteocytes. In contrast, in secondarily formed lamellar bone, which features highly arranged osteocyte networks over long ranges, the degree of mineral particle orientation is substantially higher. Interestingly, particle orientation is highest in the immediate vicinity of the primarily deposited substrate showing a long range collagen alignment which runs parallel to the surface of its substrate. The thickness of mineral particles (T-parameter) also seems to be different in these two distinct tissues. Unorganized, woven bone rather features smaller T-parameters then compared to lamellar bone. A strong distinction of mineral properties is also observed in the vicinity of the blood vessels. Here mineral crystals are barely oriented and only feature small particle thickness.
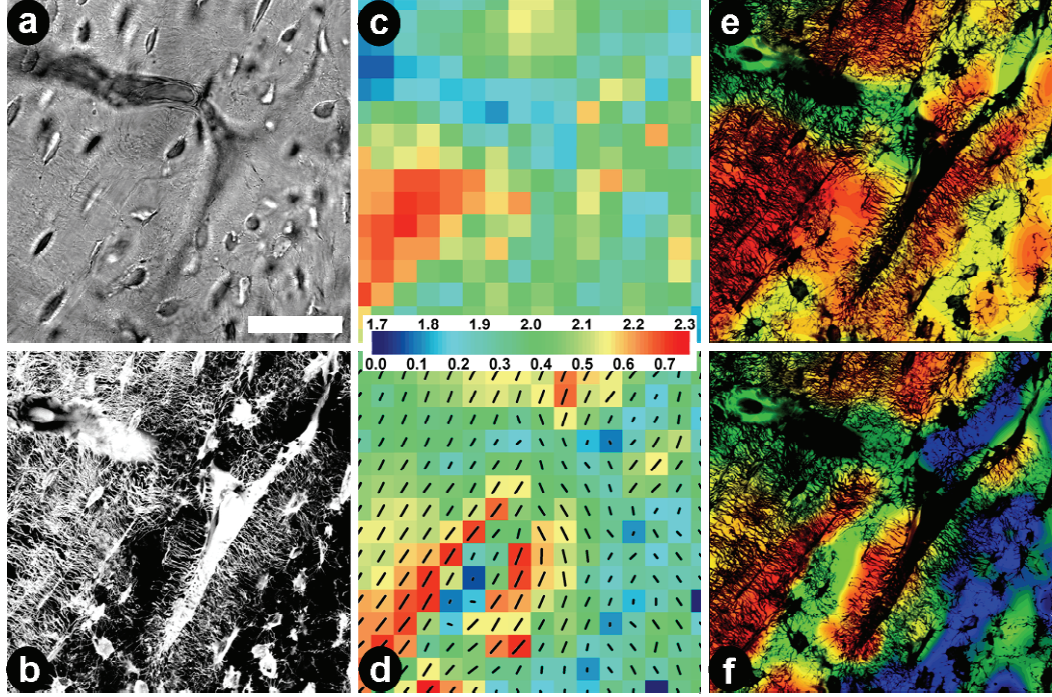
Figure 30: Murine cortical bone showing fractions of unorganized woven and lamellar bone: (a) bright field microscopy, (b) confocal microscopy showing the organization of osteocytes, (c) mineral particle thickness (T-parameter in nm), (d) absolute value and direction of mineral particle orientation (Rho-parameter), (e) shows the correspondence of smoothed T-parameter data with the osteocyte network, (f) correspondence of smoothed Rho-parameter with the osteocyte network. Scale bar: 40 μm

Fibrolamellar ovine bone is a tissue featuring high degrees of uniform material organization, which was also measured on the submicron level with scanning SAXS (Figure 31). Absolute values of mineral particle orientation in the order of 0.75 can be found throughout most of the fibrolamellar tissue. These values are notably higher then compared to murine bone which shows strong local fluctuations in tissue orientation. The mineral particle thickness shows an equivalent behavior. With 2.5 – 3 nm thickness, mineral particles are thicker then compared to those of murine bone which are in the order of 1.8 nm in the woven bone areas and 2.2 nm in areas showing higher structural organization. Only in the vicinity of the blood vessels and in the centre of the fibrolamellar bone packets where the unorganized substrate layers are present, mineral particle orientation as well as particle thickness is substantially lower showing Rho-parameters of only 0.4 and T-parameters of 2.2 nm.
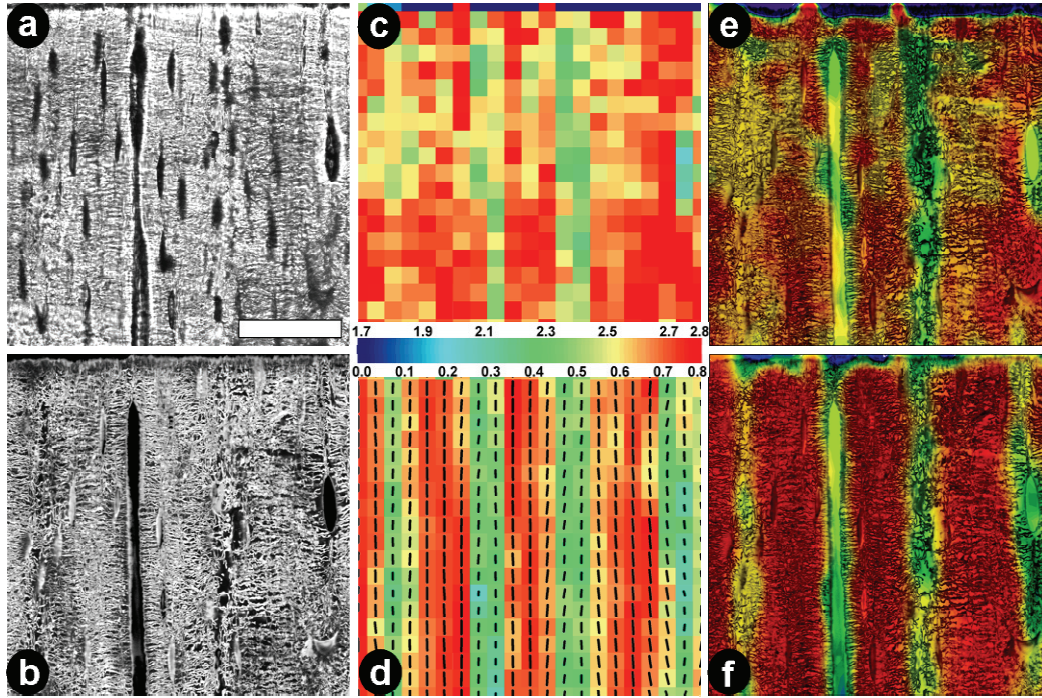
Figure 31: Ovine cortical bone: (a) bright field microscopy, (b) confocal microscopy showing the organization of osteocytes, (c) mineral particle thickness (T-parameter in nm), (d) absolute value and direction of mineral particle orientation (Rho-parameter), (e), (f) shows the correspondence of smoothed T- & Rho-parameter data with the osteocyte network, respectively. Scale bar: 60 μm

Measurement of the material properties of the submicron level in different bone types confirms the strong correspondence between the extracellular collagen matrix organization and the arrangement of the osteocyte network. It could be confirmed that primarily deposited bone which serves merely as a substrate for subsequent lamellar bone deposition is highly unorganized and tissue organization in this woven bone type is rather aligned in single domains than over long ranges (Kerschnitzki, Wagermaier et al. 2011). Furthermore, scanning SAXS offers the unique possibility to measure the difference of mineral particle thickness in different tissues (Fratzl, Fratzl-Zelman et al. 1991; Fratzl, Groschner et al. 1992). In woven bone, which is highly mineralized, mineral particles are rather small as compared to less mineralized highly organized lamellar bone. Intriguingly, in both tissue types mineral particles in the proximity of the blood vessels are substantially thinner and less oriented then those residing in the bulk of the material. However, resolution of scans was rather low due to the relatively large beam size

of more then 10 μm. Thus gradients in the material properties around relatively large structures such as blood vessels or areas of different bone tissue types could just coarsely be measured. Potential gradients around smaller structures such as osteocytes or even canaliculi could not be resolved. For this purpose, high resolution scans with beam sizes in the submicron range are needed.

6.3.2   Scanning SAXS Measurements at ESRF with 1 μm Resolution

Scanning SAXS measurements with an effective scan resolution of 1 μm was performed on fibrolamellar ovine and murine rat bone sections. Due to high scanning resolution, measured areas with sizes in the order of 200×150 μm consisted of approximately 30.000 data points which were analyzed for both, mineral particle orientation and thickness (Figure 32). Transmission scans of fibrolamellar bone packets show local beam absorption up to 10% of the initial intensity – very low absorption at blood vessels, where substantially less material is present and higher absorption with some variations within the bulk of the material which, however, can not be related to macroscopic structures such as osteocyte lacunae, visualized with confocal microscopy. Nevertheless, high resolution mapping of mineral particle orientation and thickness shows a good correlation with structural features of the bone material and exhibits interesting information on bone material properties in relation to the osteocytes.

These measurements confirm the distinct structural organization of bone material in the proximity of blood vessels and primarily deposited substrate material, which was already suspected due to low resolution measurements at μSpot at BESSY II. In substrate material, values of mineral thickness and orientation are in the range of about 2.2 nm and 0.4, respectively. T-parameters at blood vessels are continuously increasing in lateral direction from approximately 1.6 nm up to values of about 3 nm further away. This gradient is apparent up to the third osteocyte layer at which T-parameter values reach the average particle thickness which is present in the bulk. Gradients in the absolute values of mineral orientation range from approximately 0.2, directly at the blood vessel, to 0.5 up to the first osteocyte layer. Furthermore, gradients are also visible in the proximity of osteocytes with thinner and less oriented particles in the immediate vicinity of osteocytes (Figure 33).
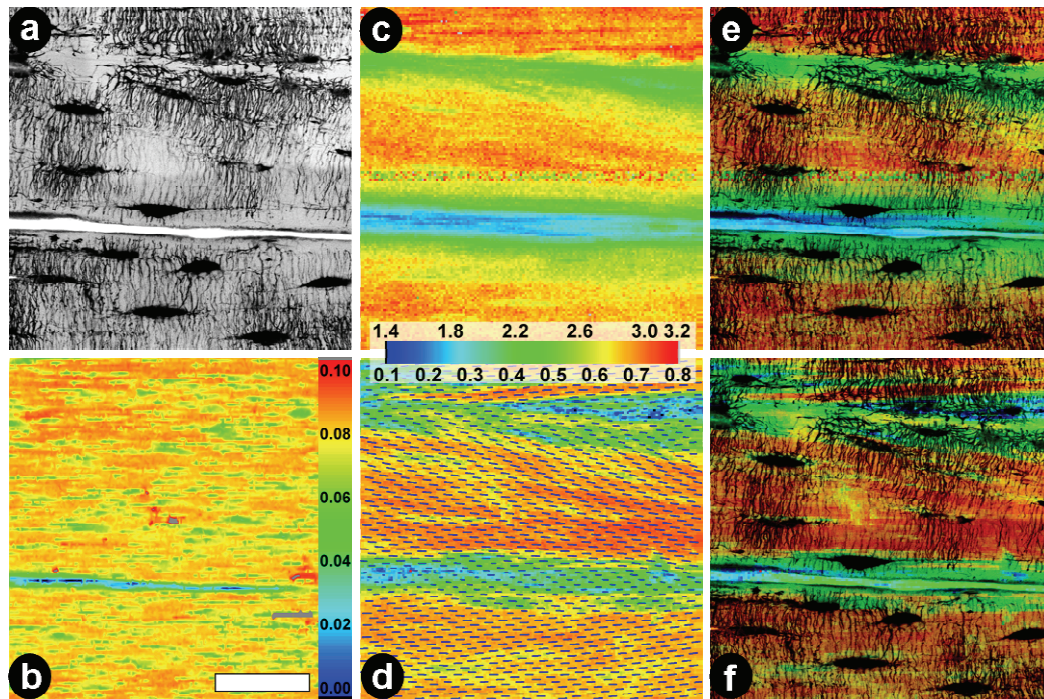
Figure 32: Overview of a SAXS scan (1 µm resolution) in ovine cortical bone: (a) confocal microscopy showing the organization of osteocytes, (b) transmission scan showing variations of beam absorption within in bulk of bone, (c) mineral particle thickness (T-parameter), (d) absolute value and direction of mineral particle orientation (Rho-parameter), (e), (f) shows the correspondence of T- & Rho-parameter data with the osteocyte network, respectively. Scale bar: 30 µm

Intriguingly, in poorly organized, primarily deposited bone (substrate material), which also shows unorganized osteocyte network with a considerably lower amount of interconnecting canaliculi, a different correlation between the osteocytes and the bone material arises. Here, the average of mineral particles, showing a thickness in the range of 2.3 nm, is thinner as compared to highly organized bone (around 3 nm). Only some mineral in the vicinity of the osteocytes or their cell processes, shows an elevated particle thickness which is even in the range of the average particle thickness in highly organized bone. This relation becomes even more apparent after plotting the distance between mineral and the nearest cell which can be calculated from the CLSM-images. Here a strong correlation between large T-parameters and short mineral – cell distances can be found (Figure 34).
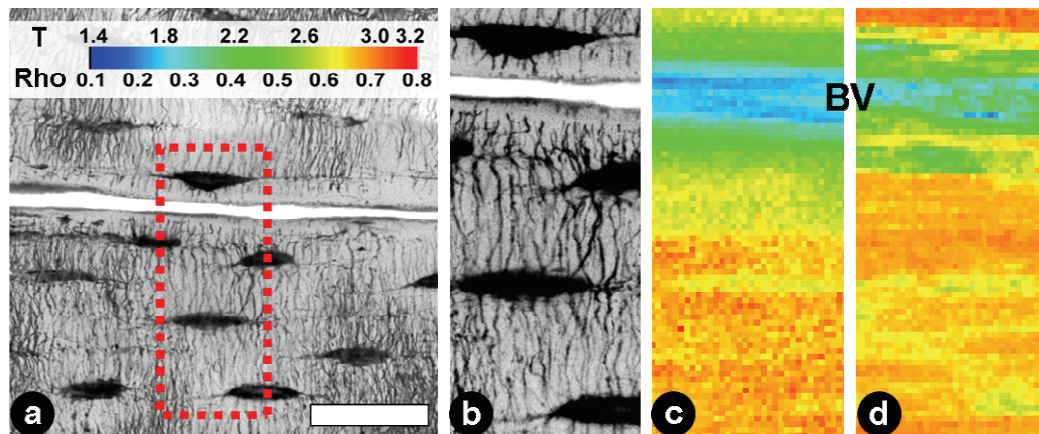
Figure 33: Mineral particles thickness and orientation around cells and blood vessels: (a) overview CLSM, (b) CLSM of magnified area, (c) particle thickness (T in nm) map showing large gradients around the blood vessel (BV) and little alterations in the proximity of osteocytes, (d) particle orientation (Rho) map showing corresponding behavior to T. Scale bar: 40 µm
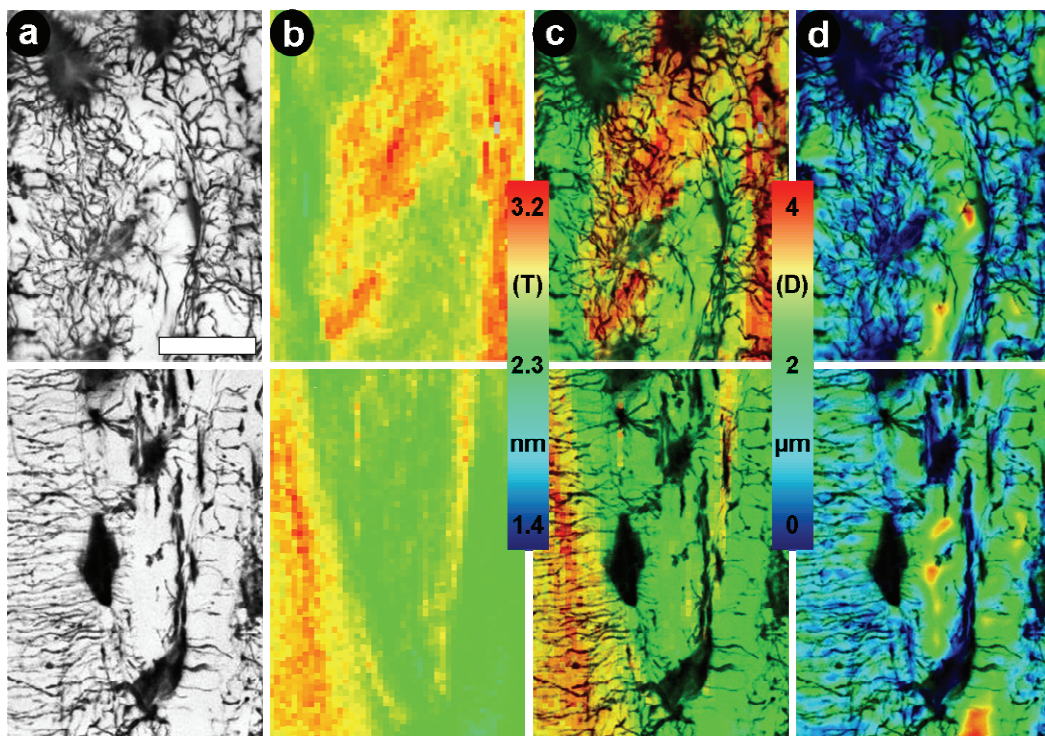
Figure 34: Correlation of mineral particle thickness -T- and cell mineral distance -D- in unorganized bone: (a) CLSM image, (b) T-parameter, (c) T merged with CLSM, (d) Distance merged with CLSM). Mineral particle thickness is elevated in areas of short cell mineral distances. Scale bar 20 µm.

6.3.3   Implications on the Interaction between Osteocytes and Mineral

Scanning SAXS measurements on murine and fibrolamellar bone shows an interesting local inhomogeneity of submicron material properties. During low resolution scans, only correlations between osteocyte network arrangements and material organization on large scale (10 μm resolution) could be shown. However, scans at ID13 at ESRF with a resolution of 1 μm reveal high local correspondence between mineral particle thickness and degree of mineral orientation. These mineral properties show strong alterations in the proximity of the cells as compared to areas further away from osteocytes.

This firstly becomes apparent in highly organized parts of the fibrolamellar bone packets which consist of parallel fibred and lamellar bone (Currey 2002). Here osteocytes are organized in linear cell layers over large distances (Kerschnitzki, Wagermaier et al. 2011). Moreover, osteocytes are interconnected via a tremendous number of homogeneously distributed canaliculi running perpendicularly to the osteocyte layers. Bone mineral residing in between two distinct cell layers – thus, within one bone lamella – shows homogeneous mineral particle thickness and orientation. Whereas in the immediate vicinity of osteocyte lacunae and even within the linear layers in which osteocytes reside, bone mineral particle thickness as well as orientation is considerably decreased (Figure 35, Figure 36).

The structural organization of lamellar bone (Weiner and Bar-Yosef 1990; Weiner and Wagner 1998) shows that bone mineral in the proximity of osteocytes is organized differently then compared to material further away. This leads to the consideration that, apart from mechanical implications, this material could be synthesized in a way, such as to be better suited for cell – mineral interactions. Furthermore, due to the uniform spatial distribution of canaliculi within bone lamellae, bone material is well controlled by the cells, leading to homogeneous mineral properties.
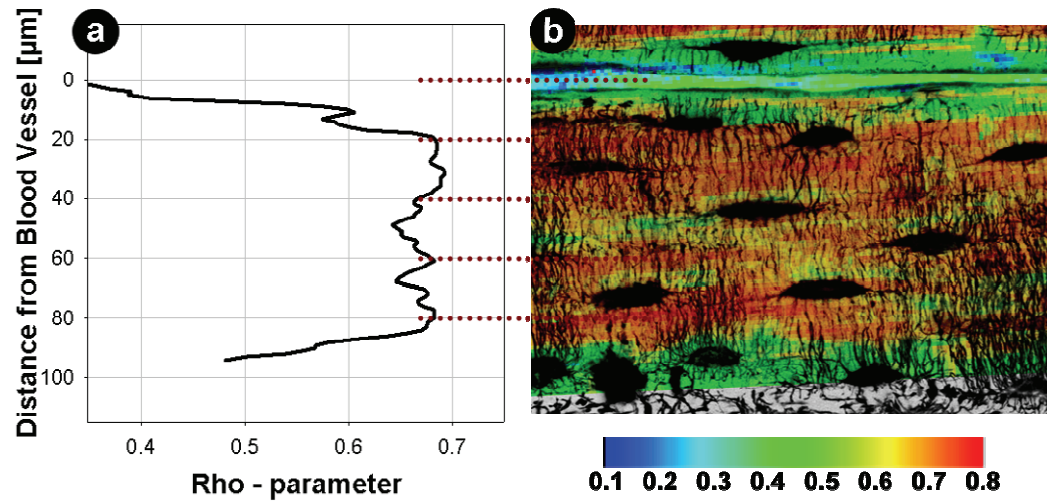
Figure 35: Averaged Rho-parameter as a function of the distance to the blood vessel: (a) plot shows lower particle orientation in the vicinity of the blood vessel (top) and in the substrate layer (bottom), note the lamellar arrangement of Rho in between osteocyte layers. (b) shows the corresponding Rho-parameter map.

Gradients in bone mineral properties in respect to osteocytes are also revealed in unorganized woven bone, present in the murine cortex or in substrate layers of fibrolamellar ovine bone. Even though, this bone type is known to be highly mineralized (Weiner and Wagner 1998; Currey 2002), the average mineral particle thickness is substantially lower then compared to highly arranged, lower mineralized lamellar bone. This denotes that during rapid processes of mineralization in woven bone more mineral crystals are nucleating simultaneously to faster reach high degrees of mineralization. Consequently, due to spatial constrains, higher packing of particles leads to smaller final mineral particle dimension. These assumptions are in line with findings from other studies in growing murine bone, in which bone mineral in different developmental stages shows thinner and smaller mineral particles in younger animals (higher fractions of unorganized woven bone). However, in older animals (higher fractions of organized lamellar bone – (Enlow 1962; Price, Herman et al. 2005) longer and thicker mineral particles were found (Lange, Li et al. 2011).

However, in unorganized woven bone mineral properties in the vicinity of osteocytes, which solely arrange to a poorly oriented osteocyte network, are altered. Here, higher mineral particle thickness is found in areas featuring short distances

to neighboring osteocytes or their cell processes. Areas which are further away from cells and in which canaliculi are absent (higher mineral – cell distances) only contain thinner mineral particles. Additional correlations of the mineral content with cell – mineral distances (see chapter 6.1.4) which are substantially lower in the proximity of cells, further imply that osteocyte are capable to directly control mineral properties in their vicinity.
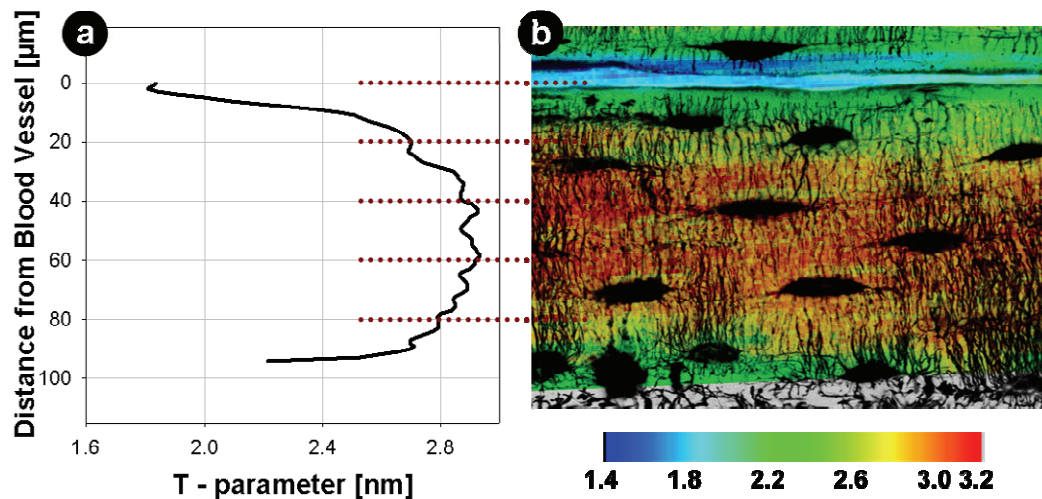
Figure 36: Averaged T-parameter as a function of the distance to the blood vessel: (a) plot shows lower particle thickness in the vicinity of the blood vessel (top) and in the substrate layer (bottom), note the lamellar arrangement of T in between osteocyte layers. (b) shows the corresponding T-parameter map.

Another interesting finding is the large lateral increase of mineral particle thickness (Figure 36) and orientation around blood vessels. Whereas mineral orientation is only altered in bone material within an area up to the first osteocyte layer, mineral particle thickness shows a strong increase up to the third layer. This leads to the assumption that – apart from mechanical implications – this bone tissue in the proximity of blood vessels could additionally serve as a reservoir for fast mineral exchange.

This consideration could explain unpublished findings in the fibrolamellar ovine cortex during fracture healing. Here, during early stages of healing, even without the presence of intracortical resorption by osteoclasts, mineralization of individual bone packets close to the fracture gap is decreasing around blood vessels.

Furthermore, scanning SAXS measurements show a continuous decrease of mineral particle thickness within the cortex during these stages of healing (Liu, Manjubala et al. 2010). Since osteoclasts, which are usually considered to be responsible for bone resorption and demineralization, are not present in that case, osteocytes might control the early "leaking" of mineral in situations of immediate calcium demands such as during early stages of fracture healing (Teti and Zallone 2009; Bonewald 2011).

6.4 Passive Mineral Extraction

High resolution measurements of submicron mineral properties in respect to osteocyte networks imply a potential interaction between osteocytes and their surrounding mineral, in particular that osteocytes can extract mineral from their mineralized vicinity. This hypothesis of osteocytic bone resorption – "Osteocytic Osteolysis" – was firstly formulated in the 1960s (Belanger 1969) and has been intensively reviewed recently (Bonucci 2009; Teti and Zallone 2009; Bonewald 2011). However, how osteocytes could demineralize bone in their vicinity is not known. Whereas conventional bone resorption by osteoclasts happens at highly acidic pH-values locally concentrated within the sealing zone of the osteoclast (Blair 1998), osteocytes are not capable of creating such highly acidic environments. Thus, potential processes of osteocytic osteolysis have to occur in a physiological environment, at pH-values in the range of 7.

In this chapter, the idea of passive mineral extraction will be described and discussed. This passive process to dissolve mineral from surfaces of the osteocyte network occurs solely due to chemical interaction between calcium rich bone mineral and calcium poor sodium chloride solution, even at physiological pH-values. Hereby bivalent calcium ions at the surface of hydroxyapatite mineral crystals get exchanged by monovalent sodium ions from solution (Bell, Posner et al. 1973). In the following, findings from back-scattered electron imaging as well as quantitative high resolution ptychographic x-ray tomography on bone samples after chemical treatment with sodium chloride solution will be shown. These techniques in particular are capable of revealing modest alterations of the mineral content in respect to microscopic bone structures such as blood vessels, osteocyte lacunae or canaliculi. Furthermore results from scanning SAXS measurements will help to understand, how submicron mineral properties are altered due to this chemical treatment.

6.4.1 Gradients in Mineral Content around Microscopic Structures after Passive Dissolution

In fibrolamellar ovine bone sections, after treatment in physiological sodium chloride solution (NaCl), back-scattered electron imaging reveals strong gradients in the degree of bone mineralization around macroscopic as well as microscopic mineral surfaces at blood vessels, osteocyte lacunae and canaliculi. However, only surfaces in the vicinity of macroscopic cutting edges of the sample are affected. Whereas, at cutting edges, gradients of demineralization are apparent over distances up to 40 μm, gradients around blood vessels are substantially smaller – in the range of 5 μm. Gradients around osteocytes and canaliculi are only apparent within the immediate vicinity of macroscopic cutting edges showing penetration depths of single microns (Figure 37).
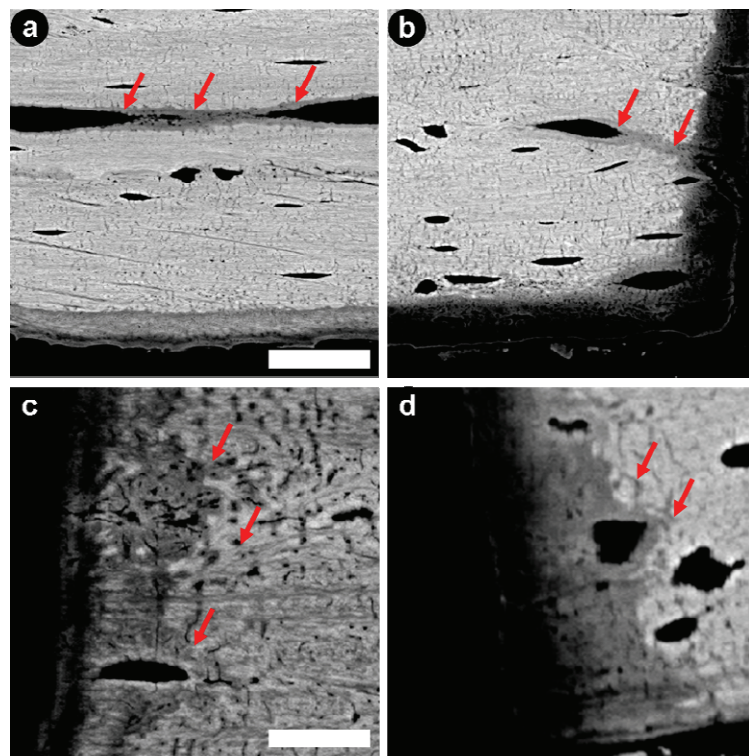
Figure 37: Back-scattered imaging of NaCl treated bone sections showing strong mineral dissolution at macroscopic cut edges, around blood vessels denoted by red arrows in (a) & (b) and around osteocyte lacunae as well as canaliculi denoted by red arrows in (c) & (d). Scale bars: (a) & (b) 40 μm, (c) & (d) 20 μm.

Application of high resolution ptychographic x-ray tomography further allows a three-dimensional visualization of gradients of bone mineral dissolution as a result of chemical treatment with sodium chloride solution. Hereby, grey level histograms describe bone mineral distribution of distinct cross sections through the gradient. Intriguingly, the degree of mineralization close to macroscopic edges does not increase consistently but shows wavy patterns (Figure 38), which are also visible in two-dimensional back-scattered electron imaging (Figure 37c, d). These patterns show low mineralization directly at the surface of the treated bone sample, higher mineralization in the immediate vicinity, a further decrease again at larger distances up to approximately 5 μm and finally a continuous increase of mineralization up to a distance in the range of 40 μm at which mineralization reaches same values as compared to those of reference areas which are far away from macroscopic surfaces. Comparable wavy patterns are also present around microscopic structures such as canaliculi and osteocyte lacunae (Figure 38). In particular, this is apparent in areas of lower mineralization (up to 5 μm from the cutting edge). Here the vicinity of canaliculi is visualized to feature higher degrees of mineralization as compared to areas further away. Furthermore, whereas in reference areas, canaliculi are hollow and easy to recognize, canalicular structures within the demineralization gradient, propagating from the macroscopic cutting edges, are hardly to identify, as they seem to be filled with material.
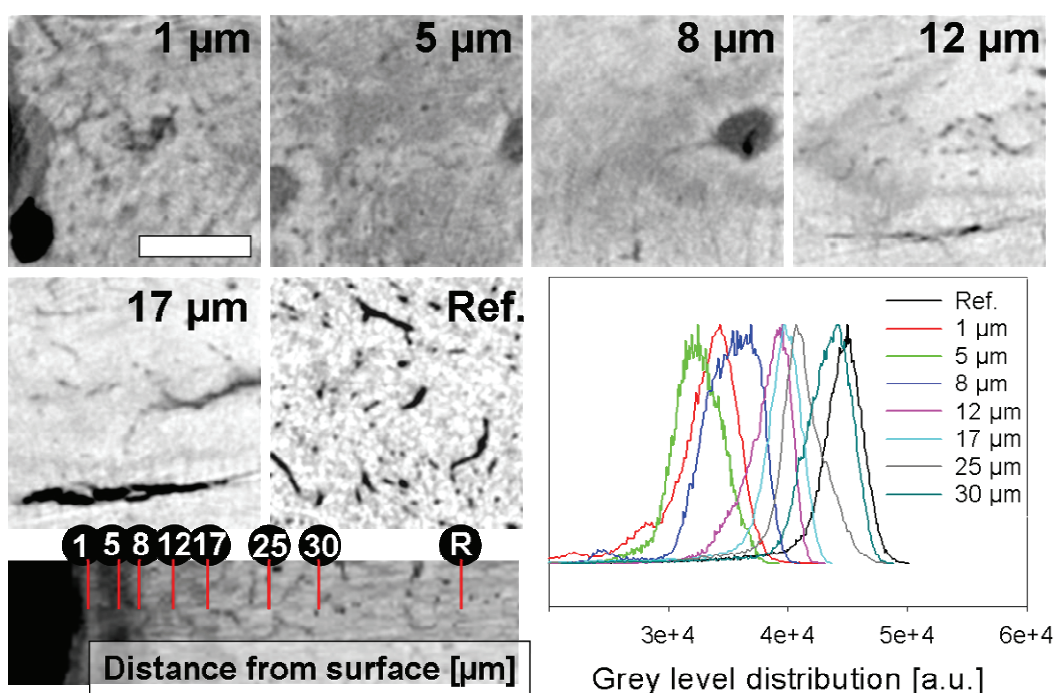
Figure 38: Ptychographic tomography: showing different cross sections at distinct distances (1, 5, 8, 12, and 17 μm – 25, 30 μm not shown) from macroscopic cutting edges. The legend at the bottom schematically shows the individual position of each cross section. The graph at the right shows the grey level distribution of each cross section which is a measure for the bone mineral density distribution at each position. Note halos around microscopical structures (osteocyte lacunae, canaliculi) which are not present in the reference image (Ref.) from a section far away from macroscopic cutting edges. Scale bar: 8 μm.

6.4.2   Submicron Mineral Properties in Areas of Passive Dissolution

To further elucidate the effect of passive dissolution on submicron mineral properties, NaCl treated bone sections were measured at the μSpot beamline at BESSY II with a scanning resolution of 10 μm. In the bulk of the scanned bone sections, the characteristic fibrolamellar organization of blood vessels, modestly arranged substrate layer and highly arranged lamellar bone is apparent. Characteristic fibrolamellar bone motifs are not evident anymore in the vicinity of macroscopic cutting edges, due to major effects of chemical treatment (Figure 39). In affected areas, the calcium fluorescence signal clearly shows a gradient in the mineral content due to passive dissolution propagating from the surface up to a distance of about 60 μm (Figure 39b). Also integral intensities of individual SAXS patterns (scan not shown), which are an additional measure of the amount

of mineral, show a corresponding behavior. Mineral particles are poorly oriented in these areas with low mineral content values of rho in the range of 0.2. However, mineral particles getting better oriented with higher degrees of mineralization (Figure 39c). On the contrary, mineral particle thickness is considerably elevated in the vicinity of the macroscopic cutting surface, showing maximum values in the range of 5 nm (Figure 39d). With increasing mineral content, mineral particle thickness continuously decreases and reaches again normal levels of about 3 nm in highly oriented areas of lamellar bone and 2.2 nm in substrate layers and the vicinity of blood vessels.

6.4.3   Implications on the Feasibility of Passive Mineral Exchange

Passive dissolution experiments reveal the modification of mineral properties due to sole treatment of bone samples with calcium poor sodium chloride solution at a pH value of 7. During treatment, the NaCl solution can easily penetrate bone through the vascular system and the osteocyte network. At internal surfaces sodium ions interact with hydroxyapatite mineral crystals and extract calcium ions even under physiological conditions (Bell, Posner et al. 1973). Hereby, the degree of calcium dissolution from the hydroxyapatite phase is determined by calcium and phosphate saturation of ambient treatment solution.

Indeed, in the vicinity of macroscopic surfaces fresh (unsaturated) solution can easily enter and subsequently be exchanged with treatment-solution which is yet locally saturated with calcium. Due to this enhanced exchange calcium is continuously dissolved from internal bone surfaces without the solution locally becoming saturated. Insufficient exchange of treatment solution leads to local calcium saturation in the bulk of the bone sections due to long distances to outer edges. Thus, further extraction of calcium ions from hydroxyapatite crystals is hampered. As a consequence, the amount of dissolved calcium is not sufficient to create recognizable gradients around internal structures such as blood vessels, osteocyte lacunae and canaliculi which reside in the bulk of the tissue. Only in the vicinity of macroscopic surfaces, featuring enhanced exchange of treatment solution the degree of dissolved calcium becomes apparent by gradients of demineralization visualized by back-scattered electron microscopy as well as ptychographic tomography. In order to obtain homogeneous extraction of calcium ions

from internal surfaces throughout the whole bone section, a continuous flow of fresh sodium chloride treatment solution through the vascular- and osteocyte lacunar porosities is required, in order to prevent the solution from local saturated. During artificial passive dissolution experiments this could be achieved, for example, by application of pressure pumps.
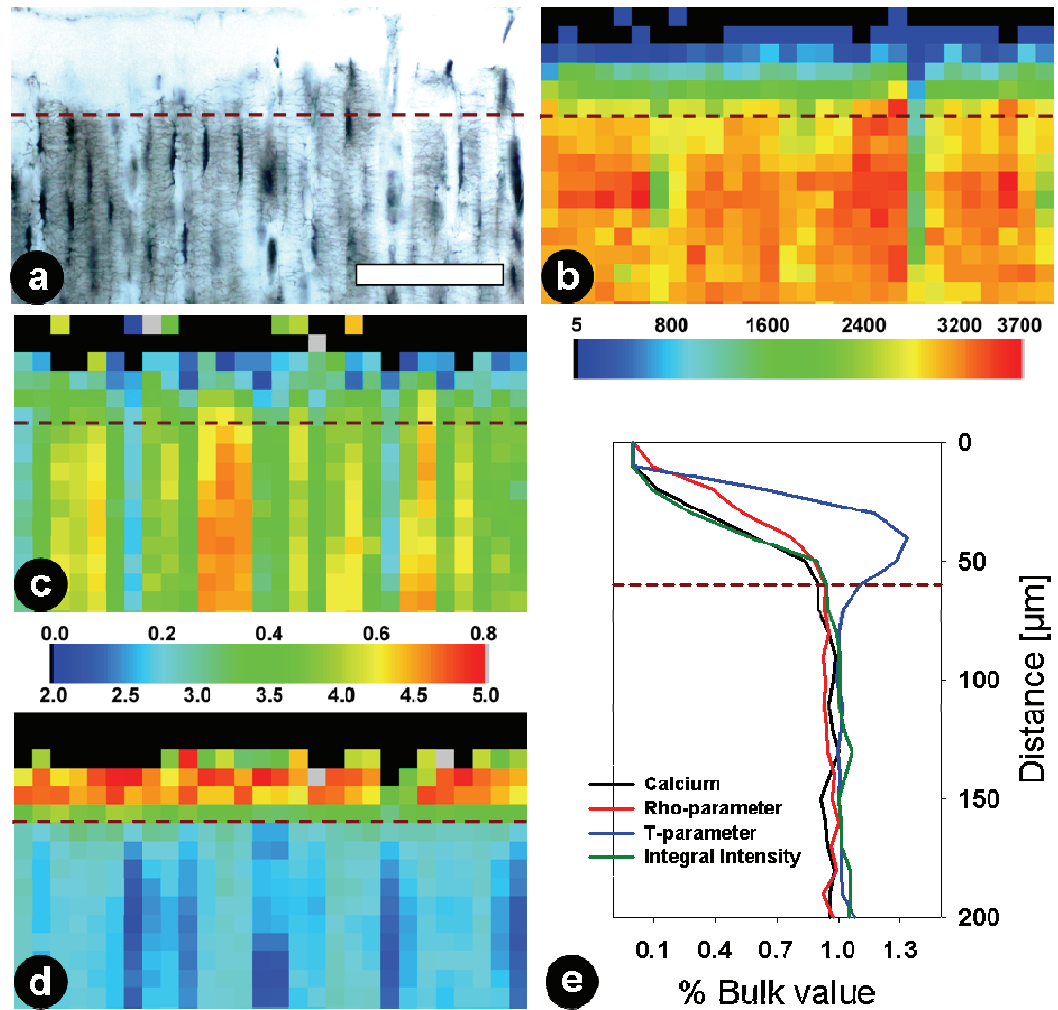

Figure 39: Scanning SAXS measurements on NaCl-treated ovine bone sections: (a) light microscopy image, (b) calcium signal (Ca), (c) mineral orientation (Rho), (d) mineral particle thickness (T), (e) plot of relative values of Ca, Rho-, & T-parameter (averaged over each scan line) compared to the bulk value as a function of the distance to the macroscopic cutting edge. Note gradients in material properties within the area of passive dissolution. Intriguingly, the T-parameter is substantially elevated within this area. Red dashed lines are guides for the eye at 60 μm distance from the macroscopic edge. Scale bar: 80 μm.

Alterations of mineral properties at the submicron scale due to chemical treatment with physiological sodium chloride solution support the idea that local saturation of treatment solution determines the degree of mineral dissolution from the solid hydroxyapatite phase. This becomes apparent at the demineralization front in the vicinity of macroscopic cutting edges of the bone sections. Here, due to dissolution of hydroxyapatite crystals, degree of mineralization (calcium fluorescence and SAXS integral intensities) and also orientation of mineral crystals is decreased. Only values of mineral particle thickness are substantially elevated in those areas. This can be explained by water evaporation within the sample, after removing those from treatment solution. When the amount of water decreases, solution gets supersaturated with dissolved mineral ions und thus spontaneous and uncontrolled reprecipitation of those ions occurs in all areas of decreasing water content. Due to an available scanning resolution of 10 μm during x-ray scattering experiments these effects could only be revealed at large macroscopic cutting surfaces and not around smaller structures such as blood vessels, osteocyte lacunae and canaliculi. Here, the amount of water and reprecipitation of formerly dissolved mineral ions within these structures is not sufficient to create recognizable effects.

These findings not only show the capability of physiological sodium chloride solution to extract calcium ions from bone mineral but also denote interesting implications on living bone tissues. On the cellular level bone is diffused with fluid, residing within spaces between osteocytes and mineralized bone tissue (Weinbaum, Cowin et al. 1994). The main constituent of this body fluid is sodium chloride which is in equilibrium with the solid hydroxyapatite phase and thus, saturated with calcium ions (Neuman 1982; Omelon, Georgiou et al. 2009). Continuous movement of bone fluid through the osteocyte lacunar and canalicular spaces due to internal pressure gradients, as a result of external mechanical stimulation is intrinsically present. This fluid flow is utilized by the osteocytes to sense external mechanical loads on the bone tissue (Cowin 2004). However, apart from mechanical sensation, osteocytes are also known to be capable of controlling calcium and phosphate saturation of the fluid within their vicinity via calcium- and phosphate-ion channels present in their cytoskeleton (Bonewald 2011). For this reason, these cells can directly trigger further ion extraction from the mineral phase by ambient body fluid, just by controlling its calcium and

phosphate saturation (Figure 40). How cells are subsequently dealing with the extracted ions, namely **(i)** how reprecipitation during the presence of high mineral ion concentrations can be inhibited and **(ii)** how these ions can be further transported through the osteocyte network, is not known. Nevertheless, several suggestions exist, such that osteocytes intracellularly store high concentrations of amorphous calcium phosphate in vesicles (Mahamid, Addadi et al. 2011; Mahamid, Sharir et al. 2011) or the extracellular storage of high amounts of calcium ions which get coordinated by polyphosphate molecules (Omelon, Georgiou et al. 2009).
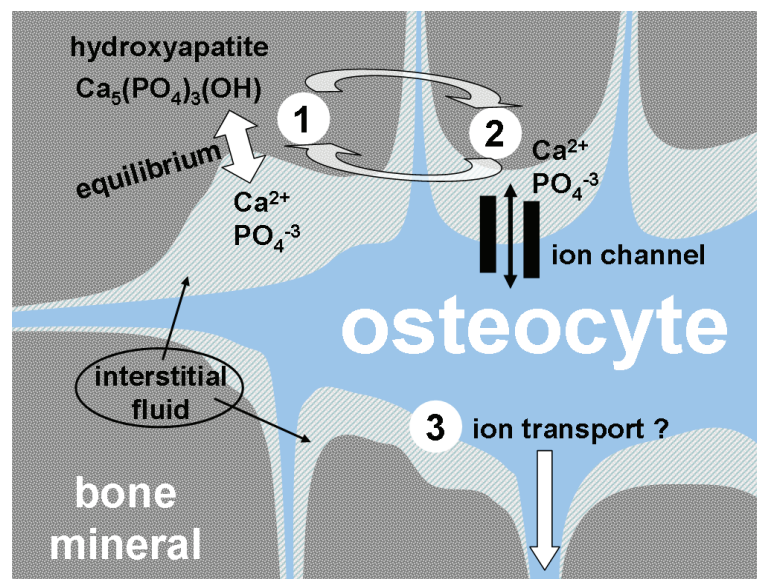
Figure 40: Scheme of osteocyte – material interactions: Between the osteocyte and the mineralized matrix interstitial fluid which is saturated with calcium- and phosphate ions is present (1 - equilibrium). Osteocytic cells can control saturation of interstitial fluid in respect to calcium and phosphate via ion channels (2). Undersaturation leads to further dissolution of hydroxyapatite crystals until resaturation (equilibrium). Mechanisms of further ion transportations through osteocyte network structures (3) are still unknown.

The idea that osteocytes can extract mineral ions just by adjusting levels of calcium and phosphate saturation in the ambient body fluid leads to interesting implications. Data from osteocyte network quantification show, that in case of highly organized bone, 80 % of the mineral is located within a distance of approximately 1 μm from the cells (chapter 6.1.4). Hence, 8 % of mineral resides within an area of only 100 nm which represents the size of a single mineralized

collagen fibril. Demineralization of the first layer of collagen fibrils at mineralized surfaces facilitates access to 8 % of whole body mineral without practically changing mechanical properties of the bone material, respectively impairing bone quality. This shows that passive mineral extraction would be an effective tool for osteocytes to control tissue mineralization and furthermore would enable those cells to directly be involved in processes of body calcium and phosphate homeostasis.

The occurrence of spontaneous and uncontrolled mineral reprecipitation due to evaporation of saturated solution or body fluid further necessitates a reconsideration of findings obtained from high resolution measurements of submicron mineral properties at the ESRF. There it was found that mineral particle orientation and thickness in the direct vicinity of osteocytes is modified. As the samples were measured dry, these different values could be an artifact of uncontrolled mineral reprecipitation due to prior drying. However, even in that case, this would imply the direct influence of osteocytes on bone mineralization which is mediated by the ionic media residing within the spaces between the mineral phase and osteocytes.

6.5 Medullary Bone in Commercial Egg Laying Hens

The most favorable circumstances to study the role of osteocytes during the process of remodeling and regeneration of bone are those when these processes occur under extreme conditions. Such a situation can be found in egg laying hens, in which calcium metabolism is incredibly intense (Dacke, Arkle et al. 1993). Commercial layers transfer about 10% of their total body calcium volume daily to the shell producing machinery in their oviducts, therefore being the most efficient calcium transporters among all vertebrates (Bar 2009). Such an intensive transport mechanism imposes severe demands on ionic calcium homeostasis. Extremely efficient calcium absorption from the food helps providing a substantial amount of the required calcium. After interruption of feeding, when the intestine of the layer is empty of calcium, considerable amounts of Ca^{2+} (20-40 %) must be derived from skeletal reserves (Mueller, Schraer et al. 1964; Zallone and Mueller 1969; Edelstein, Harell et al. 1975). To accommodate these requirements a dramatic change takes place in the bone biology of the hen at the onset of sexual maturity (Whitehead 2004). The function of the layer's osteoblasts changes from laying down cortical bone to producing a woven bone type called medullary bone (Bonucci and Gherardi 1975). This bone, unique to birds and crocodilians (Schweitzer, Elsey et al. 2007) lacks any mechanical function but is intended as a labile calcium source for shell formation (Ascenzi, FranYois et al. 1962). Medullary bone is laid down rapidly during the early stages of the lay within the medullary cavity of long bones, particularly those of the legs. The rapid cycling (25 hours) during which medullary bone is resorbed and then rebuilt makes it an ideal candidate for the study of basic questions associated with the action of osteocytes during the process of bone formation and bone resorption in its most intensive form (Taylor and Belanger 1969; Bonucci and Gherardi 1975).

In the following, preliminary experiments on medullary bone are described and their results are discussed. In this regard alterations of calcium and phosphate blood levels of hens during the egg laying cycle as well as medullary bone mineral properties will be correlated.

6.5.1 Calcium and Phosphate Ion Concentrations in Blood during the Daily Egg Laying Cycle

Alterations of ionic calcium- and phosphate blood concentrations during the daily egg laying cycle nicely show the dynamics of eggshell production (Figure 41). Within the first 6 hours after lay ionic calcium levels continuously increase whereas phosphate levels are maintained. During that time hens have high calcium uptake from food which is poor in phosphate. Calcification of the new eggshell starts 6 hours after lay, clearly apparent in the onset of a strong decrease in ionic calcium, which is in accordance with findings from an earlier study (Singh, Joyner et al. 1986), until normal levels are reached again approximately 10 hours after lay. At that time phosphate blood concentration is substantially elevating. This indicates the presence of strong bone resorption, as due to decomposition of bone mineral calcium as well as phosphate ions are extracted. Whereas calcium is subsequently used for eggshell production (Mueller, Schraer et al. 1964; Zallone and Mueller 1969) and thus levels in blood are maintained, huge amounts of unused phosphate ions lead to an increase in phosphate blood concentration. After approximately 18 hours, phosphate ion concentration reaches again normal levels probably as a consequence of new medullary bone formation. Calcium concentration keeps constant levels until animals start feeding again.
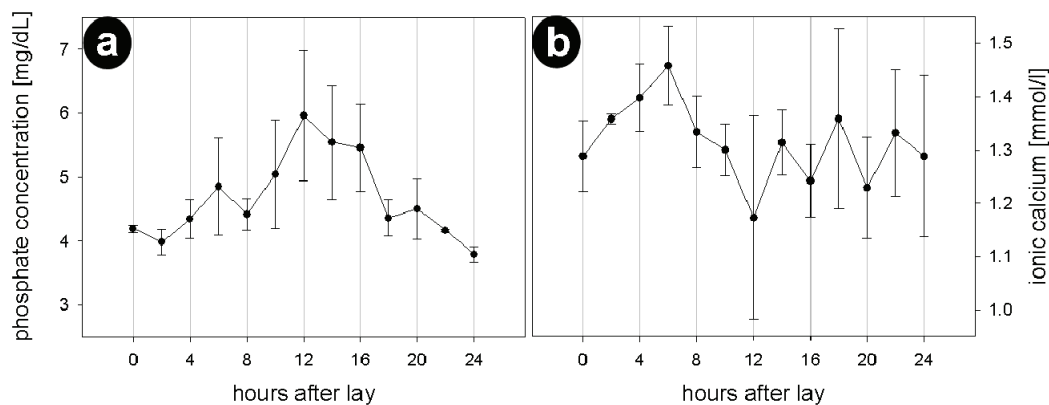
Figure 41: Phosphate (a) and ionic calcium concentration (b) in blood during the egg laying cycle of hens. Phosphate levels peak at 12 hours after lay probably due to the onset of medullary bone resorption. Calcium levels peak at 6 hours after layer due to high calcium uptake from feeding. Error bars represent the standard deviation and show a strong biological variance between individual chicken.

6.5.2   Insights into Medullary Bone Mineral

Rapid turnover rates of medullary bone involve not only extreme cell activity (Bonucci and Gherardi 1975) but potentially also bone material being optimized for fast formation and resorption (Dacke, Arkle et al. 1993). Bone mineral for example could be predominantly present in less stable and more disordered phases such as amorphous calcium phosphate or octacalcium phosphate, which are also known to play an important role during early stages of bone mineralization in mouse or zebrafish bones (Mahamid, Sharir et al. 2008; Mahamid, Aichmayer et al. 2010). During growth of animals it is beneficial to use less stable mineral phases as these are easy to decompose and reshape during later stages of growth. In case of medullary bone, which simply serves as a pool for short-term calcium storage, making use of less stable mineral phases would be feasible too.
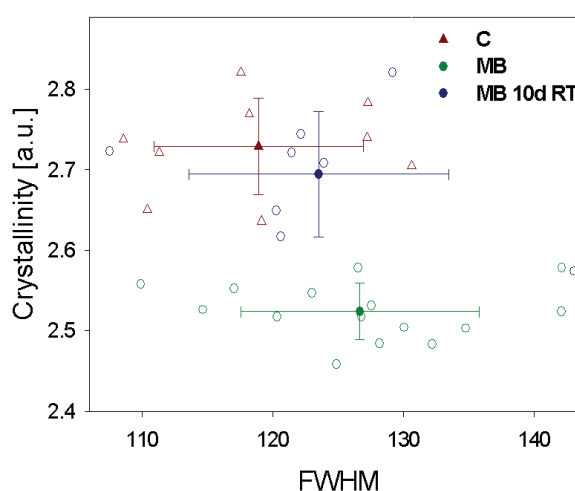
Figure 42: Splitting factors of the phosphate υ_4 double peak describing the crystallinity of medullary bone (MB) mineral and mineral in the cortex (C) of the chicken. Crystallinity is considerably lower in MB as compared to cortical bone. After 10 days storage of MB samples at room temperature (10d RT), crystallinity of MB mineral is substantially elevated almost reaching levels of cortical bone.

Infrared (IR) spectroscopy offers the possibility to measure the presence of less stable, disorganized mineral phases in bone material. Hereby, the splitting of the phosphate υ_4 double peak at wave numbers of about 600 cm^{-1} is a measure of the crystallinity. With other words, the degree of organization of bone mineral which

is smaller in amorphous less stable mineral phases as compared to stable hydroxyapatite mineral crystals.

In chicken bones, IR spectroscopy shows considerably lower crystallinity of medullary bone mineral in the range of 2.5 as compared to cortical bone mineral which shows values of about 2.75 (Figure 42). As a comparison, amorphous calcium phosphates during early stages of zebrafish bone formation also show values of mineral crystallinity in the range of 2.5 whereas in mature bone values in the range of 3 are measured (Mahamid, Sharir et al. 2008). The presence of less stable mineral phases in medullary bone is further supported by the increase of crystallinity to a value of 2.7 after 10 days storage of the samples at room temperature. This indicates that transient phases within medullary bone were already partly transformed to more stable bone mineral. This transformation can be inhibited by appropriate storage of samples in the freezer at -20°C (data not shown).

To gain further insights into medullary bone, cryo-electron microscopy imaging was used to reveal morphological characteristics of mineral present during interaction between cells and the bone material. Therefore fresh medullary bone sections were examined under cryo-conditions to prevent potential alterations in transient mineral phases present in the bone tissue (Figure 43). Intriguingly mineral globules are revealed in areas of bone formation close to osteoblasts, forming mineral islands to subsequently mineralize bone, which is in line with histochemical and electron microscopical investigations (Bonucci and Gherardi 1975). Furthermore, these globules with diameters of approximately 100 nm are found again in the vicinity of osteocytes. Whereas mineral globules bound to membranes in cell vesicles appear sphere like. Those already deposited in bone matrix seem to be rather flake like. In areas featuring rather mature bone (data not shown) these mineral globules are not apparent anymore. However, also the presence of mineral platelets is not recognizable.

Comparison with data from early stages of formation of zebrafish and murine bone in which same morphological mineral characteristics are revealed and proofed to be amorphous mineral phases (Mahamid, Sharir et al. 2008; Mahamid, Aichmayer et al. 2010; Mahamid, Sharir et al. 2011), these data together with IR-

measurements imply, that amorphous phases, which could not be found in an earlier study (Ascenzi, FranYois et al. 1962), might be also present in medullary chicken bone . However, the occurrence of transient highly unstable mineral in medullary bone would not be surprising as this tissue is designed to facilitate a fast response to tremendous calcium demands during the daily cycle of egg shell production (Dacke, Arkle et al. 1993; Bar 2009).

6.5.3 Alteration of Medullary Bone Mineralization during the Egg Laying Cycle

To further elucidate dynamics of medullary bone mineralization and resorption during the egg laying cycle, mineral density distributions at different time points can be measured with three-dimensional quantitative micro CT performed at BAMline at BESSY II. Here exemplarily 2 time points are compared – mineral distribution directly after lay and at a time point 12 hours later (Figure 44).

The distribution of medullary bone mineralization shows high peaks at low degrees of mineralization at both time points. This indicates extreme formation of new bone which has not mineralized yet. Furthermore medullary bone directly after lay shows larger fractions of higher mineralized bone as compared to medullary bone 12 hours after lay. Also maximum values of mineralization are substantially higher directly after lay (16 wt % calcium at 0 hours – 14 wt % calcium at 12 hours). Also chicken cortical bone is plotted as a reference which is not affected during the daily cycle featuring substantially higher degrees of mineralization with an average value of 18 wt % calcium.
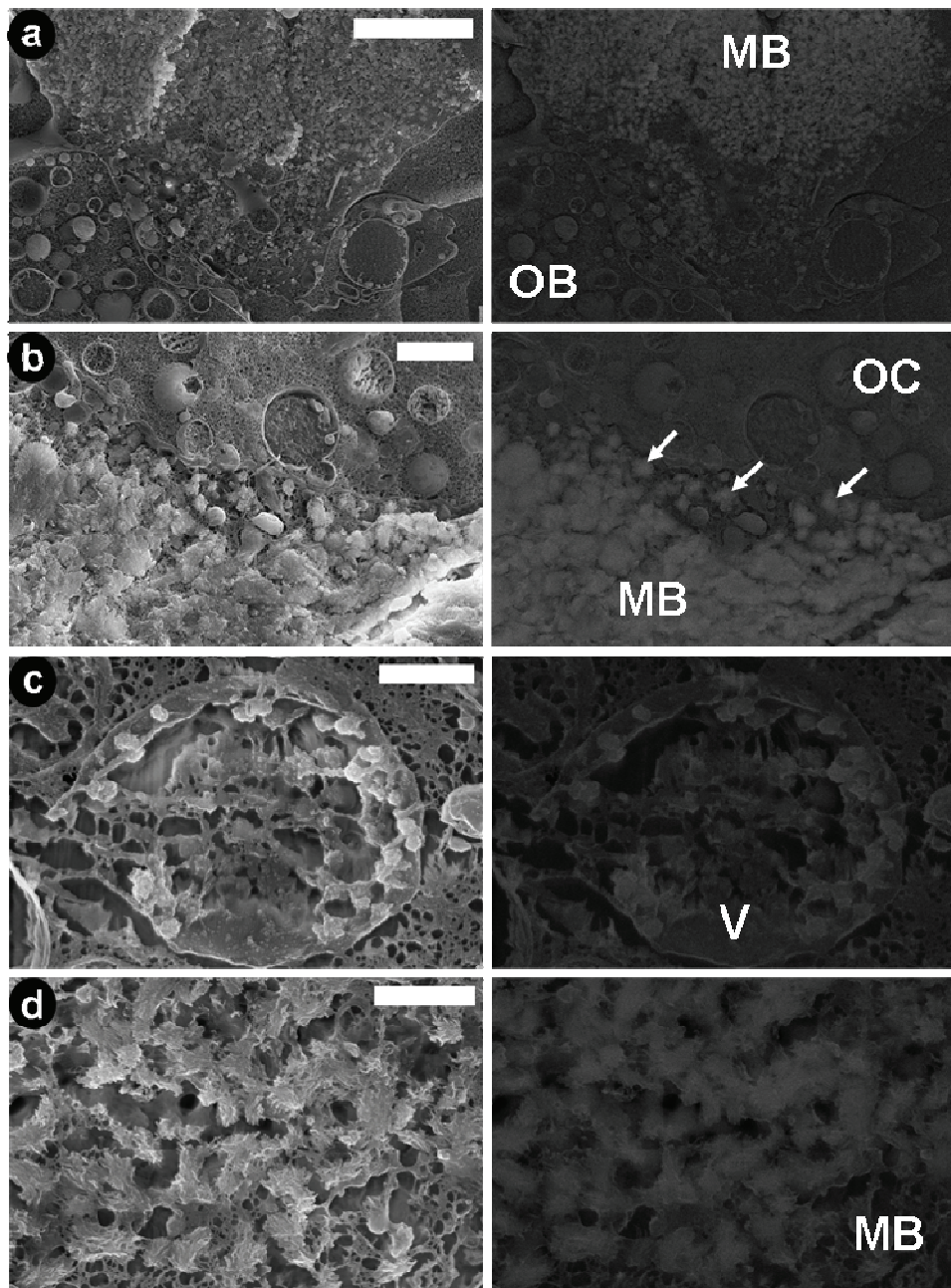
Figure 43: Cryo-electron microscopy showing medullary bone mineralization – secondary electrons (SE) left, back-scattered electrons (BSE) right. (a) An osteoblast (OB) at the surface is mineralizing the medullary bone (MB) packet. Globular mineralization islands are apparent. (b) Also an osteocyte (OC) shows mineral globules in their vicinity. (c) High magnification of mineral globules which are stored in vesicles (V) and bound to the vesicle membrane. (d) High magnification of mineral globules deposited in MB. Scale bars: (a) 3µm, (b) 1µm, (c) & (d) 400nm.
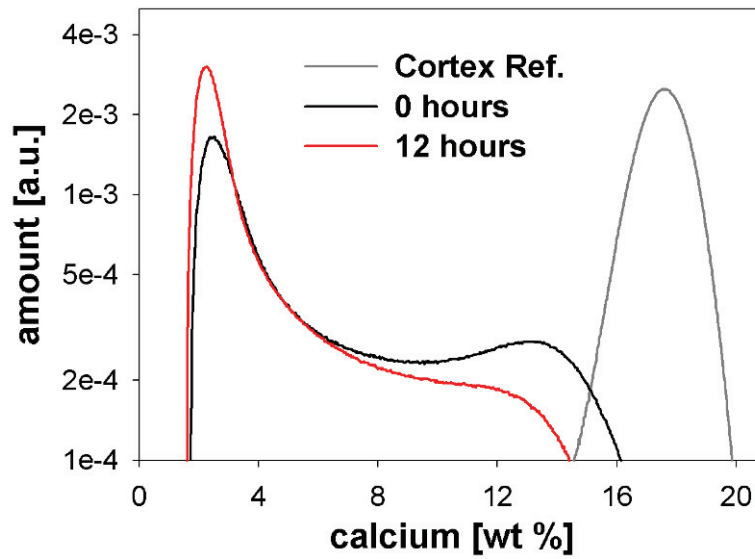
Figure 44: Normalized medullary bone mineral distribution at two different time points and chicken cortical bone as a reference. Directly after lay medullary bone features higher degrees of mineralization as compared to 12 hours after lay. During that time strong medullary bone resorption occurs as calcium is demanded for eggshell production. Both curves show a high peak at lower degrees of mineralization, indicating vast formation of medullary bone at both time points. Mineralization of cortical chicken bone as a reference is substantially higher.

Despite the fact, medullary bone mineral distribution of only two separate time points are analyzed and shown here, these already show good correlation with ionic calcium and phosphate blood concentrations measured in the animals before harvesting their bones. During early stages and even before the lay of the egg, medullary bone forms and mineralizes rapidly (Bloom, Domm et al. 1958) which becomes apparent in the relatively large fractions of higher degrees of mineralization at time point 0. Furthermore animals already started feeding and thus have higher calcium uptake. After 12 hours ionic calcium concentration in the blood reaches its minimum value, additionally phosphate blood concentration peaks at its maximum. This strongly indicates extreme bone resorption to assure extraction of calcium which is subsequently used for eggshell production (Zallone and Mueller 1969; Singh, Joyner et al. 1986). As a consequence, degree of medullary bone mineralization is decreased showing a mineral distribution

with lower fractions at higher degrees of mineralization. Intriguingly at both time points, large fractions of newly formed bone – low degrees of mineralization – are present. This could imply that excessive bone formation occurs during all stages of the daily cycle and thus is in phase with osteoclastic activity. Only when calcium demands for eggshell production decrease during the inactive period, medullary bone can further mineralize as spare calcium is available (Vandevelde, Vermeiden et al. 1984). These findings support the assumption that only the degree of calcification, but not total medullary bone volume does change during the egg-laying cycle (Kusuhara 1976). However, to better understand mineralization dynamics of medullary bone during daily eggshell production, analysis of substantially more samples at different time points is required.

6.5.4 Preliminary Conclusions and Future Experiments

Medullary bone is a fascinating model system, ideal to study processes of bone formation and resorption during situations of extreme calcium demands. Here not only excessive cell activity due to high turnover rates can be studied but also the specification of bone material respectively the mineral properties which need to fit theses dynamic requirements. Preliminary results presented, rather focus on the aspect of mineral properties such as the crystallinity and the mineral density distribution of medullary bone. These already show the dynamic of the system and suggesting the occurrence of different mineral phases which are easier to form and subsequently to resorb, a necessary condition due to the rapid responses of the system. However to understand the full picture, cellular activities during all stages of the daily cycle will be investigated by histological techniques. Furthermore high resolution scanning SAXS to measure submicron mineral properties will be performed to further elucidate how mineral is altered and extracted by the bone cells.

7   Conclusion and Outlook

The objective of this PhD thesis was to test the hypothesis whether osteocytes influence bone material properties in their direct vicinity. In this regard, a combination of techniques to reveal osteocyte network organization together with the measurement of bone ultrastructural properties on the submicron level was applied. In particular, the influence on bone material characteristics of initial cell-cell alignment during the dynamic process of bone formation and remodeling as well as the possibility of subsequent osteocyte-matrix interactions within the mature bone material was investigated.

It could be shown qualitatively that the osteocytic network alignment mirrors the extracellular matrix organization. Furthermore, it was found that formation of a highly oriented collagen matrix requires a collective action of the matrix producing cells, which is facilitated by a substrate layer whose surface directs this process. Thus, it is proposed that the process of bone formation is split into two different phases: (**i**) substrate formation by osteoblasts which are not attached to a surface and (**ii**) the following phase whereby deposition of the oriented collagen matrix is performed by osteoblasts aligned on a surface.

The assumption that initially formed bone can act as an endogenous scaffold which directs lamellar bone deposition was found to hold true also during bone fracture healing. In the context of bone tissue engineering, this reinforces the idea that scaffolds mimicking the primary bone architecture may be developed to accelerate bone regeneration in critical defect filling, for example.

Initial cell alignment during bone formation has not only a strong influence on matrix organization during growth but may also be important during bone maintenance processes within mature bone material. In highly organized bone, osteocyte networks are arranged to feature short mean mineral cell distances in order to better control mineral characteristics. This idea is supported by the obtained submicron mineral properties in different bone types, featuring different degrees of osteocyte network arrangement. These findings show that mineral properties such as particle thickness and arrangement show different values in the vicinity

of the cells as compared to tissue in which network organization results in longer distances between the cells and the mineral. This leads to interesting considerations regarding the role of bone remodeling. Remodeling predominantly transforms a less arranged, earlier formed bone type into a highly organized lamellar bone. The newly formed tissue shows higher potential of controlling bone mineral characteristics in the bulk due to highly organized osteocyte networks and thus, short mineral-cell distances. Hence, remodeling can not only be understood as a process to remediate cracks, or to adapt to external mechanical stimuli, but also to increase the efficiency of potential osteocyte-mineral interactions during bone homeostasis.

However, how osteocytes in particular can control mineral characteristics in their vicinity remains unclear. In this thesis, mechanisms of passive mineral dissolution were investigated, a process that results from the chemical interaction under physiological conditions between the solid mineral phase and the surrounding ionic medium. It could be shown that considerable amounts of calcium can be extracted from the mineralized surfaces of the osteocyte network by sole treatment with physiological sodium chloride (NaCl) solution unsaturated in calcium. Comparable mechanisms could be present during bone homeostasis in the body, whereby osteocytes could act as ionic membranes, controlling mineral ion saturation of the surrounding ionic medium (body fluid) und thus directly trigger mineral extraction from the hydroxyapatite phase. As this process occurs at mineralized surfaces, this further shows the importance of highly organized osteocyte networks in bone, maximizing the surface area to the exposed mineral.

Finally, medullary bone as a model system was investigated. Here preliminary results indicate that vast cell activity during tremendous turnover of calcium ions for eggshell production is only one part of the full picture. Furthermore, bone material properties must be specifically adapted to fit the requirements for rapid bone resorption as well as re-formation.

Moreover, a visualization technique to exhibit osteocyte network organization with confocal laser scanning microscopy, together with sample preparation techniques to allow concomitant measurement of bone material characteristics with complementary experimental techniques, was developed. The conclusion that

osteocyte network organization mirrors matrix organization and even to some extent submicron mineral properties, further allows predicting mineral properties solely based on the osteocyte network arrangement. This can be beneficial as this imaging technique is relatively fast and easy to apply as compared to sophisticated experimental techniques, such as x-ray microtomography, to measure submicron mineral properties.

However, for future experiments it would be intriguing to investigate the relation of an alteration of osteocyte network organization and the resulting modification of bone material properties such as matrix orientation and mineralization during aging and diseases related to dysfunctional bone mineral homeostasis. Those experiments could further clarify the impact of osteocyte network organization in conjunction with osteocyte activity on bone tissue characteristics determining bone quality as well as bone fragility. If this hypothesis proves to be true, osteocytes must be considered more urgently as a target for drug development in the context of bone diseases featuring deficient bone mineral homeostasis such as osteoporosis.

8   References

Aarden, E. M., E. H. Burger, et al. (1994). "Function of Osteocytes in Bone." Journal of Cellular Biochemistry **55**(3): 287-299.

Ascenzi, A., C. FranYois, et al. (1962). "On the Bone Induced by Estrogens in Birds." 5th International Congress for Electron Microscopy Philadelphia **2**: QQ 11.

Asscher, Y., S. Weiner, et al. (2011). "Variations in Atomic Disorder in Biogenic Carbonate Hydroxyapatite Using the Infrared Spectrum Grinding Curve Method." Advanced Functional Materials **21**(17): 3308-3313.

Bar, A. (2009). "Calcium Transport in Strongly Calcifying Laying Birds: Mechanisms and Regulation." Comparative Biochemistry and Physiology a-Molecular & Integrative Physiology **152**(4): 447-469.

Baud, C. A. (1962). "Morphologie Et Structure Inframicroscopique Des Osteolytes." Acta Anatomica **51**(3): 209-&.

Baylink, D., J. Wergedal, et al. (1971). "Formation,Mineralization, and Resorption of Bone in Hypophosphatemic Rats." Journal of Clinical Investigation **50**(12): 2519-&.

Belanger, L. F. (1969). "Osteocytic Osteolysis." Calcified Tissue Research **4**(1): 1-&.

Bell, L. C., A. M. Posner, et al. (1973). "Point of Zero Charge of Hydroxyapatite and Fluorapatite in Aqueous-Solutions." Journal of Colloid and Interface Science **42**(2): 250-261.

Blair, H. C. (1998). "How the Osteoclast Degrades Bone." Bioessays **20**(10): 837-846.

Bloom, M. A., L. V. Domm, et al. (1958). "Medullary Bone of Laying Chickens." American Journal of Anatomy **102**(3): 411-453.

Boivin, G., P. Mesguich, et al. (1987). "Ultrastructural Immunocytochemical Localization of Endogenous 1,25-Dihydroxyvitamin-D3 and Its Receptors in Osteoblasts and Osteocytes from Neonatal Mouse and Rat Calvaria." Bone and Mineral **3**(2): 125-136.

Bonewald, L. F. (2007). "Osteocytes as Dynamic Multifunctional Cells." Skeletal Biology and Medicine, Pt A **1116**: 281-290.

Bonewald, L. F. (2011). "The Amazing Osteocyte." Journal of Bone and Mineral Research **26**(2): 229-238.

Bonewald, L. F. and M. L. Johnson (2008). "Osteocytes, Mechanosensing and Wnt Signaling." Bone **42**(4): 606-615.

Bonucci, E. (1990). The Histology Histochemistry and Ultrastructure of Bone. Pecile, A. And B. De Bernard**:** 15-38.

Bonucci, E. (2009). "The Osteocyte: The Underestimated Conductor of the Bone Orchestra." Rendiconti Lincei-Scienze Fisiche E Naturali **20**(3): 237-254.

Bonucci, E. and G. Gherardi (1975). "Histochemical and Electron-Microscope Investigations on Medullary Bone." Cell and Tissue Research **163**(1): 81-97.

Boyde, A. and S. J. Jones (1996). "Scanning Electron Microscopy of Bone: Instrument, Specimen, and Issues." Microscopy Research and Technique **33**(2): 92-120.

Buckwalter, J. A., M. J. Glimcher, et al. (1995). "Bone Biology .2. Formation, Form, Modelling, Remodeling and Regulation of Cell-Funtion." Journal of Bone and Joint Surgery-American Volume **77A**(8): 1276-1289.

Burger, E. H. and J. Klein-Nulend (1999). "Mechanotransduction in Bone - Role of the Lacuno-Canalicular Network." <u>Faseb Journal</u> **13**: S101-S112.

Burr, D. B., M. B. Schaffler, et al. (1988). "Composition of the Cement Line and Its Possible Mechanical Role as a Local Interface Inhuman Compact-Bone." <u>Journal of Biomechanics</u> **21**(11): 939-&.

Busse, B., D. Djonic, et al. (2010). "Decrease in the Osteocyte Lacunar Density Accompanied by Hypermineralized Lacunar Occlusion Reveals Failure and Delay of Remodeling in Aged Human Bone." <u>Aging Cell</u> **9**(6): 1065-1075.

Chen, J. H., C. Liu, et al. (2010). "Boning up on Wolff's Law: Mechanical Regulation of the Cells That Make and Maintain Bone." <u>Journal of Biomechanics</u> **43**(1): 108-118.

Cowin, S. C. (2004). "Tissue Growth and Remodeling." <u>Annual Review of Biomedical Engineering</u> **6**: 77-107.

Currey, J. D. (2002). <u>Bones : Structure and Mechanics</u>. Princeton [N.J.], Princeton University Press.

Currey, J. D. (2003). "The Many Adaptations of Bone." <u>Journal of Biomechanics</u> **36**(10): 1487-1495.

Dacke, C. G., S. Arkle, et al. (1993). "Medullary Bone and Avian Calcium Regulation." <u>Journal of Experimental Biology</u> **184**: 63-88.

Dierolf, M., A. Menzel, et al. (2010). "Ptychographic X-Ray Computed Tomography at the Nanoscale." <u>Nature</u> **467**(7314): 436-U82.

Duncan, R. L. and C. H. Turner (1995). "Mechanotransduction and the Functional-Response of Bone to Mechanical Strain." <u>Calcified Tissue International</u> **57**(5): 344-358.

Ebacher, V. and R. Z. Wang (2009). "A Unique Microcracking Process Associated with the Inelastic Deformation of Haversian Bone." <u>Advanced Functional Materials</u> **19**(1): 57-66.

Edelstein, S., A. Harell, et al. (1975). "Functional Metabolism of Vitamin-D in Chicks Fed Low-Calcium and Low-Phosphorus Diets." <u>Biochimica Et Biophysica Acta</u> **385**(2): 438-442.

Enlow, D. H. (1962). "A Study of Post-Natal Growth and Remodeling of Bone." <u>American Journal of Anatomy</u> **110**(2): 79-&.

Everts, V., W. Beertsen, et al. (1988). "Effects of the Proteinase-Inhibitors Leupeptin and E-64 on Osteoclastic Bone-Resorption." <u>Calcified Tissue International</u> **43**(3): 172-178.

Franz-Odendaal, T. A., B. K. Hall, et al. (2006). "Buried Alive: How Osteoblasts Become Osteocytes." <u>Developmental Dynamics</u> **235**(1): 176-190.

Fratzl, P., N. Fratzl-Zelman, et al. (1993). "Collagen Packing and Mineralization - an X-Ray-Scattering Investigation of Turkey Leg Tendon." <u>Biophysical Journal</u> **64**(1): 260-266.

Fratzl, P., N. Fratzl-Zelman, et al. (1991). "Nucleation and Growth of Mineral Crystals in Bone Studied by Small-Angle X-Ray-Scattering." <u>Calcified Tissue International</u> **48**(6): 407-413.

Fratzl, P., M. Groschner, et al. (1992). "Mineral Crystals in Calcified Tissues - a Comparative-Study by Saxs." <u>Journal of Bone and Mineral Research</u> **7**(3): 329-334.

Fratzl, P., H. S. Gupta, et al. (2004). "Structure and Mechanical Quality of the Collagen-Mineral Nano-Composite in Bone." <u>Journal of Materials Chemistry</u> **14**(14): 2115-2123.

Fratzl, P. and R. Weinkamer (2007). "Nature's Hierarchical Materials." <u>Progress in Materials Science</u> **52**(8): 1263-1334.

Frost, H. M. (1987). "Bone Mass and the Mechanostat - a Proposal." <u>Anatomical Record</u> **219**(1): 1-9.

Gardner, J. C., R. L. van Bezooijen, et al. (2005). "Bone Mineral Density in Sclerosteosis; Affected Individuals and Gene Carriers." Journal of Clinical Endocrinology & Metabolism **90**(12): 6392-6395.

Gupta, H. S., J. Seto, et al. (2006). "Cooperative Deformation of Mineral and Collagen in Bone at the Nanoscale." Proceedings of the National Academy of Sciences of the United States of America **103**(47): 17741-17746.

Gupta, H. S., W. Wagermaier, et al. (2005). "Nanoscale Deformation Mechanisms in Bone." Nano Letters **5**(10): 2108-2111.

Hammersley, A. P., S. O. Svensson, et al. (1996). "Two-Dimensional Detector Software: From Real Detector to Idealised Image or Two-Theta Scan." High Pressure Research **14**(4-6): 235-248.

Helfrich, M. H., D. C. Aronson, et al. (1991). "Morphological Features of Bone in Human Osteopetrosis." Bone **12**(6): 411-419.

Hirose, S., M. Li, et al. (2007). "A Histological Assessment on the Distribution of the Osteocytic Lacunar Canalicular System Using Silver Staining." Journal of Bone and Mineral Metabolism **25**(6): 374-382.

Hörner, K., K. Loeffler, et al. (1997). "Vergleich Der Histologischen Struktur Der Kompakta Der Langen Röhrenknochen Bei Maus, Hamster, Ratte, Meerschweinchen, Kaninchen, Katze Und Hund Während Der Altersentwicklung." Anat. Histol. Embryol. **26**: 289-295.

Idelevich, A., M. Kerschnitzki, et al. (2011). "1,25(Oh)(2)D(3) Alters Growth Plate Maturation and Bone Architecture in Young Rats with Normal Renal Function." Plos One **6**(6): 14.

Jager, I. and P. Fratzl (2000). "Mineralized Collagen Fibrils: A Mechanical Model with a Staggered Arrangement of Mineral Particles." Biophysical Journal **79**(4): 1737-1746.

Jee, W. S. S. (2001). "Integrated Bone Tissue Physiology: Anatomy and Physiology." CRC Press, Boca Raton.

Johnson, R. (1990). Environmental Scanning Electron Microscopy: An Introduction to Esem, Philips Electron Optics.

Kerschnitzki, M. (2008). "Die Kontrolle der Mechanischen Eigenschaften von Knochen durch die Veränderung der Temperatur, der Dehnrate, des pH-Wertes und des Ionischen Mediums (Diploma Thesis)."

Kerschnitzki, M., W. Wagermaier, et al. (2011). "Poorly Ordered Bone as an Endogenous Scaffold for the Deposition of Highly Oriented Lamellar Tissue in Rapidly Growing Ovine Bone." Cells Tissues Organs **194**(2-4): 119-123.

Kerschnitzki, M., W. Wagermaier, et al. (2011). "The Organization of the Osteocyte Network Mirrors the Extracellular Matrix Orientation in Bone." Journal of Structural Biology **173**(2): 303-311.

Klein-Nulend, J., A. Vanderplas, et al. (1995). "Sensitivity of Osteocytes to Biomechanical Stress in-Vitro." Faseb Journal **9**(5): 441-445.

Koester, K. J., J. W. Ager, et al. (2008). "The True Toughness of Human Cortical Bone Measured with Realistically Short Cracks." Nature Materials **7**(8): 672-677.

Koshikaw.T and R. Shimizu (1974). "Monte-Carlo Calculation of Low-Energy Secondary-Electron Emission from Metals." Journal of Physics D-Applied Physics **7**(9): 1303-1315.

Kratky, O., G. Porod, et al. (1951). "*Einige Neuerungen in Der Technik Und Auswertung Von Rontgen-Kleinwinkelmessungen." Zeitschrift Fur Elektrochemie **55**(1): 53-59.

Kusuhara, S. (1976). "Histochemical and Microraiographical Studies of Medullary Bones in Laying Hens." Jap. J. zootech. Sci.(47): 141-146.

Landis, W. J. (1995). "The Strength of a Calcified Tissue Depends in Part on the Molecular-Structure and Organization of Its Constituent Mineral Crystals in Their Organic Matrix." Bone **16**(5): 533-544.

Landis, W. J. and M. J. Glimcher (1978). "Electron-Diffraction and Electron-Probe Microanalysis of Mineral Phase of Bone Tissue Prepared by Anhydrous Techniques." Journal of Ultrastructure Research **63**(2): 188-223.

Landis, W. J., K. J. Hodgens, et al. (1996). "Structural Relations between Collagen and Mineral in Bone as Determined by High Voltage Electron Microscopic Tomography." Microscopy Research and Technique **33**(2): 192-202.

Landis, W. J., K. J. Hodgens, et al. (1996). "Mineralization of Collagen May Occur on Fibril Surfaces: Evidence from Conventional and High-Voltage Electron Microscopy and Three-Dimensional Imaging." Journal of Structural Biology **117**(1): 24-35.

Landis, W. J., M. C. Paine, et al. (1980). "Use of Acrolein Vapors for the Anhydrous Preparation of Bone Tissue for Electron-Microscopy." Journal of Ultrastructure Research **70**(2): 171-180.

Lane, N. E., W. Yao, et al. (2006). "Glucocorticoid-Treated Mice Have Localized Changes in Trabecular Bone Material Properties and Osteocyte Lacunar Size That Are Not Observed in Placebo-Treated or Estrogen-Deficient Mice." Journal of Bone and Mineral Research **21**(3): 466-476.

Lange, C., C. Li, et al. (2011). "Fetal and Postnatal Mouse Bone Tissue Contains More Calcium Than Is Present in Hydroxyapatite." Journal of Structural Biology **176**(2): 159-167.

Lanyon, L. E., Rubin, et al. (1993). "Osteocytes, Strain Detection, Bone Modeling and Remodeling." Calcified Tissue International **53**: S102-S107.

Lee, C. L. and P. S. P. Wang (1994). A New Thinning Algorithm. Proceedings of the 12th Iapr International Conference on Pattern Recognition - Conference A: Computer Vision & Image Processing. Los Alamitos, I E E E, Computer Soc Press**:** 546-548.

Liu, Y. F., I. Manjubala, et al. (2010). "Size and Habit of Mineral Particles in Bone and Mineralized Callus During Bone Healing in Sheep." Journal of Bone and Mineral Research **25**(9): 2029-2038.

Mahamid, J., L. Addadi, et al. (2011). "Crystallization Pathways in Bone." Cells Tissues Organs **194**(2-4): 92-97.

Mahamid, J., B. Aichmayer, et al. (2010). "Mapping Amorphous Calcium Phosphate Transformation into Crystalline Mineral from the Cell to the Bone in Zebrafish Fin Rays." Proceedings of the National Academy of Sciences of the United States of America **107**(14): 6316-6321.

Mahamid, J., A. Sharir, et al. (2008). "Amorphous Calcium Phosphate Is a Major Component of the Forming Fin Bones of Zebrafish: Indications for an Amorphous Precursor Phase." Proceedings of the National Academy of Sciences of the United States of America **105**(35): 12748-12753.

Mahamid, J., A. Sharir, et al. (2011). "Bone Mineralization Proceeds through Intracellular Calcium Phosphate Loaded Vesicles: A Cryo-Electron Microscopy Study." Journal of Structural Biology **174**(3): 527-535.

Marotti, G. (2000). "The Osteocyte as a Wiring Transmission System." Journal of Musculoskeletal & Neuronal Interactions **1**(2): 133-136.

Meyers, M. A., P. Y. Chen, et al. (2008). "Biological Materials: Structure and Mechanical Properties." Progress in Materials Science **53**(1): 1-206.

Minsky, M. (1988). "Memoir on Inventing the Confocal Scanning Microscope." Scanning **10**(4): 128-138.

Mirone, A., R. Wilcke, et al. (2009). "High Speed Tomographic Reconstruction." from http://www.esrf.eu/UsersAndScience/Experiments/TBS/SciSoft/.

Mori, R., A. Hirayama, et al. (2007). "Histological and Physicochemical Studies of Hypercalcified Primear Lines in the Laminar Bone of Young Calves." Anatomical Science International **82**(2): 108-115.

Mori, R., T. Kodaka, et al. (2003). "Comparative Histology of the Laminar Bone between Young Calves and Foals." Cells Tissues Organs **175**(1): 43-50.

Mueller, W. J., H. Schraer, et al. (1964). "Calcium Metabolism + Skeletal Dynamics of Laying Pullets." Journal of Nutrition **84**(1): 20-&.

Nakashima, T., M. Hayashi, et al. (2011). "Evidence for Osteocyte Regulation of Bone Homeostasis through Rankl Expression." Nature Medicine **17**(10): 1231-1234.

Neuman, M. W. (1982). "Blood - Bone Equilibrium." Calcified Tissue International **34**(2): 117-120.

Nicolella, D. P., L. F. Bonewald, et al. (2005). "Measurement of Microstructural Strain in Cortical Bone." European Journal of Morphology **42**(1-2): 23-29.

Nicolella, D. P., D. E. Moravits, et al. (2006). "Osteocyte Lacunae Tissue Strain in Cortical Bone." Journal of Biomechanics **39**(9): 1735-1743.

Nudelman, F., K. Pieterse, et al. (2010). "The Role of Collagen in Bone Apatite Formation in the Presence of Hydroxyapatite Nucleation Inhibitors." Nature Materials **9**(12): 1004-1009.

Olszta, M. J., X. G. Cheng, et al. (2007). "Bone Structure and Formation: A New Perspective." Materials Science & Engineering R-Reports **58**(3-5): 77-116.

Omelon, S., J. Georgiou, et al. (2009). "Control of Vertebrate Skeletal Mineralization by Polyphosphates." Plos One **4**(5): 16.

Owan, I., D. B. Burr, et al. (1997). "Mechanotransduction in Bone: Osteoblasts Are More Responsive to Fluid Forces Than Mechanical Strain." American Journal of Physiology-Cell Physiology **273**(3): C810-C815.

Palumbo, C., M. Ferretti, et al. (2004). "Osteocyte Dendrogenesis in Static and Dynamic Bone Formation: An Ultrastructural Study." Anatomical Record Part a-Discoveries in Molecular Cellular and Evolutionary Biology **278A**(1): 474-480.

Parfitt, A. M. (2003). "Misconceptions (3): Calcium Leaves Bone Only by Resorption and Enters Only by Formation." Bone **33**(3): 259-263.

Paris, O., C. H. Li, et al. (2007). "A New Experimental Station for Simultaneous X-Ray Microbeam Scanning for Small- and Wide-Angle Scattering and Fluorescence at Bessy Ii." Journal of Applied Crystallography **40**: S466-S470.

Peterlik, H., P. Roschger, et al. (2006). "From Brittle to Ductile Fracture of Bone." Nature Materials **5**(1): 52-55.

Petruska, J. A. and A. J. Hodge (1964). "Subunit Model for Tropocollagen Macromolecule." Proceedings of the National Academy of Sciences of the United States of America **51**(5): 871-&.

Poole, K. E. S., R. L. van Bezooijen, et al. (2005). "Sclerostin Is a Delayed Secreted Product of Osteocytes That Inhibits Bone Formation." Faseb Journal **19**(10): 1842-+.

Porod, G. (1951). "Die Rontgenkleinwinkelstreuung Von Dichtgepackten Kolloiden Systemen .1." Kolloid-Zeitschrift and Zeitschrift Fur Polymere **124**(2): 83-114.

Porod, G. (1952). "Die Rontgenkleinwinkelstreuung Von Dichtgepakten Kolloiden Systemen .2." Kolloid-Zeitschrift and Zeitschrift Fur Polymere **125**(1): 51-57.

Price, C., B. C. Herman, et al. (2005). "Genetic Variation in Bone Growth Patterns Defines Adult Mouse Bone Fragility." Journal of Bone and Mineral Research **20**(11): 1983-1991.

Price, R. and W. Jerome (2011). Basic Confocal Microscopy, Springer New York Dordrecht Heidelberg London.

Pudney, C. (1998). "Distance-Ordered Homotopic Thinning: A Skeletonization Algorithm for 3d Digital Images." Computer Vision and Image Understanding **72**(3): 404-413.

Qing, H. and L. F. Bonewald (2009). "Osteocyte Remodeling of the Perilacunar and Pericanalicular Matrix." International Journal of Oral Science **1**(2): 59-65.

Rack, A., S. Zabler, et al. (2008). "High Resolution Synchrotron-Based Radiography and Tomography Using Hard X-Rays at the Bamline (Bessy Ii)." Nuclear Instruments & Methods in Physics Research Section a-Accelerators Spectrometers Detectors and Associated Equipment **586**(2): 327-344.

Ravesloot, J. H., R. J. Vanhouten, et al. (1990). "Identification of Ca2+-Activated K+ Channels in Cells of Embryonic Chick Osteoblast Cultures." Journal of Bone and Mineral Research **5**(12): 1201-1210.

Ravesloot, J. H., R. J. Vanhouten, et al. (1991). "High-Conductance Anion Channels in Embryonic Chick Osteogenic Cells." Journal of Bone and Mineral Research **6**(4): 355-363.

Rho, J. Y., L. Kuhn-Spearing, et al. (1998). "Mechanical Properties and the Hierarchical Structure of Bone." Medical Engineering & Physics **20**(2): 92-102.

Rinnerthaler, S., P. Roschger, et al. (1999). "Scanning Small Angle X-Ray Scattering Analysis of Human Bone Sections." Calcified Tissue International **64**(5): 422-429.

Rodan, G. A. and T. J. Martin (2000). "Therapeutic Approaches to Bone Diseases." Science **289**(5484): 1508-1514.

Roschger, P., P. Fratzl, et al. (1998). "Validation of Quantitative Backscattered Electron Imaging for the Measurement of Mineral Density Distribution in Human Bone Biopsies." Bone **23**(4): 319-326.

Roschger, P., E. P. Paschalis, et al. (2008). "Bone Mineralization Density Distribution in Health and Disease." Bone **42**(3): 456-66.

Roschger, P., H. Plenk, et al. (1995). "A New Scanning Electron-Microscopy Approach to the Quantification of Bone-Mineral Distribution - Backscattered Electron Image Grey-Levels Correlated to Calcium K-Alpha-Line Intensities." Scanning Microscopy **9**(1): 75-88.

Ruffoni, D., P. Fratzl, et al. (2008). "Effect of Temporal Changes in Bone Turnover on the Bone Mineralization Density Distribution: A Computer Simulation Study." Journal of Bone and Mineral Research **23**(12): 1905-1914.

Schell, H., D. R. Epari, et al. (2005). "The Course of Bone Healing Is Influenced by the Initial Shear Fixation Stability." Journal of Orthopaedic Research **23**(5): 1022-1028.

Schneider, P., M. Meier, et al. (2010). "Towards Quantitative 3d Imaging of the Osteocyte Lacuno-Canalicular Network." Bone **47**(5): 848-858.

Schneider, P., M. Meier, et al. (2011). "Serial Fib/Sem Imaging for Quantitative 3d Assessment of the Osteocyte Lacuno-Canalicular Network." Bone **49**(2): 304-311.

Schweitzer, M. H., R. M. Elsey, et al. (2007). "Do Egg-Laying Crocodilian (Alligator Mississippiensis) Archosaurs Form Medullary Bone?" Bone **40**(4): 1152-1158.

Shapiro, F. (1988). "Cortical Bone Repair - the Relationship of the Lacunar-Canalicular System and Intercellular Gap-Junctions to the Repair Process." Journal of Bone and Joint Surgery-American Volume **70A**(7): 1067-1081.

Shapiro, F. (2008). "Bone Development and Its Relation to Fracture Repair. The Role of Mesenchymal Osteoblasts and Surface Osteoblasts." European Cells & Materials **15**: 53-76.

Singh, R., C. J. Joyner, et al. (1986). "Changes in the Concentrations of Parathyroid-Hormone and Ionic Calcium in the Plasma of Laying Hens During the Egg Cycle in Relation to Dietary Deficiencies of Calcium and Vitamin-D." General and Comparative Endocrinology **61**(1): 20-28.

Skedros, J. G., J. L. Holmes, et al. (2005). "Cement Lines of Secondary Osteons in Human Bone Are Not Mineral-Deficient: New Data in a Historical Perspective." Anatomical Record Part a-Discoveries in Molecular Cellular and Evolutionary Biology **286A**(1): 781-803.

Stover, S. M., R. R. Pool, et al. (1992). "Histological Features of the Dorsal Cortex of the 3rd Metacarpal Bone Mid-Diaphysis During Postnatal-Growth in Thoroughbred Horses." Journal of Anatomy **181**: 455-469.

Stroncek, J. D. and W. M. Reichert (2008). Overview of Wound Healing in Different Tissue Types. Indwelling Neural Implants: Strategies for Contending with the in Vivo Environment. W. M. Reichert. Boca Raton (FL), Taylor & Francis Group, LLC.

Sugawara, Y., H. Kamioka, et al. (2005). "Three-Dimensional Reconstruction of Chick Calvarial Osteocytes and Their Cell Processes Using Confocal Microscopy." Bone **36**(5): 877-83.

Tai, K., M. Dao, et al. (2007). "Nanoscale Heterogeneity Promotes Energy Dissipation in Bone." Nature Materials **6**(6): 454-462.

Taylor, T. G. and L. F. Belanger (1969). "Mechanism of Bone Resorption in Laying Hens." Calcified Tissue Research **4**(2): 162-&.

Teti, A. and A. Zallone (2009). "Do Osteocytes Contribute to Bone Mineral Homeostasis? Osteocytic Osteolysis Revisited." Bone **44**(1): 11-16.

Thompson, A. (1992). "On Growth and Form - the Complete Revised Edition (Unaltered Republication of Cambridge Univ. Press, 1942)." Dover Publications.

Toyosawa, S., S. Shintani, et al. (2001). "Dentin Matrix Protein 1 Is Predominantly Expressed in Chicken and Rat Osteocytes but Not in Osteoblasts." Journal of Bone and Mineral Research **16**(11): 2017-2026.

van Bezooijen, R. L., B. A. J. Roelen, et al. (2004). "Sclerostin Is an Osteocyte-Expressed Negative Regulator of Bone Formation, but Not a Classical Bmp Antagonist." Journal of Experimental Medicine **199**(6): 805-814.

Vanderplas, A. and P. J. Nijweide (1988). "Cell Cell-Interactions in the Osteogenic Compartment of Bone." Bone **9**(2): 107-111.

Vandevelde, J. P., J. P. W. Vermeiden, et al. (1984). "Changes in Activity of Chicken Medullary Bone Cell-Populations in Relation to the Egg-Laying Cycle." Metabolic Bone Disease & Related Research **5**(4): 191-193.

Vuong, J. and C. Hellmich (2011). "Bone Fibrillogenesis and Mineralization: Quantitative Analysis and Implications for Tissue Elasticity." Journal of Theoretical Biology **287**: 115-130.

Weinbaum, S., S. C. Cowin, et al. (1994). "A Model for the Excitation of Osteocytes by Mechanical Loading-Induced Bone Fluid Shear Stresses." Journal of Biomechanics **27**(3): 339-360.

Weiner, S. and O. Bar-Yosef (1990). "States of Preservation of Bones from Prehistoric Sites in the near-East - a Survey." Journal of Archaeological Science **17**(2): 187-196.

Weiner, S. and W. Traub (1992). "Bone-Structure - from Angstroms to Microns." Faseb Journal **6**(3): 879-885.

Weiner, S. and H. D. Wagner (1998). "The Material Bone: Structure Mechanical Function Relations." Annual Review of Materials Science **28**: 271-298.

Whitehead, C. C. (2004). "Overview of Bone Biology in the Egg-Laying Hen." Poultry Science **83**(2): 193-199.

Zallone, A. Z. and W. J. Mueller (1969). "Medullary Bone of Laying Hens During Calcium Depletion and Repletion." Calcified Tissue Research **4**(2): 136-&.

Zeng, Y., S. C. Cowin, et al. (1994). "A Fiber-Matrix Model for Fluid-Flow and Streaming Potentials in the Canaliculi of an Osteon." Annals of Biomedical Engineering **22**(3): 280-292.

Zizak, I., P. Roschger, et al. (2003). "Characteristics of Mineral Particles in the Human Bone/Cartilage Interface." Journal of Structural Biology **141**(3): 208-217.

9 Figure List

10 Acknowledgements

11   Eidesstattliche Erklärung

Hiermit versichere ich, dass ich meine Dissertation mit dem Titel "Bone Material Characteristics Influenced by Osteocytes" selbstständig angefertigt und keine anderen, als die von mir angegebenen Hilfsmittel und Quellen verwendet habe. Ich versichere, dass ich bisher an keiner Universität, weder im In- noch im Ausland, einen Promotionsversuch unternommen habe.

Ich erkläre hiermit außerdem, dass ich die Promotionsordnung der Mathematisch- Naturwissenschaftlichen Fakultät I der Humboldt-Universität zu Berlin in der Fas-sung vom 01. September 2005 anerkenne.

Michael Kerschnitzki

Potsdam, Dezember 2011